

APPENDIX V




Subsidence assessment



**COWAL GOLD OPERATIONS
SURFACE SUBSIDENCE ASSESSMENT FOR OPEN PIT
EXPANSION**

**PREPARED FOR
EMM & EVOLUTION MINING**

DOCUMENT CONTROL

Date	Version	Comments	Signed
2023FEB03	DRAFT01	Initial draft for client review & comments.	
2023FEB16	DRAFT02	Second draft following client feedback.	
2023APR13	FINAL	Final version accepted by client.	
COPYRIGHT NOTICE Copyright of this document is retained by Beck Engineering Pty Ltd. Copyright is enforced to protect client interests.			

EXECUTIVE SUMMARY

Beck Engineering (BE) has conducted a life-of-mine (LOM) surface subsidence assessment for the proposed open pit mine expansion project, located at the Cowal Gold Operations of Evolution Mining, near West Wyalong, New South Wales. The aim of this project was to address the Secretary's Environmental Assessment Requirements (SEARs) from the Department of Planning, Industry and Environment (DPIE) for the Environmental Impact Study (EIS) of the proposed mine expansion. The project scope included:

1. Simulate the proposed open pit and future underground mining using a 3D finite element numerical model.
2. Forecast surface impacts, subsidence and pit wall displacements during future open pit mine expansion. This includes surface maps of displacement, horizontal strain, angular distortion (tilt) and plastic strain,
3. Assess water draw-down effects on surface subsidence.
4. Assess geotechnical interaction between the proposed open pit expansion and the planned underground mine, including forecasts for stress, strain and displacement.

Our assessment is based on numerical modelling using finite element (FE) methods. An overview of the assessment, including the main findings, risks and recommendations is summarized below. More extensive details are provided in Section 3 of this report.

Main findings

E42, E46 & GR Open Pits

- Vertical displacements of the original topography around the perimeter of the E42, E46 & GR open pits are forecast to be less than 0.1 m at the end of the mine plan (Y2037 M06). The direction of the forecast displacements of the pit walls is uplift. This is a typical response for large open pit mines as the overburden load is removed from the slopes over time.
- The forecast open pit mining-induced surface displacements and rockmass damage around the perimeter of the E42, E46 & GR open pits can be classified as Negligible and of a magnitude which would not present any visible evidence of disturbance to the natural topography or man-made features outside the pits. Displacements beyond the crest of the open pits are elastic in nature and near-zero. No plastic (i.e. permanent) rock mass damage is forecast beyond the crest of the pits at the natural surface level and therefore no visible surface cracking or other forms of visible damage are expected to occur.
- Rock mass damage of a Significant nature within the E42 pit is concentrated along the major faults in the oxide domains and along the Central Shear zone, including areas of the fresh rock slope both above and below the planned haul ramp in the north wall. The damage is not forecast to extend beyond the crest of the open pit and would therefore not affect surface terrain or infrastructure.
- The E46 pit slopes accumulate a higher severity of rockmass damage than the other open pits due to the slope loading effect of the E46 in-pit backfilling, which takes place during 2031/32. However, as the slopes are confined by that backfill, there would be no adverse subsidence or slope instability as a result.
- Potential for minor subsidence events in the E46 in-pit backfill material exists if weak oxides or other fine materials are deposited above coarser fragmentation backfill, such as fresh rock fill. This could occur if the overlying finer fill materials migrate through the coarser underlying fill over time, due to either water or gravity-driven vertical movement of the fines within the pore space of the coarse fill zones. These risks can be reliably avoided if a consistent source of backfill is utilised for the E46 in-pit backfilling campaign.
- The 36 degree final slope angle assumed for the E46 backfill slope may be too steep to achieve, as some damage is assumed in the model. However, in reality the tipped fill material would naturally rill to a stable slope angle.

E41 Open Pit

- Mining of the E41 open pit is not forecast to generate total displacements exceeding 0.1 m anywhere beyond the physical limits of the pit itself. The small magnitude elastic displacements at the surface are insufficient to cause visible subsidence effects or any permanent damage, such as tension cracking or ground depressions.

- Within the pit, maximum horizontal displacements of the slopes are forecast to approach 0.15 m in three locations within the Soft Oxide domain. This is a Negligible magnitude of displacement and primarily related to uplift of the slopes due to overburden removal, not subsidence or slope instability. Total displacements of the E41 pit slopes approach 0.3 m within the Soft Oxides only. This is also related to uplift of the slopes during overburden removal, not subsidence.
- There are total (i.e. 3D) displacements approaching 0.2 m to the immediate north of the E41 pit, through the permanent bridging pillar of rock that separates the E41 pit from the E42. These displacements are also classified as Negligible.

Lake Protection Bund & Other Infrastructure

- The final lake protection bund (LPB) and vast majority of the surface, including the processing infrastructure precinct, are forecast to experience a Negligible subsidence impact as a result of the proposed open pit mine plan. A Very Slight impact is forecast to affect a minority of the ROM Pad to the west of the final E42 pit, but the effect is unlikely to present as any visible subsidence damage or lead to any adverse consequences.
- Vertical displacements of the natural topographic surface of up to 0.5 m are forecast to occur during the deposition of the waste dumps (NWRD and SWRD) to the northwest and southwest of the open pits. These displacements are caused by the overburden load applied to the weak and weathered cover sequence materials at the surface. They are not a result of open pit mining-induced subsidence. The displacements only affect the ground beneath the waste dumps and do not extend outwards to affect any nearby areas.

Effect of Mining on Groundwater Conditions

- The numerical simulation of the Lake Cowal mine plan was hydro-mechanically coupled. This means that groundwater characteristics of the local geological environment, such as the phreatic surface level, hydraulic conductivity and pore water pressure, and their effect on the rock mass, were included in the mechanical solutions of the simulation. The action of groundwater and pore water pressure within the model space influences the mining-induced rock mass damage. Similarly, the simulated hydraulic conductivity of the rock does change over time, as a function of the mining-induced rockmass fracturing.
- The model forecasts indicate that the majority of the rock mass between the mining excavations and Lake Cowal water body experiences minimal change in hydraulic conductivity or flux over the life-of-mine plan.
- There are some regions of forecast conductivity increase of up to 1.7×10^{-6} m/s within the oxide weathering domain in the immediate abutments of the open pit slopes. There are also conductivity increases in the order of 1.5×10^{-7} m/s forecast along some fault structures that are within close proximity to the open pit and/or underground workings in the upper eastern precinct of the mine. These structures are not persistent between the planned mining excavations and the lake, given the current geological understanding.
- Due to the draw-down of the phreatic surface in the vicinity of the mine, there is a forecast minor increase in the hydraulic flux from the lake towards the pit. By the end of mining in 2037 this increase in flux is forecast to be in the order of 2×10^{-8} m/s.
- Overall, the proposed open pit mine expansion plan is not forecast to cause any significant change in either hydraulic conductivity or flux between Lake Cowal and the mining excavations.

Main geotechnical risks

- The main geotechnical risk affecting surface subsidence and relating to open pit mining is a large-scale instability of the pit slope which either undermines or causes displacement of the surface terrain. Such an event is likely to be either a circular failure through the near-surface weathered rock material or else structurally controlled. In the worst case, the affected area would be unlikely to extend more than several tens of metres from the pit crest limits at the time. The mine already has a detailed structural model, which includes many major faults through the open pit precinct and these have been included in the numerical simulation. The existing geology knowledge and simulation results, which indicate that the pit crest region will remain stable, both reduce the probability of an unforeseen slope instability event occurring. Further structural data collection, interpretation and model updates are recommended to be conducted on an ongoing basis during mine planning and operations.

Recommendations

- Engage a qualified structural or civil engineer to review the following detailed subsidence forecasts for all pieces of major mining-related infrastructure, including but not limited to the final LPB, major plant in the processing precinct and tailings storage facilities etc, in order to confirm that the forecast strains, displacements and angular distortions do not exceed the service limits of any assets.
- Review and where necessary update the underground mine design to ensure that no stopes are excavated beneath the open pit with a fresh rock crown pillar height of less than 20-30 m (i.e. maintain a minimum stope width to fresh rock crown pillar ratio of 1:2). Where any non-compliant stopes do exist in the mine plan, remove them. BE re-iterate the recommendations made previously by Campbell (2020) in relation to subsidence interactions between the underground and open pit vicinity.
- When backfilling the E46 open pit, consider the fill material types used and the sequence of the deposition in order to avoid creation of voids within the fill, which might lead to subsidence over time. Ideally, fill material(s) with minimal porosity should be used to backfill the E46 pit.
- In order to mitigate and contain any potential slumping of the E46 final backfill slope, it is recommended to construct fresh rock bunds at the toe of the slope.
- Continue and expand the open pit slope displacement and groundwater monitoring activities at the mine in order to record trends as the open pit increases in size and to periodically evaluate those trends against the numerical model forecasts. Valuable future data collection programs would include some or all of the following: pit slope radar, prism monitoring, INSAR displacement surveys of the entire mining lease, GPS survey stations around the pit crest and critical/valuable assets, piezometers in the local bore network to record groundwater elevation changes etc.
- Continue to collect and interpret rock mass characterisation data from the open pit and underground mining domains, especially regarding the strength properties of the various lithologies as well as the location, orientation and characteristics of the geological structures (i.e. mine scale faults, shears, intermediate scale faults and small scale joint sets). Use this information to inform future slope stability and hydrogeology assessments.

Limitations

In addition to the normal resolution limits associated with the current finite element model, the main limitations of this project are:

- The current understanding of rockmass strength and its' spatial variability, which affects forecasts of damage.
- The resolution and accuracy of the structural model, including the large and intermediate scale discontinuities which may affect the performance of the excavations.
- Knowledge of the hydrogeological characteristics of the Lake Cowal site, including conductivity and storativity parameters of the orebody, nearby host rock and faults, the location and characteristics of local aquifers and aquitard structures, and also the nature of the groundwater sources and sinks, such as inflow/outflow rates.

Enquiries

Please direct further enquiries to the undersigned.



Christopher Drover

PhD MEngSc BE (Hons) BSc

Principal Engineer, Mining & Rock Mechanics

TABLE OF CONTENTS

1	INTRODUCTION	10
1.1	Geometric Data.....	10
2	PROJECT WORKFLOW, BACKGROUND DATA & MODEL COMPOSITION	13
2.1	Project workflow & simulation framework.....	13
2.2	Topography.....	13
2.3	Stress Field.....	14
2.4	Geotechnical domain assignment.....	16
2.4.1	Estimated material properties for modelling	16
2.5	Hydrogeological conditions	16
2.6	Mining methods, geometry & sequence	22
2.7	Stope filling methodology & fill properties	27
2.8	Structural model resolution.....	27
2.9	Rockmass damage and surface subsidence classification methods	30
3	FORECASTS, INTERPRETATION & DISCUSSION	33
3.1	Open pit design.....	33
3.2	E42, E46 & GR Open Pits	33
3.3	E41 Open Pit.....	45
3.4	Lake Protection Bund & Other Infrastructure	50
3.5	Open Pit / Underground Interaction.....	58
3.6	Asset Reports.....	63
3.7	Mining effect on groundwater conditions.....	77
4	CONCLUSIONS, RECOMMENDATIONS & LIMITATIONS.....	80
5	REFERENCES.....	83
6	APPENDIX A - LRX CONSTITUTIVE FRAMEWORK	84
6.1	Constitutive model and physical composition.....	84
6.1.1	The LR2 constitutive framework	84
6.2	Constitutive model for the continuum parts	84
6.3	Representation of explicit structure	88
6.4	Extension for the case of transversal isotropy	88
6.5	Model parameter to determine rock strength.....	90
6.6	Modelling softening behaviour.....	91
6.7	The common damage scale	92
6.8	Assessing seismic potential with RER	92
6.9	Mechanical response in the presence of pore-water pressure	93
6.10	References	93
7	APPENDIX B – MATERIAL STRENGTH ENVELOP PLOTS	94

LIST OF FIGURES

Figure 1-1	Open pit and underground mining excavation geometry included in the numerical model (view southeast, dumps & lake bund not shown).	12
Figure 2-1	Principal stress orientations for the Lake Cowal mine model.....	14
Figure 2-2	Pre-mining stress state along a vertical sample path for three locations in the model space.....	15
Figure 2-3:	Lithology domains included in the model and list of included 3D wireframes.....	17
Figure 2-4:	Indicative rockmass softening curve demonstrating the plastic strain transition points ϵ_1 and ϵ_2	21
Figure 2-5	Variation in hydraulic conductivity as a function of mining-induced rockmass damage.	21
Figure 2-6	Variation of hydraulic conductivity (Y-axis) with plastic strain (X-axis) in the hydro-coupled model (Flatten, et al., 2016).	22
Figure 2-7	Global geometry of the finite-element simulation domain for the CGO model.....	23
Figure 2-8	Simulated extraction sequence for the mine plan (view southeast from below).	24
Figure 2-9	Simulated extraction sequence for the mine plan (view west).....	25
Figure 2-10	Simulated extraction & waste dumping sequence for the mine plan (top view).	26
Figure 2-11	Modelled fault and shear zone structures in the vicinity of the open pits.....	27
Figure 2-12	Explicitly modelled geological faults and shear zones included in the model (top view).....	28
Figure 2-13:	Rockmass damage scale.....	30
Figure 2-14	Stress vs. Strain chart showing corresponding rockmass damage levels.	30
Figure 2-15	Example of surface subsidence following a large-scale slope failure at another mine.....	32
Figure 2-16	Surface infrastructure subsidence impact severity assessment scheme based on Boscardin & Cording (1989). 32	
Figure 3-1	Forecast vertical displacements of the E42, E46 & GR open pit slopes and surrounding natural surface topography (2037 M06).	35
Figure 3-2	Forecast horizontal displacements of the E42, E46 & GR open pit slopes and surrounding natural surface topography (2037 M06).	36
Figure 3-3	Forecast total displacements of the E42, E46 & GR open pit slopes and surrounding natural surface topography (2037 M06).	37
Figure 3-4	Forecast rockmass damage of the E42, E46 & GR open pit slopes and surrounding natural surface topography (2037 M06).	38
Figure 3-5	Rock mass damage forecasts for the E42 open pit showing elevated damage in the Central Shear and oxides (2037 M06).	39
Figure 3-6	Rock mass damage forecasts for the E46 open pit after in-pit backfilling (2037 M06).	40
Figure 3-7	North-South long section showing forecast total displacements and directions in the E42 open pit slopes. 41	
Figure 3-8	East-West cross section showing forecast total displacements and directions in the E42 open pit slopes. 42	
Figure 3-9	North-South long section showing induced major principal stress conditions in the E42 open pit slopes. 43	
Figure 3-10	East-West cross section showing induced major principal stress conditions in the E42 open pit slopes. 44	
Figure 3-11	Forecast vertical displacements of the E41 open pit slopes and surrounding natural surface topography. 46	
Figure 3-12	Forecast horizontal displacements of the E41 open pit slopes and surrounding natural surface topography. 47	

Figure 3-13	Forecast total displacements of the E41 open pit slopes and surrounding natural surface topography.	48
Figure 3-14	Forecast rockmass damage of the E41 open pit slopes and surrounding natural surface topography....	49
Figure 3-15	Mine-scale view of forecast vertical displacements (Y2037 M06).....	51
Figure 3-16	Mine-scale view of forecast total displacements (Y2037 M06).....	52
Figure 3-17	Rock mass damage showing impact of open pit mining to the Lake Protection Bund and nearby surface (2037 M06).....	53
Figure 3-18	Classification system for the severity of surface subsidence based on Boscardin & Cording (1989).	54
Figure 3-19	Contours of surface subsidence impact severity for the open pit district (top view).....	55
Figure 3-20	Contours of surface subsidence impact severity for CGO after completion of the proposed pit mining (global top view).....	56
Figure 3-21	Contours of surface subsidence impact severity for the major surface plant adjacent the western pit crest (top view).....	57
Figure 3-22	3D volume render of rockmass damage forecasts in the regional pillar separating the open pit and underground mine.	59
Figure 3-23	Northeast-Southwest oriented vertical section of forecast major principal stress concentrations in the regional pillar between the open pit and underground mine.....	60
Figure 3-24	Northeast-Southwest oriented vertical section of forecast total displacement in the regional pillar between the open pit and underground mine.	61
Figure 3-25	Isosurfaces of 100 mm and 200 mm total displacement surrounding the open pit and underground mines at the end of the LOM.....	62
Figure 3-26	Location of asset subsidence reporting points for the Lake Protection Bund (LPB)	64
Figure 3-27	Subsidence reports for LPB #1 and #2 locations.....	65
Figure 3-28	Subsidence reports for LPB #3 and #4 locations.....	66
Figure 3-29	Subsidence reports for LPB #5 and #6 locations.....	67
Figure 3-30	Subsidence reports for LPB #7 and #8 locations.....	68
Figure 3-31	Location of asset subsidence reporting points for the processing plant & ROM precinct.	69
Figure 3-32	Subsidence reports for the ROM pad & crusher.	70
Figure 3-33	Subsidence reports for processing plant silos and ore stockpile cone.....	71
Figure 3-34	Subsidence reports for the metallurgy processing plant and ball mill.	72
Figure 3-35	Subsidence reports for the workshop and D6 pond.....	73
Figure 3-36	Subsidence reports for the main warehouse and surface transformer station.	74
Figure 3-37	Location of asset subsidence reporting points for the TSF dams.....	75
Figure 3-38	Subsidence reports for the north and south tailings storage facilities (closest points to the open pit) ..	76
Figure 3-39	Forecast hydraulic conductivity between Lake Cowal and the orebodies before and after mining.	78
Figure 3-40	Forecast hydraulic flux between Lake Cowal and the orebodies before and after mining.....	79

LIST OF TABLES

Table 2-1 In-situ stress field for the Lake Cowal mine model (after Bird & Hulls, 2020). 14

Table 2-2: Material properties used the Lake Cowal numerical simulation..... 18

Table 2-3 Strength properties used for Mohr-Coulomb-like materials. 20

Table 2-4 Hydraulic conductivity values applied to the major geological domains in the model..... 21

Table 2-5 List of all explicitly modelled geological structures in the Lake Cowal model..... 29

Table 2-6 Surface subsidence impact classification criteria..... 31

Table 3-1 List of mine assets with detailed subsidence reports (precise locations in mine grid coordinates). 63

1 INTRODUCTION

Beck Engineering (BE) has assessed mining-induced subsidence impacts relating to the proposed open pit mine expansion at the Cowal Gold Operations (CGO) of Evolution Mining, located near West Wyalong in New South Wales.

The aim of this project was to address the Secretary's Environmental Assessment Requirements (SEARs) from the Department of Planning, Industry and Environment (DPIE) for the Environmental Impact Study (EIS). The project scope included:

1. Simulation of proposed open pit and future underground mining using a 3D finite element numerical model.
2. Forecast surface impacts, subsidence and pit wall displacements during future open pit mine expansion. This includes surface maps of displacement, horizontal strain, angular distortion (tilt) and plastic strain,
3. Assess water draw-down effects on surface subsidence.
4. Assess geotechnical interaction between the proposed open pit expansion and the planned underground mine, including forecasts for stress, strain and displacement.

This assessment did not include:

- Sub-modelling of any part of the mine,
- Modelling of ground support,
- Detailed stability or seismic forecasting for the underground workings,
- A site visit. This was not required for the scope of the project.

This report documents our analysis method, results, associated interpretation, conclusions and our recommendations for EMM and Evolution Mining's consideration.

1.1 Geometric Data

The numerical assessments were constructed using the 3D geometric data files of the mine design and local geology, as were provided to us. These were:

For the as-built open pit mine:

- *OP_EOM_SEPT22_HARD.dxf*

For the future open pit mine, surface waste dumps and lake protection bund (design files dated 23.08.2022):

- *CGO_EIS_EOFY_2023-Contour_EOFY_23_CONTOUR.dxf*
- *CGO_EIS_EOFY_2024-Contour_EOFY_24_CONTOUR.dxf*
- *CGO_EIS_EOFY_2025-Contour_EOFY_25_CONTOUR.dxf*
- *CGO_EIS_EOFY_2026-Contour_EOFY_26_CONTOUR.dxf*
- *CGO_EIS_EOFY_2027-Contour_EOFY_27_CONTOUR.dxf*
- *CGO_EIS_EOFY_2028-Contour_EOFY_28_CONTOUR.dxf*
- *CGO_EIS_EOFY_2029-Contour_EOFY_29_CONTOUR.dxf*
- *CGO_EIS_EOFY_2030-Contour_EOFY_30_CONTOUR.dxf*
- *CGO_EIS_EOFY_2031-Contour_EOFY_31_CONTOUR.dxf*
- *CGO_EIS_EOFY_2032-Contour_EOFY_32_CONTOUR.dxf*
- *CGO_EIS_EOFY_2033-Contour_EOFY_33_CONTOUR.dxf*
- *CGO_EIS_EOFY_2034-Contour_EOFY_34_CONTOUR.dxf*
- *CGO_EIS_EOFY_2035-Contour_EOFY_35_CONTOUR.dxf*

- *CGO_EIS_EOFY_2036-Contour_EOFY_36_CONTOUR.dxf*
- *CGO_EIS_EOFY_2037-Contour_EOFY_37_CONTOUR.dxf*

For the as-built underground mining excavations:

- *currentsolids_17102022.dxf*

For the future underground mine excavations (MOSS_Mod1, design files dated 17.10.2022):

- *MOS_FY_2022.dxf*
- *MOS_FY_2023.dxf*
- *MOS_FY_2024.dxf*
- *MOS_FY_2025.dxf*
- *MOS_FY_2026.dxf*
- *MOS_FY_2027.dxf*
- *MOS_FY_2028.dxf*
- *MOS_FY_2029.dxf*
- *MOS_FY_2030.dxf*
- *MOS_FY_2031.dxf*
- *MOS_FY_2032.dxf*
- *MOS_FY_2033.dxf*
- *MOS_FY_2034.dxf*
- *MOS_FY_2035.dxf*
- *MOS_FY_2036.dxf*

For the geotechnical (i.e. lithology) domains:

- *Various files provided by EMM RFI_003 (see lithology material types described in Section 2.4).*

For the local geological structures (i.e. faults & shear zones):

- *Various files provided by EMM RFI_002 (see structures listed in Section 2.7).*

The open pit and underground mining excavations included in the numerical simulation are illustrated in Figure 1-1.

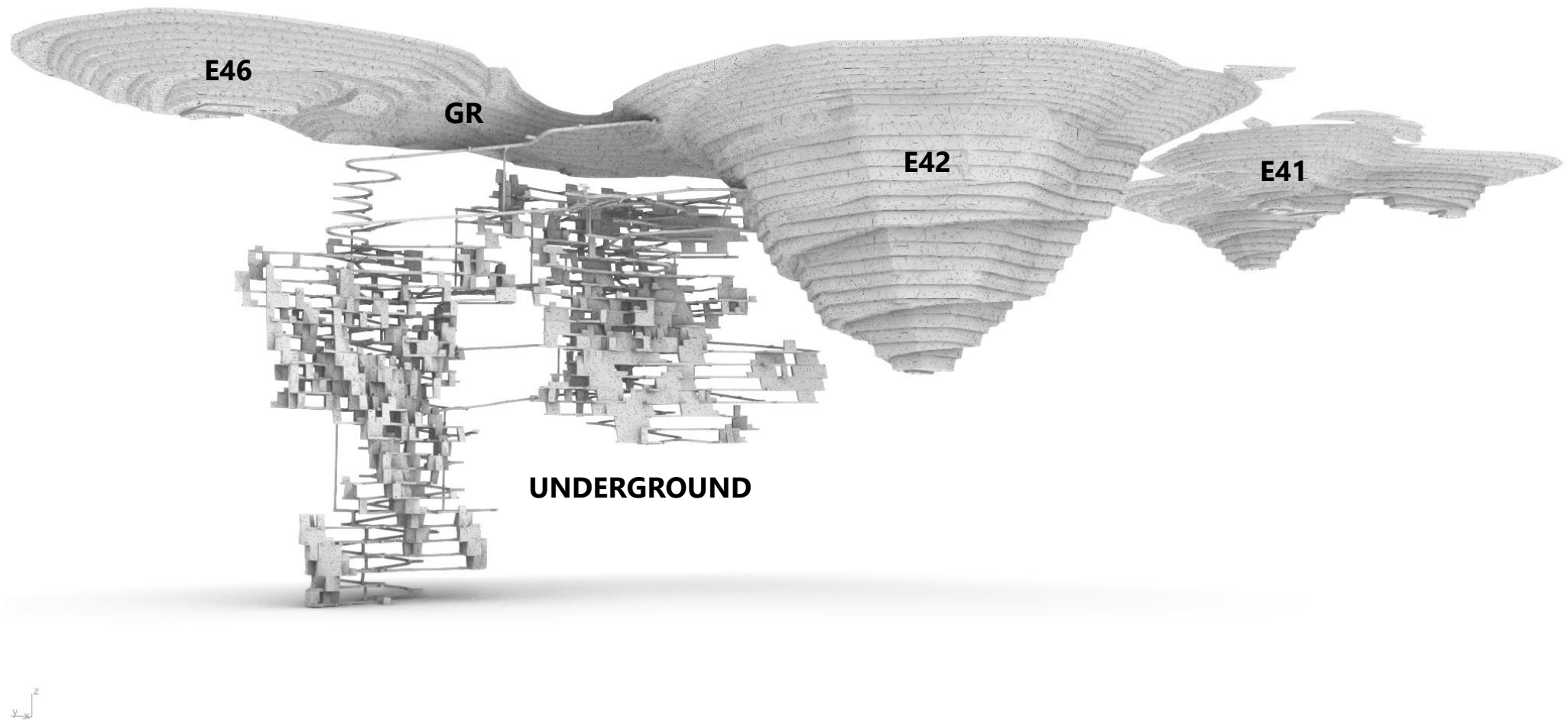


Figure 1-1 Open pit and underground mining excavation geometry included in the numerical model (view southeast, dumps & lake bund not shown).

2 PROJECT WORKFLOW, BACKGROUND DATA & MODEL COMPOSITION

This section summarises the project workflow, the available background data and assumptions relevant to the project and describes how these data and assumptions have been incorporated into the workflow.

2.1 Project workflow & simulation framework

The modelling workflow for this project was:

1. Collation of all relevant geometric data into a 3D CAD database using commercial software.
2. Discontinuum finite element (FE) mesh construction using commercial software and in-house scripting tools. Higher-order finite elements were used for all volume elements.
3. Assignment of the geotechnical domains, material properties, initial conditions, boundary conditions and the mining, waste tipping and backfilling sequence to the FE mesh.
4. Solution of the stress, strain and displacement fields and released energy for each step in the modelled mining sequence using the Abaqus Explicit FE solver. Abaqus Explicit is a commercial, general purpose, 3D, non-linear, continuum or discontinuum FE analysis package designed specifically for analysing problems with significant plasticity, large strain gradients, high deformation levels and large numbers of material domains. Commercial software and in-house post-processing scripts are used to process the Abaqus output and visualise the results.
5. Forecasting of future rockmass behaviour for the current LOM plan. Section 3 documents the model results, our interpretation of the results in a mining context and associated discussion.

The Levkovitch-Reusch (LRx) discontinuum constitutive framework was applied in Abaqus to describe the mechanical behaviour of the rockmass and structures. The LRx framework includes:

1. Three-dimensional (3D) geometry, with the mine excavations sequenced in a sufficient number of separate excavation steps (called frames) to capture the necessary temporal resolution for the project scope.
2. Strain-softening dilatant constitutive model for the rockmass and structures with a generalised Hoek-Brown yield criterion. Different material properties are assigned to each geotechnical domain.
3. Discontinuum formulation using cohesive finite elements to model discrete structures. Cohesive elements are free to dislocate, dilate and degrade and can realistically capture the behaviour of thin structures which tetrahedral finite elements cannot achieve as effectively. The complete interpreted structural model at the required resolution can be included, and where appropriate, can be supplemented with a discrete fracture network (DFN) to improve the structural resolution.
4. Structures less persistent than those modelled explicitly can be represented by “smearing” the effects of structures within the continuum regions of the modelled rockmass.
5. Hydromechanical coupling, where necessary, to capture the effects of pore water pressure on the rockmass yield surface, or to estimate water flow rates.

The LRx modelling framework aims for physical similitude, by making the fewest possible assumptions about the governing physics of the entire mine system within a single physics-based numerical model, at the required scale of the analysis. This results in a realistic but complex model since complexity is the reality of all mines. Building a realistic mine model by including the governing physics means that realistic rockmass behaviour evolves naturally in the model, and is therefore essential for developing a detailed understanding of the likely rockmass response to mining.

2.2 Topography

The natural ground surface at Cowal Gold Operations is generally flat with only low topographical relief (± 40 m) in the near vicinity of the mine. The supplied topographic data were used to build the natural surface topography, with extensions out to the model boundaries. The main surface topographical feature of note is the Lake Cowal basin, located to the immediate east of the current open pit.

2.3 Stress Field

Evolution Mining specified that the input stress field to the subsidence model should match that which Mining One Consultants (Bird & Hulls, 2020) have previously recommended to be adopted as the pre-mining in-situ stress regime for CGO. This stress field is summarised in Table 2-1 and Figure 2-1 below. This input has previously been used by BE for other modelling projects at CGO. In the model input stress regime the major and intermediate principal stress orientations are reversed with respect to those of the regional stress regime of the Lachlan Orogen, as reported by Lee, et al. (2010).

Table 2-1 In-situ stress field for the Lake Cowal mine model (after Bird & Hulls, 2020).

Principal stress component	Magnitude gradient (MPa/km)	Dip (degrees)	Dip azimuth (degrees)
σ_1	53	22°	195°
σ_2	34	17°	292°
σ_3	28	62°	056°
Stress gradients applied from reference $z = 1,205$ mRL.			

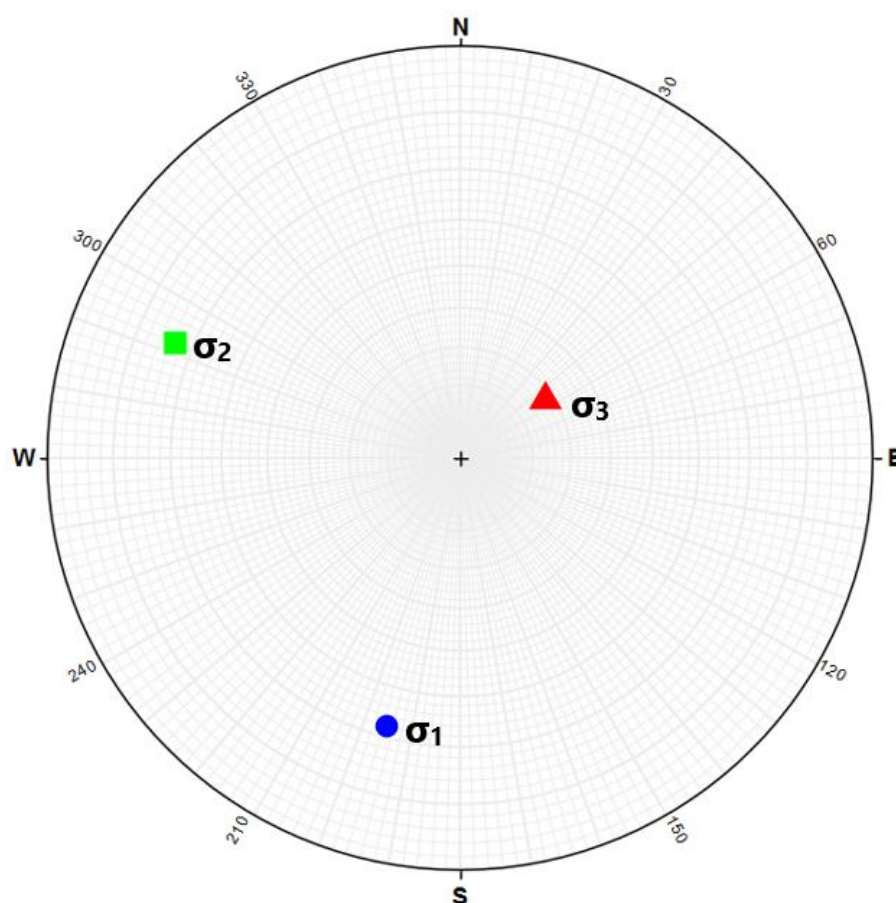


Figure 2-1 Principal stress orientations for the Lake Cowal mine model.

The pre-mining stress field was generated in the FE model by ramping the stresses in each element from an initial zero stress state to the target initial stress gradients over an appropriate number of computational steps. This part of the simulation procedure is called the equilibrium step and aims to evolve an initial stress field in the mine precinct that is mechanically compatible with the modelled structures, geotechnical domains, material properties and topography. This procedure generates a variable in situ stress field in the mine precinct which is characteristic of the variability typically measured in mines. This normal variability in the principal stress orientation and magnitude with depth is illustrated in Figure 2-2, which shows the modelled principal stresses sampled along a vertical path at three locations in the model space at the completion of the equilibrium step.

Project	COWAL2022047
Angles	bearing + plunge

Model	COWAL2022047_R04M_G02Mv1_S01_Q01_M01_D01
Offset coordinates	x=0m; y=0m; z=0m

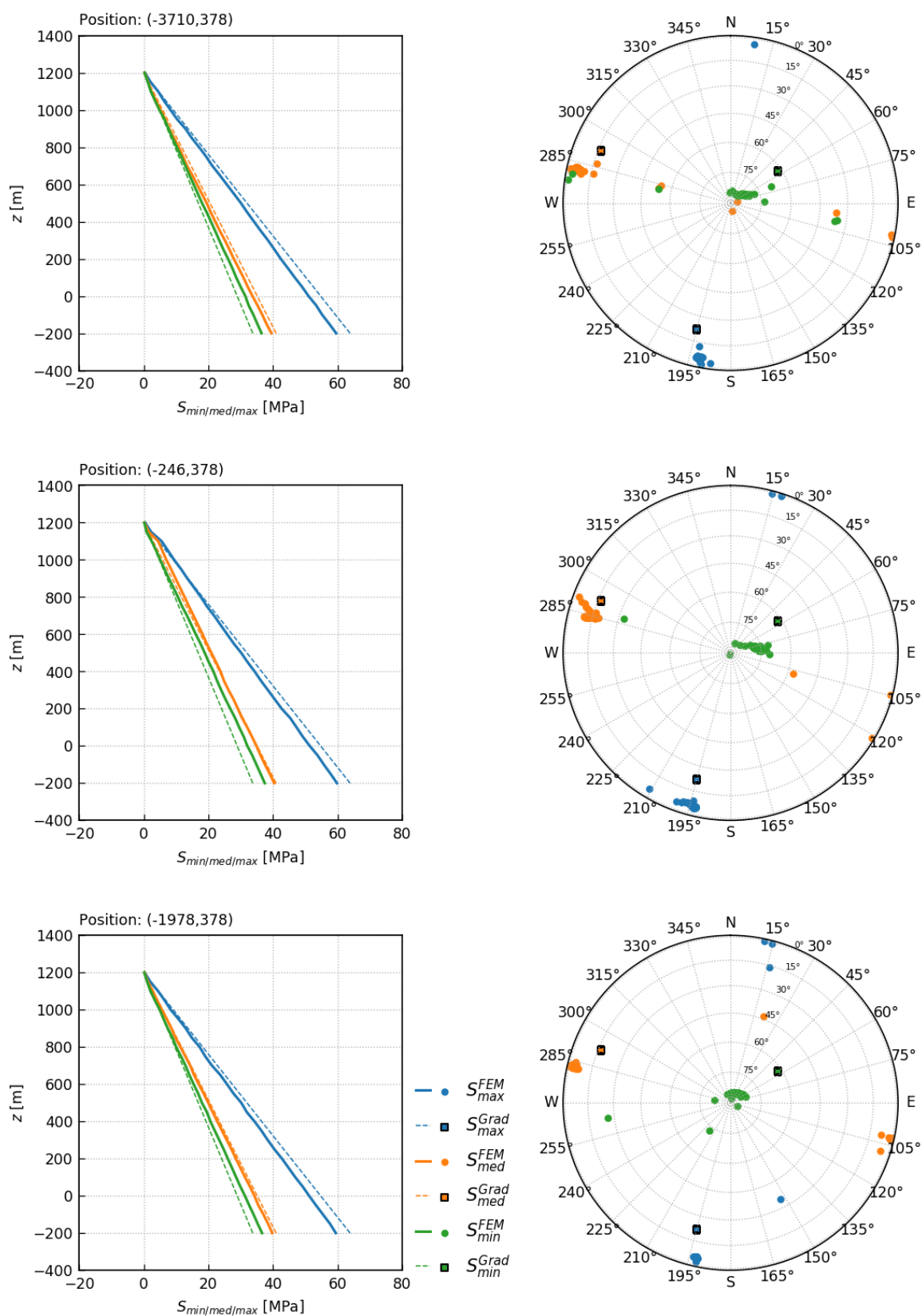


Figure 2-2 Pre-mining stress state along a vertical sample path for three locations in the model space.

2.4 Geotechnical domain assignment

The material properties have been applied according to the lithology. This domaining approach is a necessary assumption in the absence of a separate detailed geotechnical domain model, but from our general understanding of the rockmass conditions at CGO, this assumption is appropriate.

2.4.1 Estimated material properties for modelling

The material properties assigned to the lithology domains of the model were carried over directly from the prior simulations that BE has conducted for CGO. The latest available geological wireframes were used to define all domains, as listed in Figure 2-3. The strength parameter values used for the LRx materials of the model are given in Table 2-2. Table 2-3 presents the strength properties of the weaker, near-surface lithologies, which were simulated as Mohr-Coulomb-like materials. Strength envelope definitions for all materials are provided in Appendix A. The Cowal and Central Shear zones were modelled as volume faults and assigned the residual strength of the contained rock materials.

The following nomenclature is used in Table 2-2:

UCS	= uniaxial compressive strength.
GSI	= geological strength index.
ϵ_0	= 0 = plastic strain at start of peak strength stage (see Figure 2-4).
ϵ_1	= plastic strain at start of transitional strength stage (see Figure 2-4).
ϵ_2	= plastic strain at start of residual strength stage (see Figure 2-4).
E	= Young's modulus for the rockmass.
ν	= Poisson's ratio for the rockmass.
s, m, a	= generalised HB yield parameters for the rockmass.
d	= rockmass dilation parameter.
e	= deviatoric eccentricity constant.

2.5 Hydrogeological conditions

The numerical simulation of the Lake Cowal mine that was conducted as a part of this project was hydro-mechanically coupled. The methodology for applying the groundwater in the model is outlined below:

- The direction-dependent values of hydraulic conductivity (k_w) for the major lithology domains of the mine were provided to BE by EMM Consulting. Since BE's current generation of hydro-coupled simulations do not accept anisotropic fluid conductivity inputs, the east-directional conductivities for the rockmass materials were taken as the model inputs, as listed in Table 2-4.
- Based on the findings reported by Best (2008), the pre-mining groundwater elevation was set to 1,201 mAHD by applying this phreatic surface as an external boundary condition. The boundaries of the model were approximately 3.5 km away from the mine. This reflects the pre-mining groundwater level.
- At every stage in the model as the mine advances and the open pit grows, the excavations both new and old are assumed to be drained by firing the pore water pressure at the void boundary to near-zero. This becomes an internal boundary condition and the permeability in the damaged rock around the open pit and underground workings is adjusted to account for the mining-induced fracturing.
- As the open pit grows and plastic strain (rockmass damage) evolves around the excavations, the hydraulic conductivities change as a function of the equivalent deviatoric plastic strain using the equation below. In simple terms, as rock becomes more damaged, it cracks and dilates and the hydraulic conductivity increases.

$$K_w(PST) = K_{w0} \exp\{a \cdot PST\} \leq K_{wmax}.$$

- A schematic illustrating the effects of rockmass damage on hydraulic conductivity is provided in Figure 2-5. A graphical representation of hydraulic conductivity change relative to plastic strain is provided in Figure 2-6.
- In the model, a *pgH* pore water pressure boundary condition was applied at the floor of Lake Cowal (east of the Lake Protection Bund) in order to simulate a constant water level of 4 m. While the lake is understood to be ephemeral, this assumption was applied for conservatism. The spatial extent of this boundary condition was modified during the simulation sequence in order to reflect the change in the position of the Lake Protection Bund (LPB) as the pit is expanded.

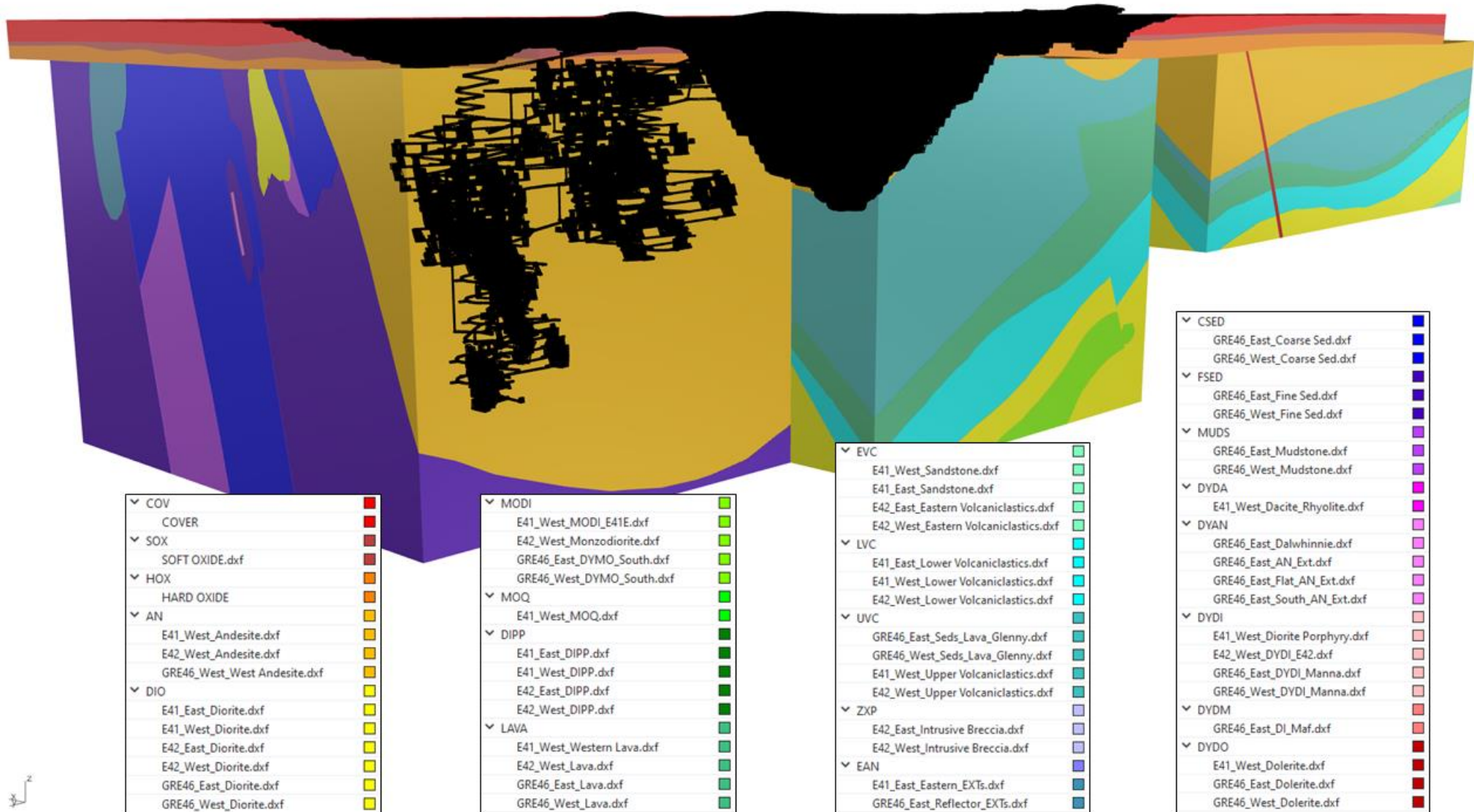


Figure 2-3: Lithology domains included in the model and list of included 3D wireframes.

COWAL GOLD OPERATIONS: SURFACE SUBSIDENCE ASSESSMENT FOR OPEN PIT EXPANSION

Table 2-2: Material properties used the Lake Cowal numerical simulation.

MAT #	Name	Code	Input Parameters					LRx Calculated Rockmass Parameters								
			Density (kg/m ³)	UCS (MPa)	GSI	Anisotropy		Stage	Plastic strain	E (GPa)	ν	s	m	a	d	e
						n	s									
1	Hard Oxide	HOX	2000	15	30	1.0	1.0	Peak	$\epsilon_0 = 0.00$	4.25	0.25	6.34E-5	0.32	0.53	0.05	0.60
								Residual	$\epsilon_2 = 30.84$	4.24	0.25	1.00E-5	0.32	0.53	0.00	0.60
2	Andesite	AN	2770	125	65	1.0	1.0	Peak	$\epsilon_0 = 0.00$	26.27	0.25	2.10E-3	1.97	0.50	0.33	0.60
								Transition	$\epsilon_1 = 0.96$	22.53	0.25	5.82E-4	1.34	0.50	0.22	0.60
								Residual	$\epsilon_2 = 7.32$	19.38	0.25	1.00E-5	0.67	0.50	0.00	0.60
3	Diorite	DIO	2800	132	60	1.0	1.0	Peak	$\epsilon_0 = 0.00$	25.17	0.25	1.27E-3	1.75	0.51	0.29	0.60
								Transition	$\epsilon_1 = 0.52$	23.14	0.25	6.12E-4	1.40	0.51	0.23	0.60
								Residual	$\epsilon_2 = 6.56$	19.80	0.25	1.00E-5	0.70	0.51	0.00	0.60
4	Monzodiorite	MODI	2800	132	75	1.0	1.0	Peak	$\epsilon_0 = 0.00$	30.58	0.25	5.70E-3	2.74	0.50	0.46	0.60
								Transition	$\epsilon_1 = 1.59$	23.14	0.25	6.12E-4	1.40	0.50	0.23	0.60
								Residual	$\epsilon_2 = 7.63$	19.80	0.25	1.00E-5	0.70	0.50	0.00	0.60
5	Quartz Monzonite	MOQ	2710	132	60	1.0	1.0	Peak	$\epsilon_0 = 0.00$	25.02	0.25	1.27E-3	1.73	0.51	0.29	0.60
								Transition	$\epsilon_1 = 0.54$	22.97	0.25	6.04E-4	1.39	0.51	0.23	0.60
								Residual	$\epsilon_2 = 6.66$	19.68	0.25	1.00E-5	0.69	0.51	0.00	0.60
6	Plagioclase Phyric Diorite	DIPP	2770	132	60	1.0	1.0	Peak	$\epsilon_0 = 0.00$	25.17	0.25	1.27E-3	1.75	0.51	0.29	0.60
								Transition	$\epsilon_1 = 0.52$	23.14	0.25	6.12E-4	1.40	0.51	0.23	0.60
								Residual	$\epsilon_3 = 6.56$	19.80	0.25	1.00E-5	0.70	0.51	0.00	0.60
7	Lava	LAVA	2760	159	70	1.0	1.0	Peak	$\epsilon_0 = 0.00$	30.57	0.25	3.46E-3	2.66	0.50	0.44	0.60
								Transition	$\epsilon_1 = 0.96$	25.08	0.25	7.13E-4	1.65	0.50	0.28	0.60
								Residual	$\epsilon_2 = 5.99$	21.11	0.25	1.00E-5	0.78	0.50	0.00	0.60
8	Eastern Volcanics	EVC	2770	127	60	1.0	1.0	Peak	$\epsilon_0 = 0.00$	26.79	0.25	2.32E-3	2.04	0.50	0.34	0.60
								Transition	$\epsilon_1 = 1.01$	22.71	0.25	5.91E-4	1.36	0.50	0.23	0.60
								Residual	$\epsilon_2 = 7.27$	19.50	0.25	1.00E-5	0.68	0.50	0.00	0.60

COWAL GOLD OPERATIONS: SURFACE SUBSIDENCE ASSESSMENT FOR OPEN PIT EXPANSION
Table 2-2 (Cont'd): Material properties used in the Lake Cowal numerical simulation.

MAT #	Name	Code	Input Parameters					LRx Calculated Rockmass Parameters								
			Density (kg/m ³)	UCS (MPa)	GSI	Anisotropy		Stage	Plastic strain	E (GPa)	ν	s	m	a	d	e
						n	s									
9	Lower Volcaniclastics	LVC	2770	127	75	1.0	1.0	Peak	$\epsilon_0 = 0.00$	30.12	0.25	5.70E-3	2.68	0.50	0.45	0.60
								Transition	$\epsilon_1 = 1.67$	22.71	0.25	5.91E-4	1.36	0.50	0.23	0.60
								Residual	$\epsilon_2 = 7.94$	19.50	0.25	1.00E-5	0.68	0.50	0.00	0.60
10	Upper Volcaniclastics	UVC	2700	127	74	1.0	1.0	Peak	$\epsilon_0 = 0.00$	29.74	0.25	5.16E-3	2.60	0.50	0.43	0.60
								Transition	$\epsilon_1 = 1.60$	22.71	0.25	5.91E-4	1.36	0.50	0.23	0.60
								Residual	$\epsilon_2 = 7.86$	19.50	0.25	1.00E-5	0.68	0.50	0.00	0.60
11	Intrusive Breccia	ZXP	2800	132	40	1.0	1.0	Peak	$\epsilon_0 = 0.00$	20.83	0.25	1.72E-4	0.96	0.52	0.16	0.60
								Residual	$\epsilon_2 = 2.77$	19.80	0.25	1.00E-5	0.7	0.52	0.00	0.60
12	Eastern Andesite	EAN	2800	127	66	1.0	1.0	Peak	$\epsilon_0 = 0.00$	26.79	0.25	2.32E-3	2.04	0.50	0.34	0.60
								Transition	$\epsilon_1 = 1.01$	22.71	0.25	5.91E-4	1.36	0.50	0.23	0.60
								Residual	$\epsilon_2 = 7.27$	19.50	0.25	1.00E-5	0.68	0.50	0.00	0.60
13	Coarse Sediments	CSED	2700	145	68	1.0	1.0	Peak	$\epsilon_0 = 0.00$	28.90	0.25	2.83E-3	2.36	0.50	0.39	0.60
								Transition	$\epsilon_1 = 0.96$	24.15	0.25	6.64E-4	1.53	0.50	0.25	0.60
								Residual	$\epsilon_2 = 6.46$	20.49	0.25	1.00E-5	0.74	0.50	0.00	0.60
14	Fine Sediments	FSED	2800	127	66	1.0	1.0	Peak	$\epsilon_0 = 0.00$	26.79	0.25	2.32E-3	2.04	0.50	0.34	0.60
								Transition	$\epsilon_1 = 1.01$	22.71	0.25	5.91E-4	1.36	0.50	0.23	0.60
								Residual	$\epsilon_3 = 7.27$	19.50	0.25	1.00E-5	0.68	0.50	0.00	0.60
15	Mudstone	MUDS	2700	70	67	1.0	1.0	Peak	$\epsilon_0 = 0.00$	19.99	0.25	2.56E-3	1.54	0.50	0.26	0.60
								Transition	$\epsilon_1 = 2.34$	15.70	0.25	2.96E-4	0.80	0.50	0.13	0.60
								Residual	$\epsilon_2 = 12.41$	14.36	0.25	1.00E-5	0.50	0.50	0.00	0.60
16	Dacite Dyke	DYDA	2756	129	70	1.0	1.0	Peak	$\epsilon_0 = 0.00$	28.42	0.25	3.46E-3	2.33	0.50	0.39	0.60
								Transition	$\epsilon_1 = 1.28$	22.89	0.25	6.00E-4	1.38	0.50	0.23	0.60
								Residual	$\epsilon_2 = 7.45$	19.62	0.25	1.00E-5	0.69	0.50	0.00	0.60

COWAL GOLD OPERATIONS: SURFACE SUBSIDENCE ASSESSMENT FOR OPEN PIT EXPANSION

Table 2-2 (Cont'd): Material properties used in the Lake Cowal numerical simulation.

MAT #	Name	Code	Input Parameters					LRx Calculated Rockmass Parameters								
			Density (kg/m ³)	UCS (MPa)	GSI	Anisotropy		Stage	Plastic strain	E (GPa)	ν	s	m	a	d	e
						n	s									
17	Andesite Dyke	DYAN	2770	125	65	1.0	1.0	Peak	$\epsilon_0 = 0.00$	26.27	0.25	2.10E-3	1.97	0.50	0.33	0.60
								Transition	$\epsilon_1 = 0.96$	22.53	0.25	5.82E-4	1.34	0.50	0.22	0.60
								Residual	$\epsilon_2 = 7.32$	19.38	0.25	1.00E-5	0.67	0.50	0.00	0.60
18	Diorite Dyke	DYDI	2900	155	69	1.0	1.0	Peak	$\epsilon_0 = 0.00$	29.94	0.25	3.13E-3	2.54	0.50	0.42	0.60
								Transition	$\epsilon_1 = 0.93$	24.83	0.25	7.00E-4	1.62	0.50	0.27	0.60
								Residual	$\epsilon_2 = 6.09$	20.95	0.25	1.00E-5	0.77	0.50	0.00	0.60
19	Diorite Mafic Dyke	DYDM	2770	125	65	1.0	1.0	Peak	$\epsilon_0 = 0.00$	26.27	0.25	2.10E-3	1.97	0.50	0.33	0.60
								Transition	$\epsilon_1 = 0.96$	22.53	0.25	5.82E-4	1.34	0.50	0.22	0.60
								Residual	$\epsilon_2 = 7.32$	19.38	0.25	1.00E-5	0.67	0.50	0.00	0.60
20	Dolerite Dyke	DYDO	2800	132	75	1.0	1.0	Peak	$\epsilon_0 = 0.00$	30.58	0.25	5.70E-3	2.74	0.50	0.46	0.60
								Transition	$\epsilon_1 = 1.59$	23.14	0.25	6.12E-4	1.40	0.50	0.23	0.60
								Residual	$\epsilon_2 = 7.63$	19.80	0.25	1.00E-5	0.70	0.50	0.00	0.60
21	Faults	FAULTS	2800	50	40	1.0	1.0	Peak	$\epsilon_0 = 0.00$	12.07	0.25	1.72E-4	0.59	0.52	0.10	0.60
								Residual	$\epsilon_2 = 14.92$	11.47	0.25	1.00E-5	0.43	0.52	0.00	0.60
22	Country Rock	HOST	2700	130	65	1.0	1.0	Peak	$\epsilon_0 = 0.00$	26.68	0.25	2.10E-3	2.01	0.50	0.34	0.60
								Transition	$\epsilon_1 = 0.90$	22.97	0.25	6.04E-4	1.39	0.50	0.23	0.60
								Residual	$\epsilon_3 = 7.03$	19.68	0.25	1.00E-5	0.69	0.50	0.00	0.60

* The Country Rock material properties were applied anywhere that was not enclosed within one of the 3D lithology wireframes provided.

Table 2-3 Strength properties used for Mohr-Coulomb-like materials.

Name	Code	ρ [kg/m ³]	n_{aniso}	s_{aniso}	Level	ϵ_{plast} [%]	E [GPa]	ν	cohesion [kPa]	ϕ [°]	dilation
Transported Cover Sequence	TRANS	1850.00	1.00	1.00	PEAK	0.00	0.40	0.23	26.00	27.00	0.25
Soft Oxide	SOX	1950.00	1.00	1.00	PEAK	0.00	0.40	0.23	28.00	24.00	0.25

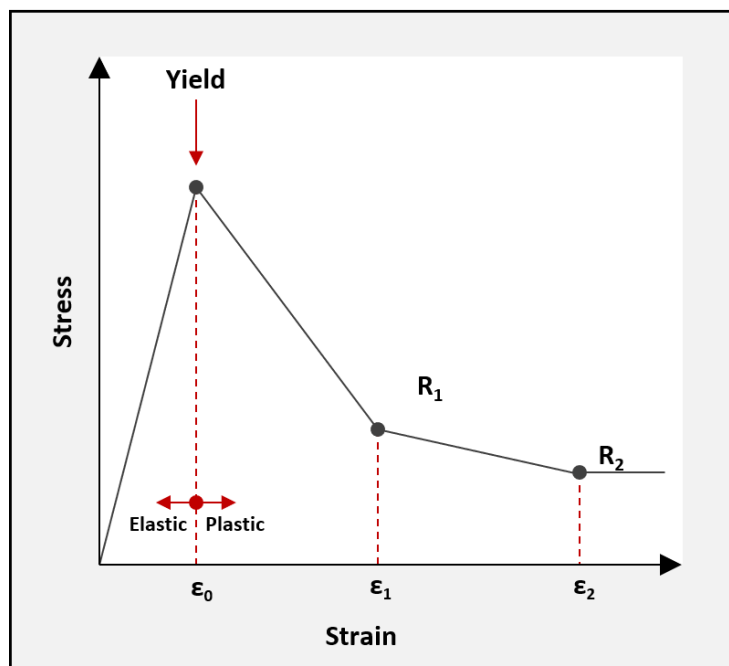


Figure 2-4: Indicative rockmass softening curve demonstrating the plastic strain transition points ϵ_1 and ϵ_2 .

Table 2-4 Hydraulic conductivity values applied to the major geological domains in the model.

Hydrological Unit	k_{w0} [m/s]	k_{max} [m/s]
TRANS (Transported Sequence)	2.51E-7	1.00E-5
SOX (Soft Oxide)	1.30E-7	1.00E-5
HOX (Hard Oxide_)	1.06E-7	1.00E-5
HARDROCK (All unweathered rock)	1.17E-8	1.00E-5
FAULT (High Conductivity)	2.50E-7	1.00E-5
FAULT (Low Conductivity)	5.00E-8	1.00E-5

Permeability	Pervious				Semi-Pervious					Impervious			
Unconsolidated Sand & Gravel	Well Sorted Gravel		Well Sorted Sand or Sand & Gravel		Very Fine Sand, Silt, Loess, Loam								
Unconsolidated Clay & Organic					Peat		Lignite			Unweathered Clay			
Consolidated Rocks			Highly Fractured Rocks		Oil Reservoir Rocks					Fresh Limestone, Dolomite		Fresh Granite	
κ (cm ²)	0.001	0.0001	10 ⁻⁵	10 ⁻⁶	10 ⁻⁷	10 ⁻⁸	10 ⁻⁹	10 ⁻¹⁰	10 ⁻¹¹	10 ⁻¹²	10 ⁻¹³	10 ⁻¹⁴	10 ⁻¹⁵
κ (millidarcy)	10 ⁺⁸	10 ⁺⁷	10 ⁺⁶	10 ⁺⁵	10,000	1,000	100	10	1	0.1	0.01	0.001	0.0001

Source: modified from Bear, 1972

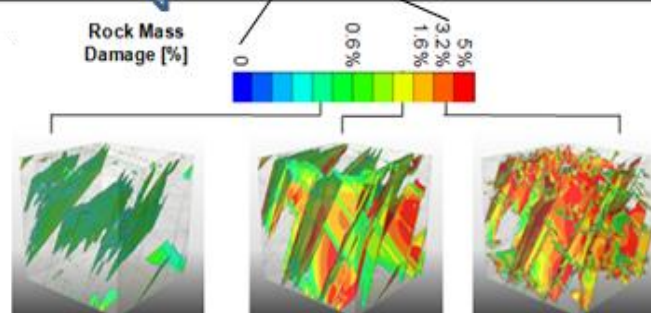


Figure 2-5 Variation in hydraulic conductivity as a function of mining-induced rockmass damage.

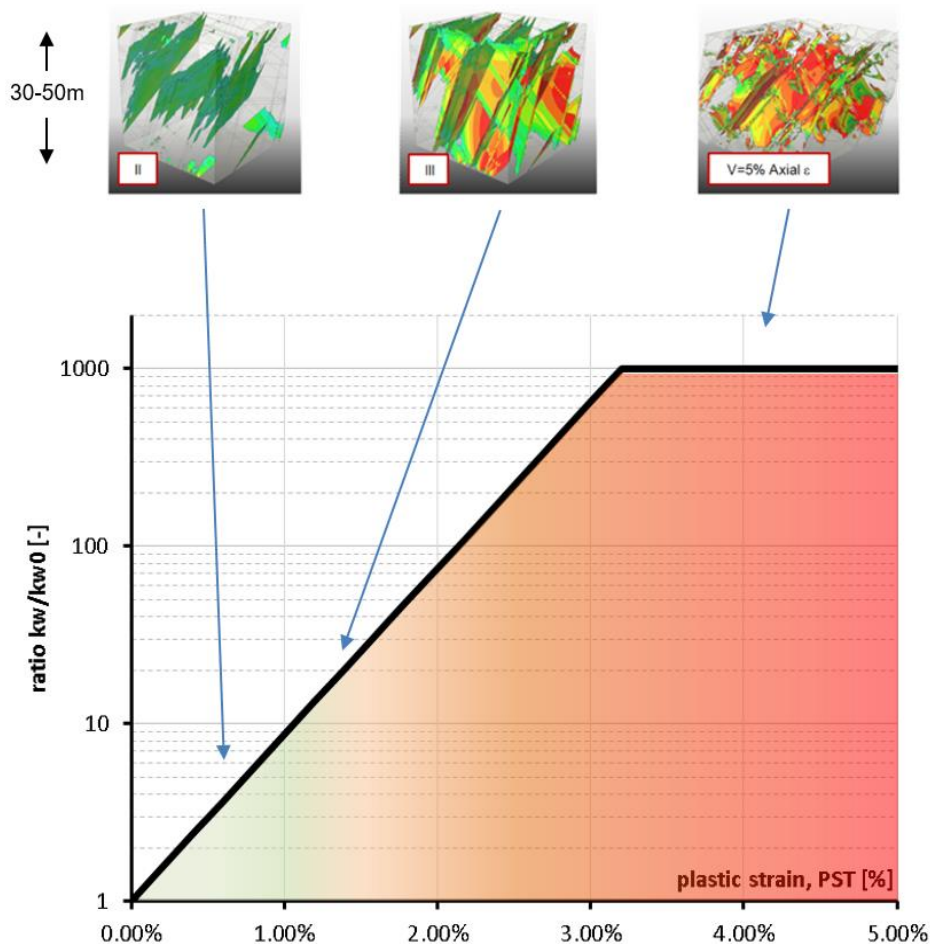


Figure 2-6 Variation of hydraulic conductivity (Y-axis) with plastic strain (X-axis) in the hydro-coupled model (Flatten, et al., 2016).

2.6 Mining methods, geometry & sequence

The FE simulation domain extended approximately 3.5 kilometres from the mining zone in all directions in order to eliminate artificial boundary loading effects (Figure 2-7). The modelling included the complete life-of-mine excavation geometry and lithological/structural models, comprising:

- As built and proposed open pits and waste dumps (including some areas of pit backfilling),
- As built and future underground excavations (footwall decline access design),
- Proposed Tailings Storage Facility (TSF) extensions,
- Proposed Lake Protection Bund reconfiguration,
- Geotechnical domains and major geological structures.

The progressive extraction of the orebodies at CGO via open pit and underground mining methods was simulated in annual mining excavation steps following the scheduled geometric information of the open pit benching, underground development and stoping that was provided. The future LOM schedule for the open pit mine ends in June 2037 (end of financial year). Several viewpoints of the simulated mining, surface dumping and pit backfilling sequence are illustrated in Figure 2-8 to Figure 2-10.

MODEL BOX

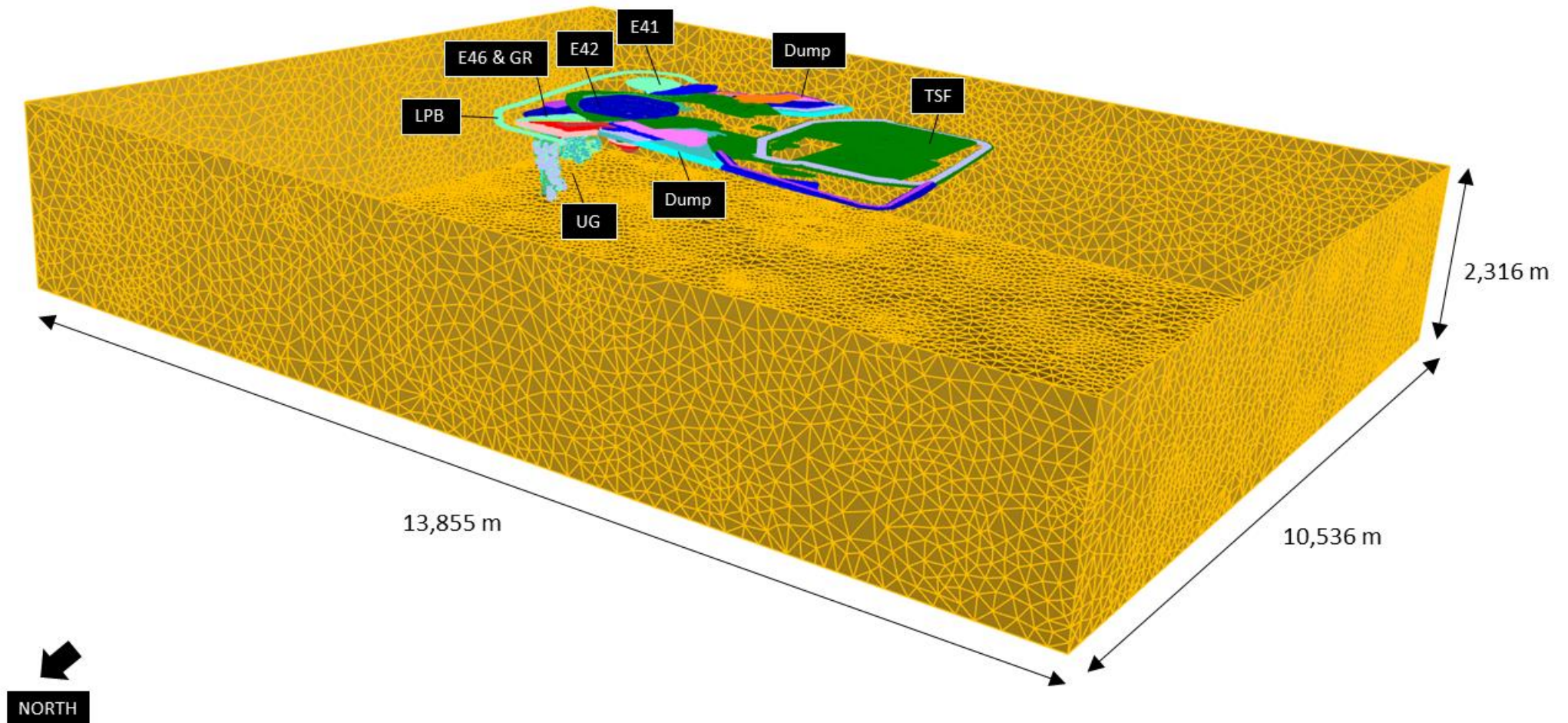


Figure 2-7 Global geometry of the finite-element simulation domain for the CGO model.

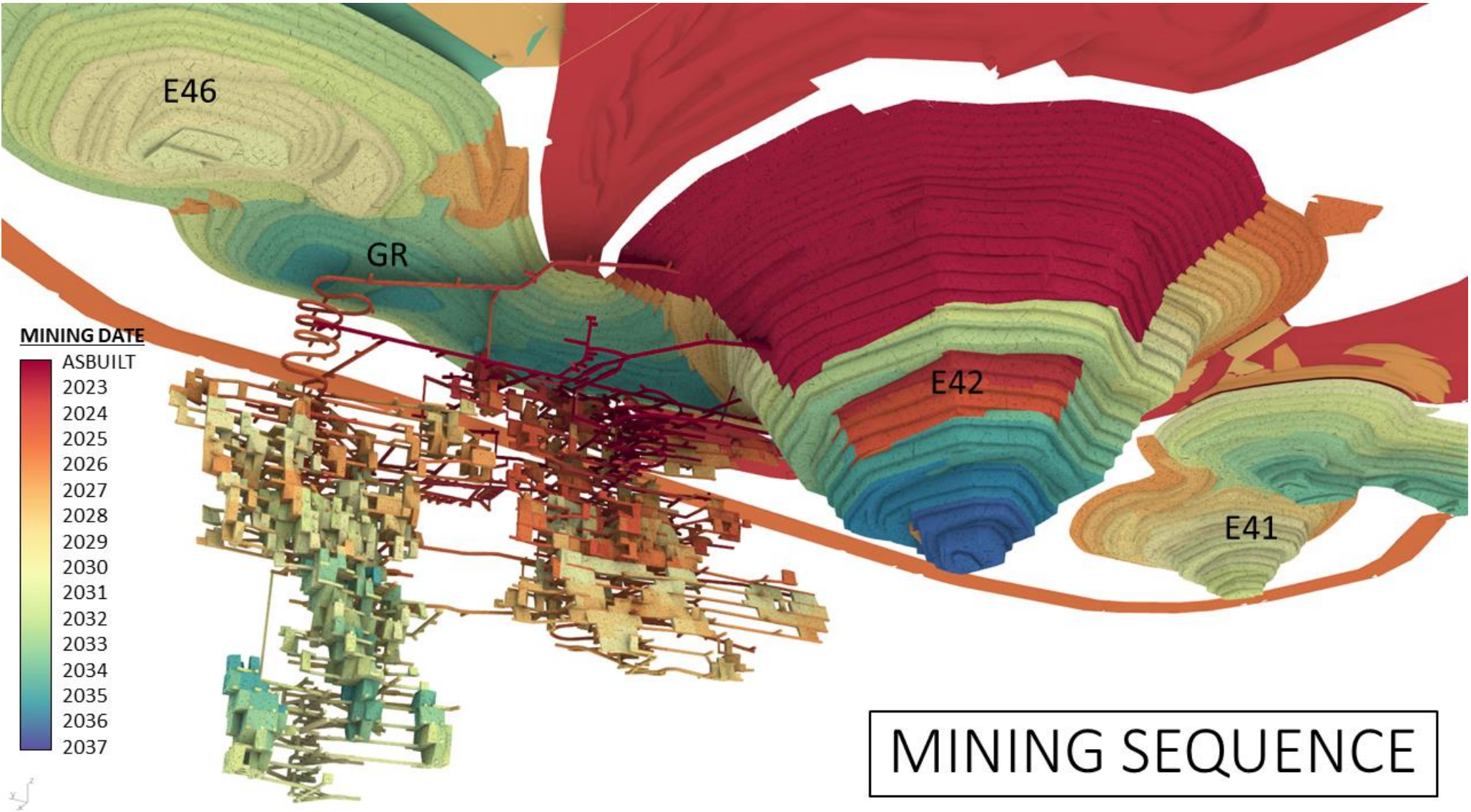


Figure 2-8 Simulated extraction sequence for the mine plan (view southeast from below).

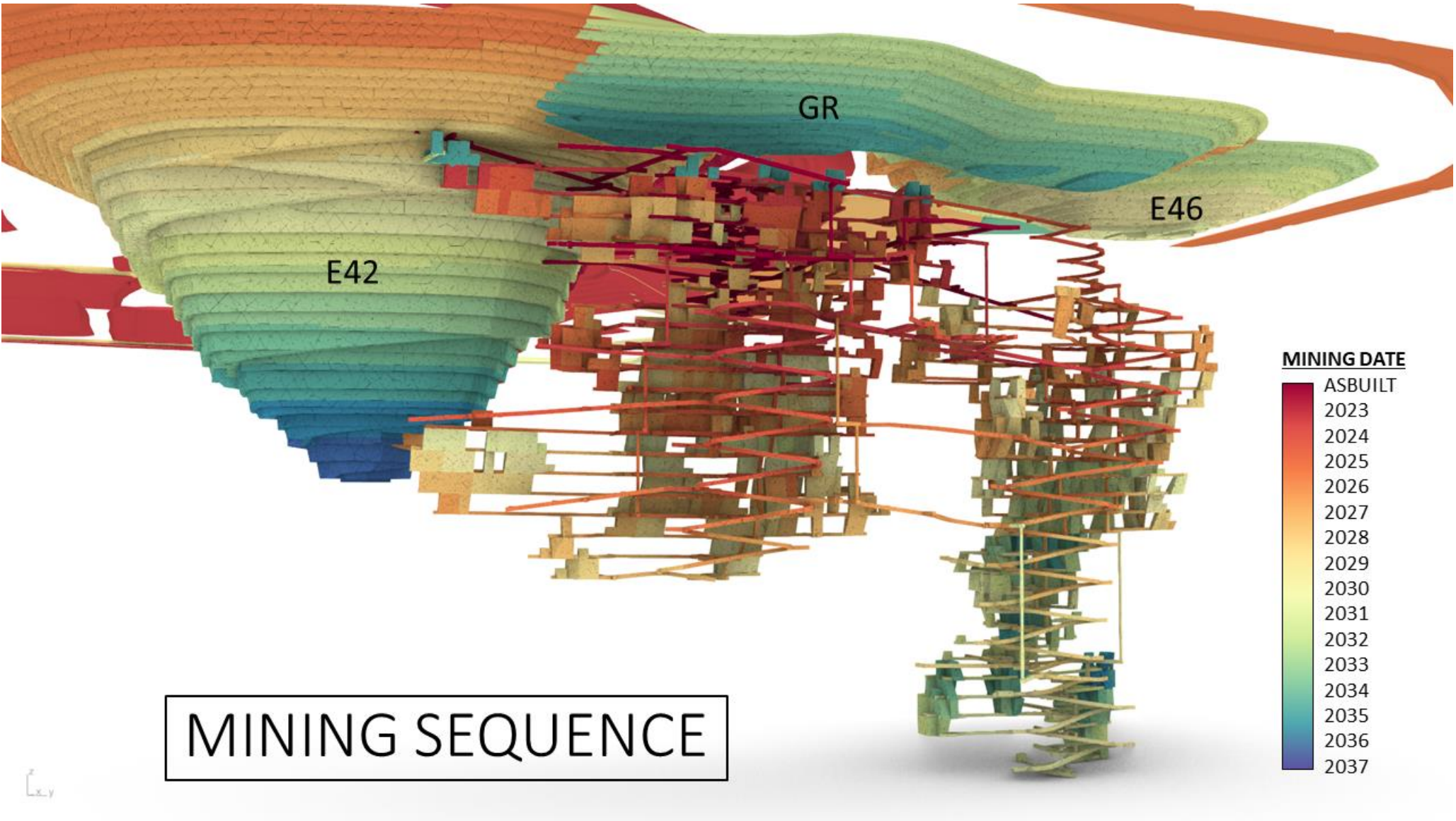


Figure 2-9 Simulated extraction sequence for the mine plan (view west).

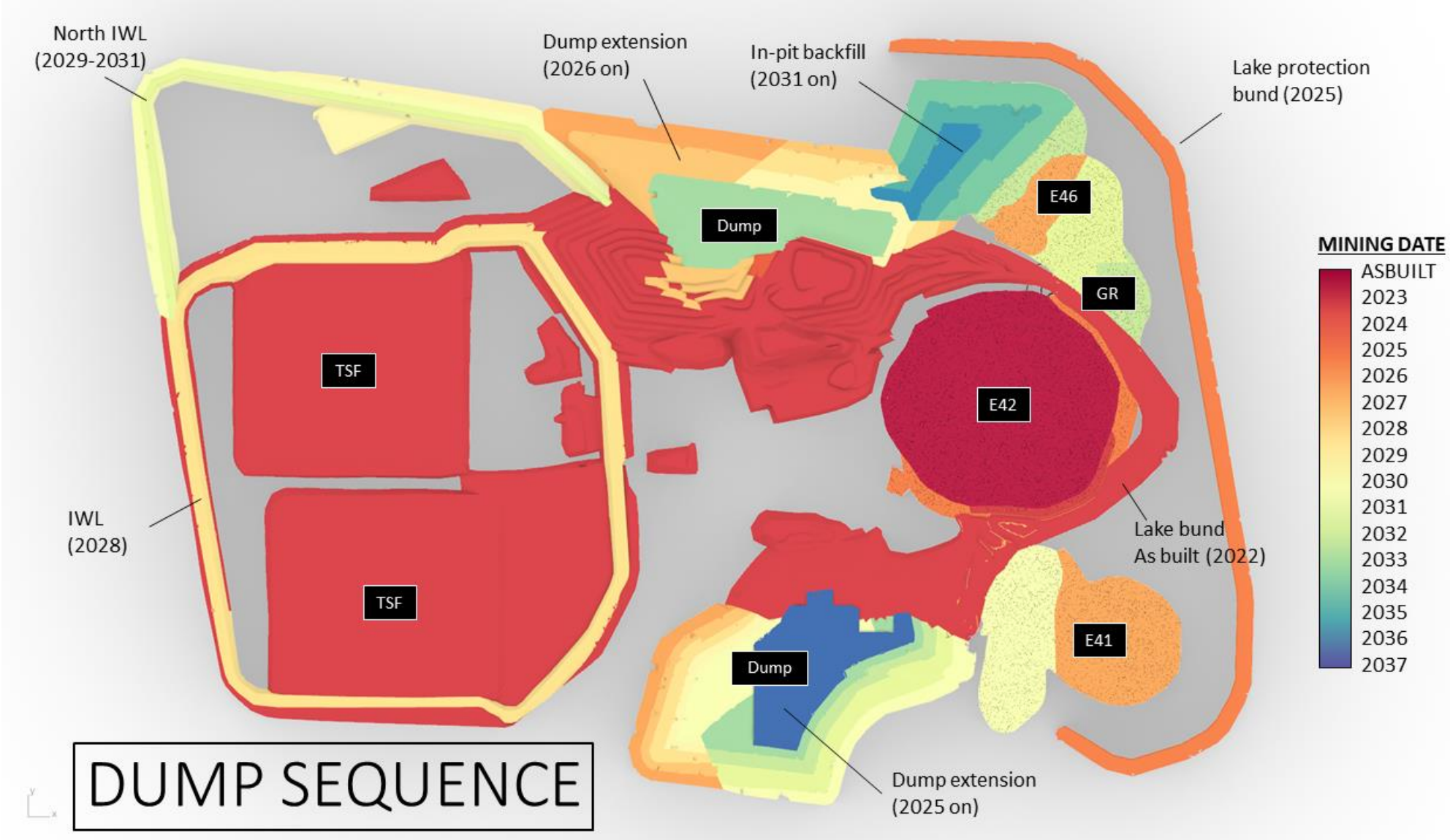


Figure 2-10 Simulated extraction & waste dumping sequence for the mine plan (top view).

2.7 Stope filling methodology & fill properties

In the model, stopes to be mined in frame i starting at time t_i are excavated over the period t_i to $t_i + 0.1$ s by ramping down the Young's modulus from the rockmass value to the void value of 100 kPa. Stopes are filled at the end of the frame (at $t_i + 3.0$ s) by setting the elastic constants of the stope void to fill properties. In practice, the mine could leave stopes open for longer than modelled and may not always achieve tight filling.

For this project, the following elastic constants were applied for fill:

- Young's modulus $E_{\text{fill}} = 200$ MPa.
- Poisson's ratio $\nu_{\text{fill}} = 0.20$.

2.8 Structural model resolution

The resolution of the available structural information allows mine-scale and precinct scale interpretations of the model results. This means that average strains across the rockmass between modelled structures can be simulated and interpreted, but local strains due to structures smaller than those modelled explicitly cannot develop in the model. To obtain forecasts of potential peak strains, which may be needed to assess the potential for locally high deformation levels around individual open pit batters, for example, a model incorporating structures with persistence smaller than the scale of the excavation batters themselves would be needed. The model does allow general interpretations of excavation stability based on, for example, forecast deformation arising from weaker rockmass conditions, adverse geometric configurations and sequences, but explicit forecasts at a small scale are not possible without greater detail on the rockmass characteristics. Selected images of the modelled geological structures are presented in Figure 2-11 and Figure 2-12. Eighty-five faults and two shear zones were incorporated into the model, as listed in Table 2-5.

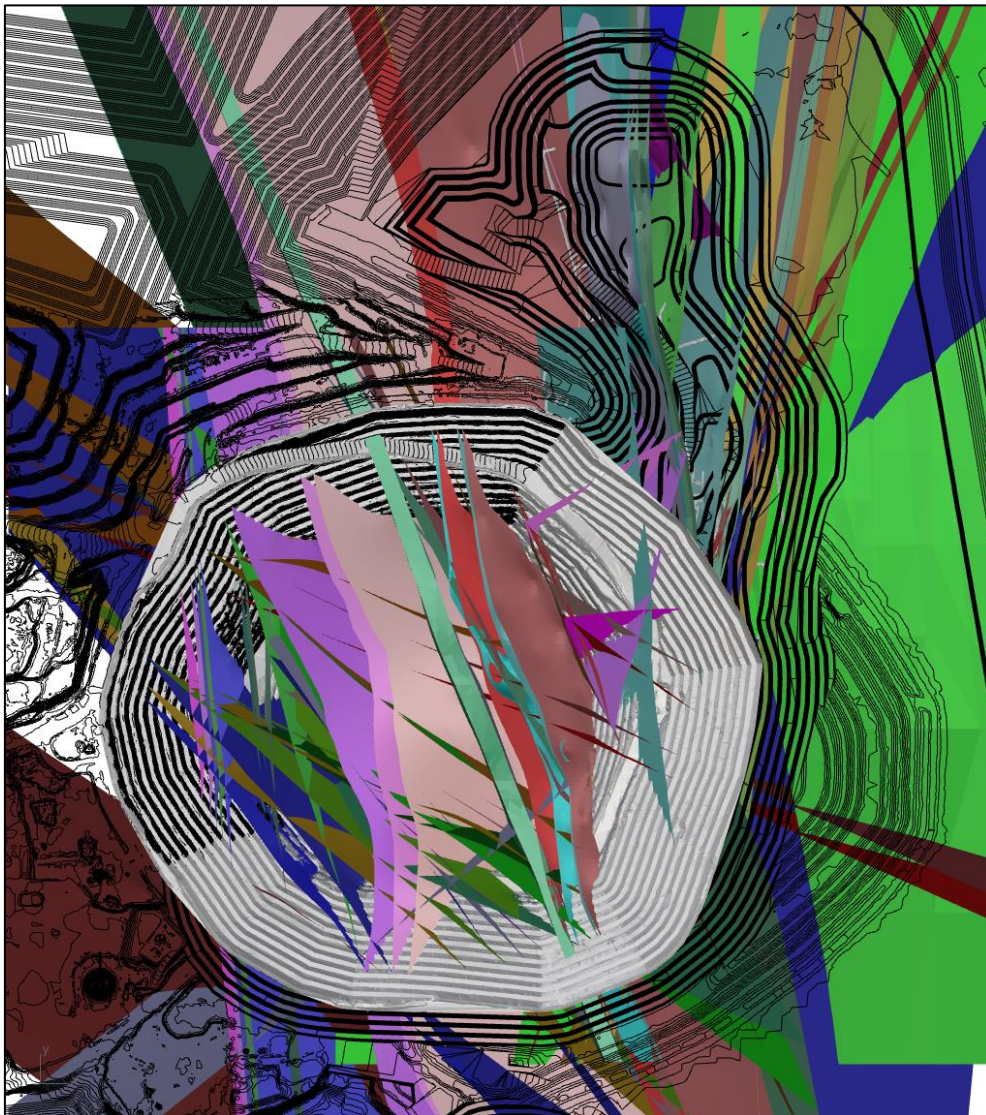


Figure 2-11 Modelled fault and shear zone structures in the vicinity of the open pits.

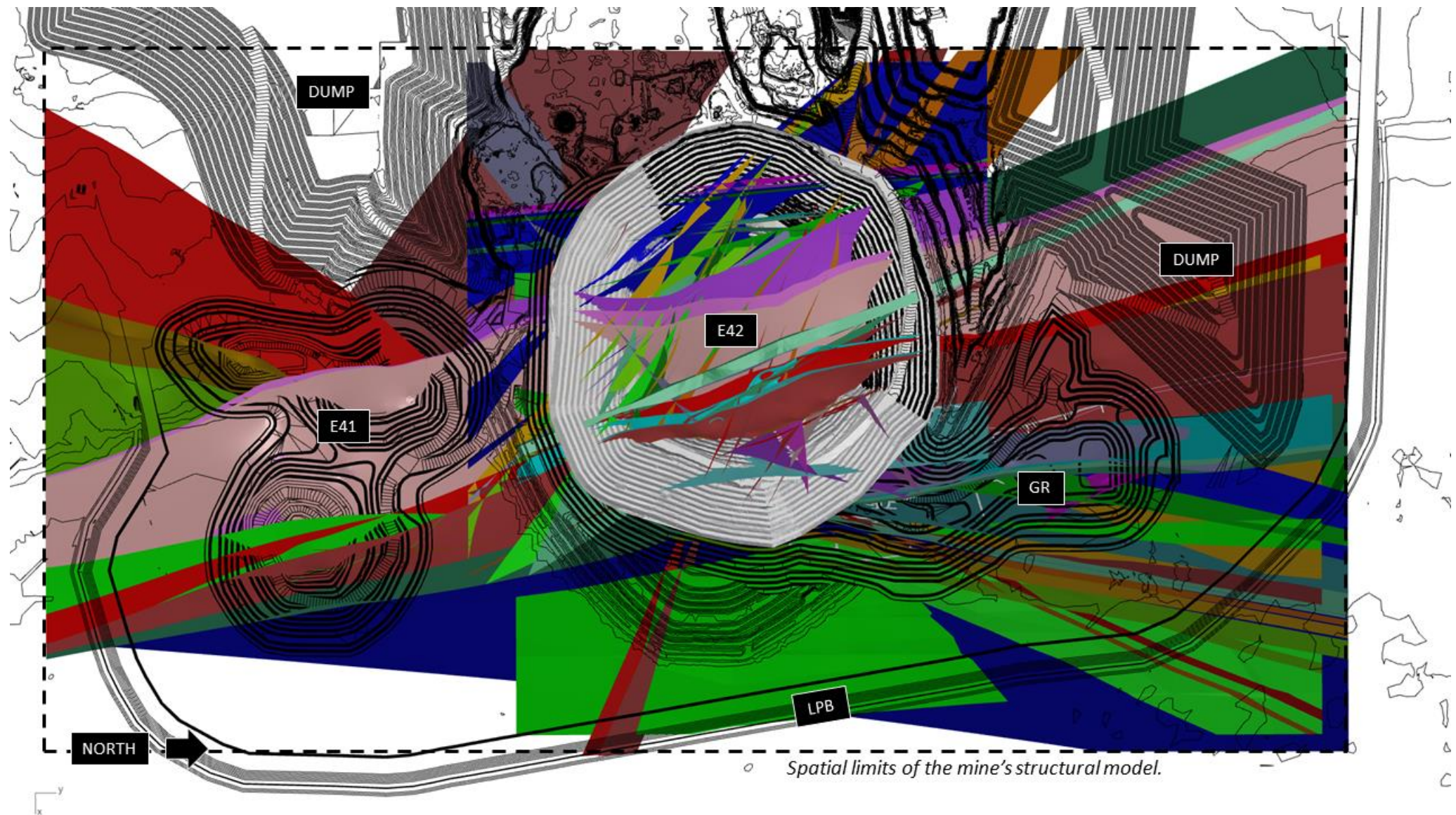


Figure 2-12 Explicitly modelled geological faults and shear zones included in the model (top view).

Table 2-5 List of all explicitly modelled geological structures in the Lake Cowal model.

CATEGORY 1 FAULTS

DYDI_2_COWAL_SHEAR
 DYDI_6_COWAL_SHEAR
 DYF_CENTRAL
 E41_GLENFIDDICH_W
 E41_KILLARA
 E41_PULLABOOKA
 GLENNFIDDICH_MAIN
 GRE46_GALWAY_IIEL1
 GRE46_GALWAY_IIEL2
 GRE46_GALWAY_IIEL3
 GRE46_GALWAY_IIEL4
 GRE46_GALWAY_SPLAY3
 GRE46_GALWAY_SPLAY7
 GRE46_GLENNFIDDICH_W
 GRE46_JURA_M1
 GRE46_LAVA_DYKE
 GRE46_MANNA_LOWER
 GRE46_MANNA_UPPER
 M1_WIDE_STRUCTURE
 ME41_TUPOLEV_HW
 NERANG_THRUST2
 NERANG_THRUST_FW
 NERANG_THRUST_HW
 SPEYBURN
 SPEYBURN3
 WESTERN_FW
 WESTERN_HW

CATEGORY 2 FAULTS

E41_WEST_POD_PHYLLIC_SHEAR
 E42_BALLANTINE
 E42_BLOW_CLEAR1
 E42_BLOW_CLEAR2
 E42_BLOW_CLEAR3
 E42_BLOW_CLEAR4
 E42_BODELS5
 E42_BOWMORE
 E42_BULLDOG
 E42_BULLDOG2
 E42_BURCHER
 E42_BURCHER2
 E42_BURCHER3
 E42_BURCHER4
 E42_FAULT_WYRRA3
 E42_GIRRAL_A
 E42_GIRRAL_A3
 E42_GIRRAL_B
 E42_GIRRAL_B2
 E42_GIRRAL_B3
 E42_GROUSE
 E42_SEAGRAMS
 E42_TALISKER
 E42_TEACHERS
 E42_TEACHERS2
 E42_TEMORA
 E42_TEMORA2
 E42_WAMBOYNE
 E42_WEST_BODELS3

CATEGORY 2 FAULTS

E42_WEST_BODELS4
 E42_WEST_BODELS6
 E42_WEST_BODELS7
 E42_WEST_CORRINGAL
 E42_WEST_CROSSHOUNDS
 E42_WEST_CROSSHOUNDS2
 E42_WEST_CROSSHOUNDS3
 E42_WEST_GIRRAL_A2
 E42_WEST_GIRRAL_A4
 E42_WEST_GIRRAL_A5
 E42_WEST_GIRRAL_A6
 E42_WEST_WAMBOYNE
 E42_WHISKEY
 E42_WHISKEY2
 E42_WHISKEY3
 E42_WHISKEY4
 E42_WYRRA
 E42_WYRRA2
 GRE46_GLENNF1
 GRE46_GLENNF2

UG MAJOR FAULTS

E42_NERANG_THRUST_2
 GRE46_COWAL_FW
 GRE46_CRAGGANMORE

UG MINOR FAULTS

GALWAY_SPLAY_1
 GALWAY_SPLAY_2
 GALWAY_SPLAY_4
 GALWAY_SPLAY_5
 GALWAY_SPLAY_6
 GALWAY_SPLAY_8

VOLUME FAULTS

COWAL SHEAR
 CENTRAL SHEAR

2.9 Rockmass damage and surface subsidence classification methods

Figure 2-13 shows BE's rockmass damage scale. Rockmass damage is plotted on a logarithmic scale called logP, where $\log P = \log_{10}(1000\epsilon_p + 1)$ and ϵ_p is the deviatoric equivalent plastic strain. This damage allows a wide range of plastic strain magnitudes to be plotted with a convenient linear colour scale. The damage scale in terms of stress and strain is shown in Figure 2-14. In open pit and stoping underground mines such as Lake Cowal:

1. Minor rockmass damage indicates a low likelihood of instability.
2. Moderate rockmass damage indicates an increased likelihood of instability,
3. Significant rockmass damage is characterised by relatively high frequency of instability, leading to reduced recovery productivity, higher dilution, increased rehabilitation and associated mining costs.
4. Very significant rockmass damage is characterised by severe stability problems which often necessitate major alteration of the mine plan and potentially alternative mining methods.

It is essential to note that these damage categories are indicative only. Persistent structures present at length scales below the inherent resolution of the model are likely to exist and these would strongly influence the stability of the mining excavations.

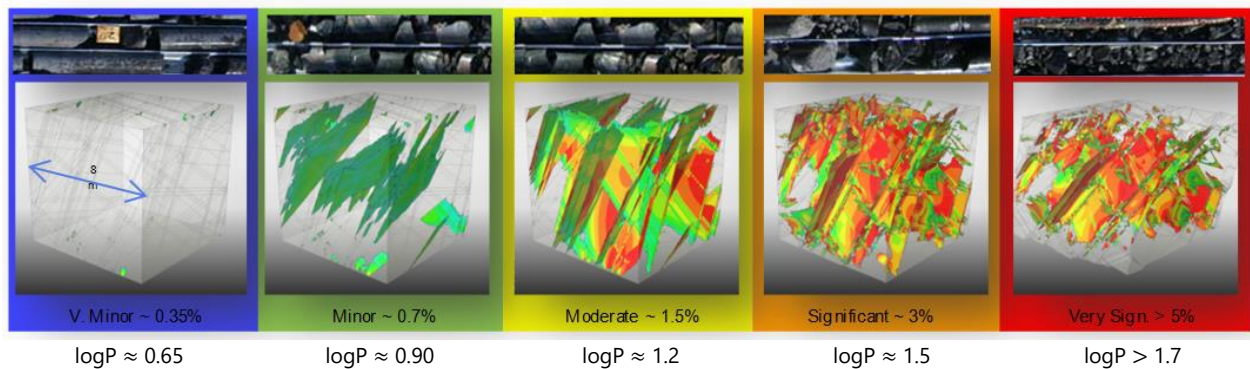


Figure 2-13: Rockmass damage scale.

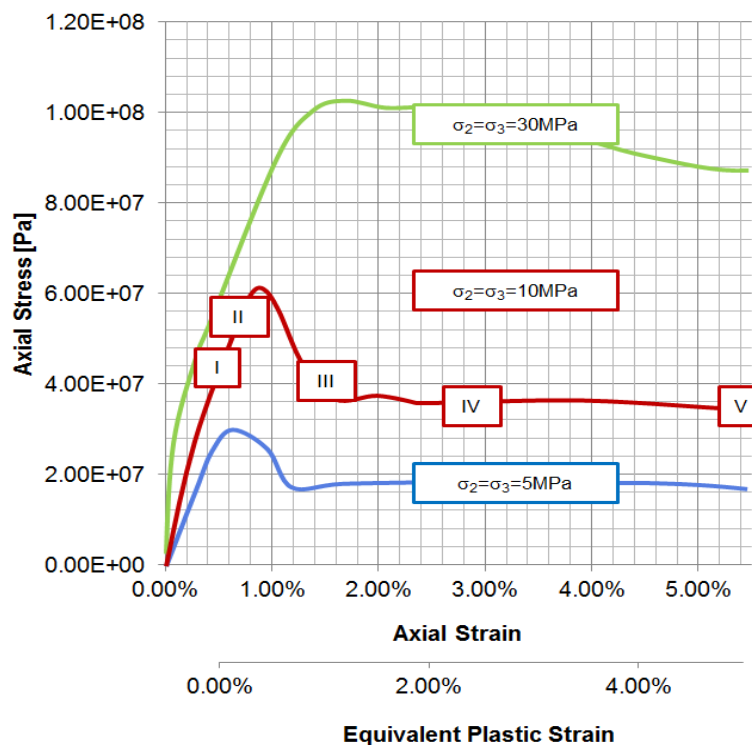
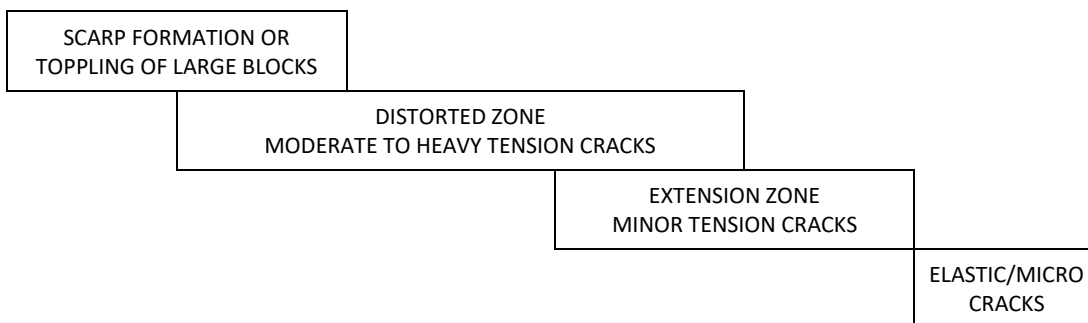


Figure 2-14 Stress vs. Strain chart showing corresponding rockmass damage levels.

Beck Engineering have conducted numerical simulations for surface and underground mass-mining operations across a wide variety of commodities and geological conditions worldwide. Our simulations are routinely calibrated to the real observations of subsidence induced damage. In our experience, the subsidence impacts induced by mining can be conveniently classified according to displacement, strain and angular distortion criteria, as outlined in Table 2-6. Subsidence impacts transition through various stages of severity during mining. Initially, during the early onset of subsidence, there is elastic deformation or micro cracking of the rockmass. Due to the small scale of the response, this is not visible to the naked eye, but it may be detected by sensitive monitoring equipment (e.g. GPS). With increasing displacement and plastic strain, the rockmass experiences non-reversible damage and minor tension fractures or hairline cracks may become visible at the surface within the extension zone. Tension cracking becomes progressively more severe as displacements increase and eventually wide fractures measuring many tens of centimetres across may form at the surface. In certain circumstances, such as above caving underground mines or adjacent unstable open pit slopes, it may be possible for high vertical scarps to form, with toppling or slumping failure of large blocks at the edge of the worst subsidence-affected region (Figure 2-15).

Table 2-6 Surface subsidence impact classification criteria.

DESCRIPTION				
Very significant movement with moderate to heavy fracturing with scarp formation and toppling failure of large blocks into the subsidence crater	Very significant movement with moderate fracturing with localised heavy fracturing or scarp formation	Moderate movement with minor fracturing	Minor movement with sparse hairline cracks	Minor movement with no visible cracks



Degree of Influence	Very Severe		Severe	Moderate	Slight	Negligible
Subsidence or Horizontal Displacement	> 5-10 m	> 2 m	> 1 m	> 0.5 m	> 0.2 m	< 0.2 m
Horizontal Strain	$\sim 10^{-1}$	$\sim 10^{-2}$	$> 3 \times 10^{-3}$	$> 1.5 \times 10^{-3}$	$> 0.5 \times 10^{-3}$	$< 0.5 \times 10^{-3}$
Angular Distortion	$\sim 10^{-1}$	$\sim 10^{-2}$	$> 7 \times 10^{-3}$	$> 3 \times 10^{-3}$	$> 1 \times 10^{-3}$	$< 1 \times 10^{-3}$
Plastic Strain	> 5 %	1 - 5 %	0.7 - 1 %	0.3 - 0.7 %	0.1 - 0.3 %	< 0.1 %

In addition to this empirical subsidence classification scheme described in Table 2-6, a methodology that BE also apply for assessing the impact of subsidence on surface infrastructure is based on the work of Boscardin & Cording (1989), also known as the Harrison Plot. This method can be used to classify and assess the severity of the impact to critical assets located close to mining excavations. The plot is only applicable for surface infrastructure, not underground facilities. It is primarily formulated for rigid surface infrastructure, such as buildings, but can be used for other structures, like earth dams, as a high-level, first-pass subsidence impact assessment. If a particular asset is forecast as being subject to a Moderate subsidence impact or higher, BE suggest that an assessment of the horizontal strain & angular distortion tolerance limits should be conducted by a relevant structural expert.



Figure 2-15 Example of surface subsidence following a large-scale slope failure at another mine.

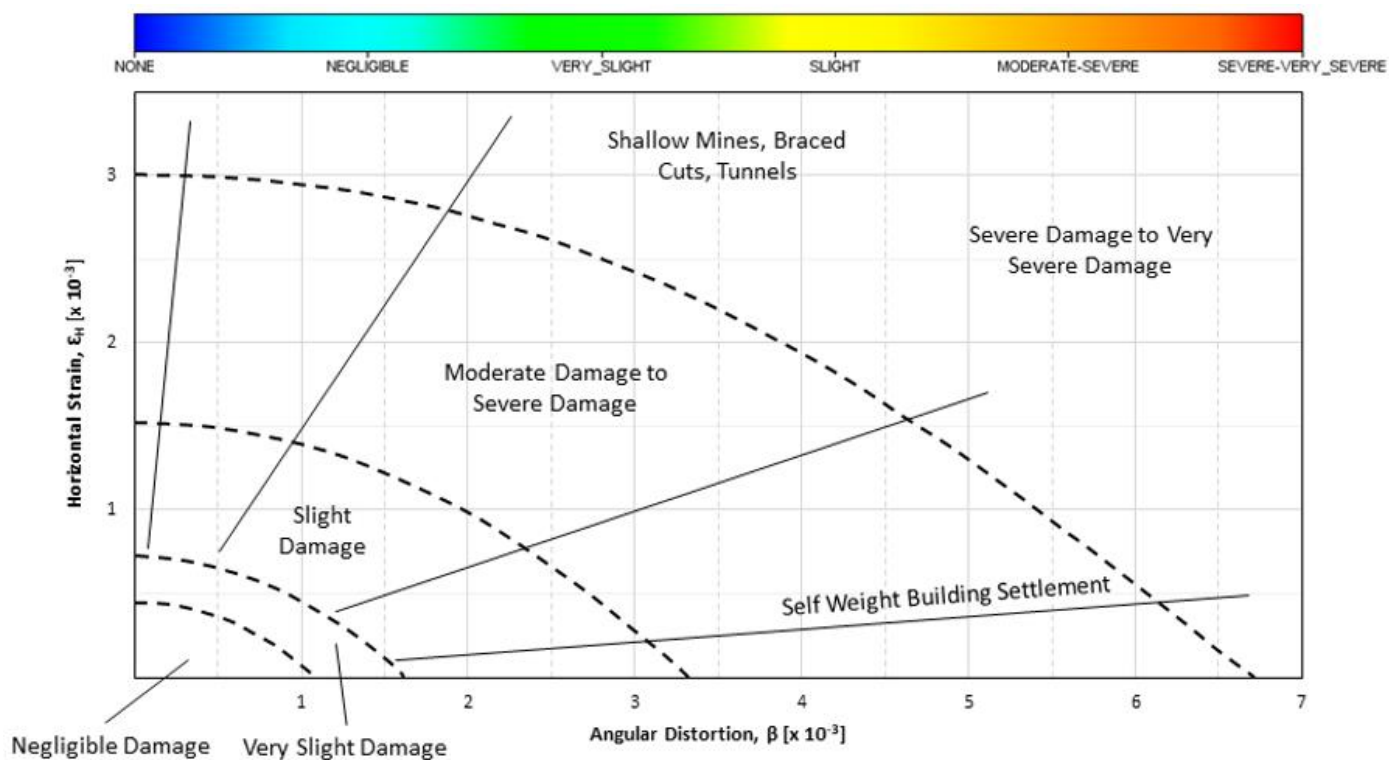


Figure 2-16 Surface infrastructure subsidence impact severity assessment scheme based on Boscardin & Cording (1989).

3 FORECASTS, INTERPRETATION & DISCUSSION

This section summarises the model results and forecasts of the surface subsidence impacts due to the proposed future mine plan at CGO, including the open pit extension and underground stoping. The results are best reviewed and interpreted using 3D visualisation software such as Voxler, so here we present a comparatively brief summary of the results and our interpretation of the expected behaviour, possible impacts on surface infrastructure and possible risk mitigation measures, where appropriate.

3.1 Open pit design

The deepest point of the E42 open pit at the current time is approximately the 755 mAHD, or 450 m below surface (mbs). The proposed future mine plan will initially involve continuation of pit floor benching, during which time a slope cutback will be initiated in the southeast quadrant of the pit, starting from the surface. The mining will then be progressively expanded to include initiation of cutbacks from surface in the northeast and southwest quadrants of the pit, with approximately three quarters of the circumference of the pit subject to cutback mining operations by 2025. Prior to initiation of those cutbacks there would be a reconfiguration of the Lake Protection Bund (LPB) to prevent interaction of the open pit mining and the water body of the lake. Meanwhile, the deeper benches of the original pit would remain underway and those would be completed to the 670 level (535 mbs) during 2026.

During 2026, the excavation of the E46 and E41 satellite pits to the north and south of the E42 main pit would also commence and the three open pit zones would be mined without physically intersecting one another until 2031. In 2031 the initial surface stripping would occur for the GR pit. Backfilling of the E46 pit gets underway earlier, in 2030, and this would occur concurrently with the planned GR pit mining activities during 2031 and 2032. The mining of the satellite pits would continue until completion in 2035, and the remaining cutback mining of the E42 main pit would be finalised in 2037. The final floor of the E42 pit is planned to be excavated to the 627 level, which is an ultimate depth of 580 mbs.

3.2 E42, E46 & GR Open Pits

Selected images of the simulation forecasts for the rockmass response of the E42, E46 and GR open pits and nearby surrounding surface topography at the conclusion of the life-of-mine plan in 2037 are presented in the following figures, as listed below.

- Figure 3-1 to Figure 3-3: Forecast vertical, horizontal and total displacements, respectively, of the E42, E46 and GR open pits and nearby natural surface topography at the end of the current mine plan,
- Figure 3-4 & Figure 3-5: Rockmass damage forecasts (various views) at the end of the mine plan,
- Figure 3-7 & Figure 3-8: Long section (north-south) and cross section (east-west) of total displacement magnitude and vectors at the end of the mine plan (i.e. Y2037 M06),
- Figure 3-9 & Figure 3-10: Long section (north-south) and cross section (east-west) of forecast major principal stress at the end of the mine plan.

The model indicates the following:

- Vertical displacements around the perimeter of the E42, E46 and GR open pits are forecast to be less than 0.1 m at the end of the mine plan (Y2037 M06). The direction of the forecast displacements of the pit walls is primarily uplift, indicating that subsidence of the surface region is effectively zero as a direct result of the open pit mining (Figure 3-1).
- Some downward vertical displacements of the natural ground surface to the immediate northwest of the E42 pit are forecast by the model beneath the deposited waste dump materials. These displacements of up to 0.45 m are caused by the static overburden load of the waste dump mass atop the weak cover sequence materials of the natural terrain and are not a result of open pit mining-induced subsidence (Figure 3-1).
- Mining-induced horizontal displacements of the natural surface around the perimeter of the E42 pit are forecast to reach a maximum of 0.15 m in only three locations where fault-related movement is forecast on the adjacent pit slopes in the weathered oxide zone (Figure 3-2). The horizontal displacements at the surface around the E42 pit are in the *Negligible* category at the end of the LOM (Y2037 M06).
- Elevated total displacements approaching 0.45 m are forecast in three locations of the E42 pit throughout the near-surface oxide, due to fault-related movement (Figure 3-3). In the fresh rock domains, the highest pit slope

displacements are forecast to occur in the Lava and Volcaniclastics of the south and west walls. They are mostly elastic displacements. Total displacements at the surface are in the Negligible category.

- Rock mass damage in the E42 pit is concentrated along the major faults in the oxide domains and along the Central Shear zone, including areas of the fresh rock slope both above and below the planned haul ramp in the north wall (Figure 3-4 & Figure 3-5). Otherwise, elevated damage occurs at scattered locations at the confluence between the slope and faults and mainly affects the batter crests at a small scale. The Lava and Volcaniclastic units in the south and west walls are forecast to experience a Very Minor to Negligible severity of rock mass damage (Figure 3-5).
- Rockmass damage is forecast to accumulate to a higher severity in the E46 pit slopes than in any of the other open pits at CGO (Figure 3-4). This is a consequence of the loading effect that the in-pit backfilling has on the slopes. Prior to backfilling this pit in 2031/32, the slope damage in the oxides is comparable to the other pits. Only when introducing the backfill does the slope damage increase to a Significant level (i.e. plastic strain of > 3 %) or higher. The damage primarily affects the berm crests in the oxide zone. Since the pit slopes are fully confined by the backfill, there would be no adverse effect to this increase in damage.
- Much of the E46 pit is planned to be backfilled during 2031/32, with a final fill slope angle design of 36°. This angle may be too steep to achieve in practice, depending on the material used for the fill (Figure 3-6). However, fill material would naturally rill to a stable angle when deposited, or when re-excavated to a slope, as is planned to occur in some places.
- In order to ensure that the E46 in-pit fill slopes remain stable over the long-term without slumping, and to avoid subsidence within the backfill zone more generally, it is recommended that the backfilling campaign be completed using a consistent source of suitable fill material with minimal internal void space. Deposition or layering of fill materials of significant contrast in internal void space should be avoided, due to the potential for particles to migrate vertically within the fill over time, due to gravity and/or water action, causing larger voids to form and potentially subsidence at the surface. Bunding at the toe of the final fill slope using a fresh rock material would also be advisable, in order to mitigate and contain any localised slumping of the fill slope over time.
- Within the fresh-rock domain of the open pits, the movements of the slopes reflect a minor amount of uplift (Figure 3-7 & Figure 3-8). This is a consequence of removal of the overburden load from within the pit and a primarily elastic response of the surrounding rock mass. The E42 southern pit slope is forecast to experience a more substantial uplift than the north slope. Total displacements of the final E42 pit slope face rarely exceed 0.25 m at the end of the LOM.
- Concentrations of the major principal stress in the open pit slopes do vary with depth and around the open pit perimeter. The northern wall of the E42 open pit experiences a transition of induced stress from < 5 MPa close to surface and up to 30 MPa at depth, whereas the southern wall of the pit is largely destressed to < 5 MPa across most of the elevation range of the mine (Figure 3-9). The east and west slopes of the pit experience a similar stress gradient with depth, close to the slope face. However, the mining-induced stress field is disturbed around numerous major structures which show sharp stress gradients (Figure 3-10). These conditions are not forecast to adversely affect the mining or subsidence on surface.

In summary, the forecast mining-induced surface displacements and damage around the perimeter of the E42, E46 and GR open pits can be classified as Negligible and of a magnitude which would not present any visible evidence of disturbance to the natural topography or man-made structures outside the pits. Displacements beyond the crest of the open pit are elastic in nature and near-zero. No plastic (i.e. permanent) rock mass damage is forecast beyond the crest of the pit at the natural surface level and therefore no visible surface cracking or other forms of visible damage are expected to occur.

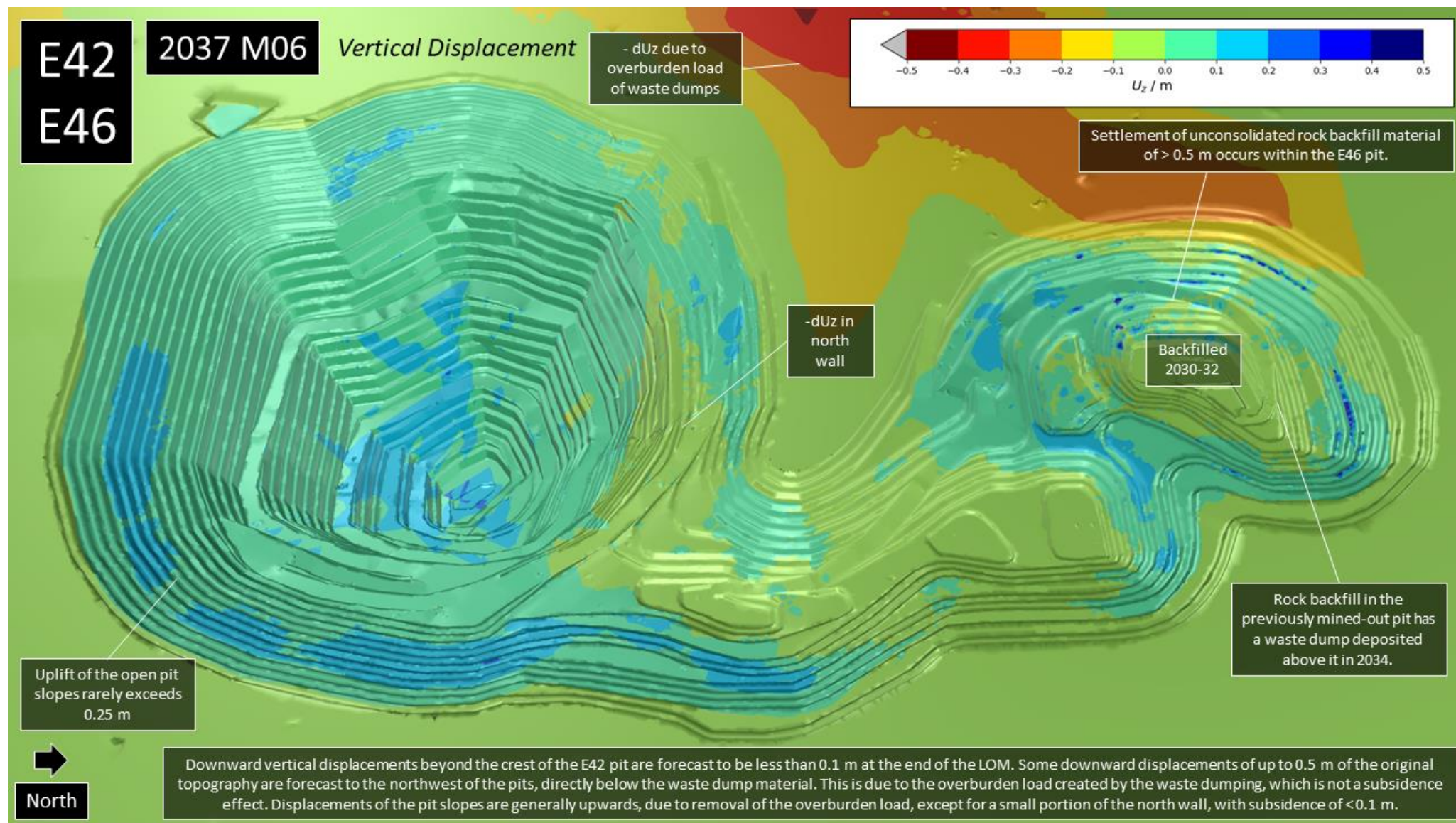


Figure 3-1 Forecast vertical displacements of the E42, E46 & GR open pit slopes and surrounding natural surface topography (2037 M06).

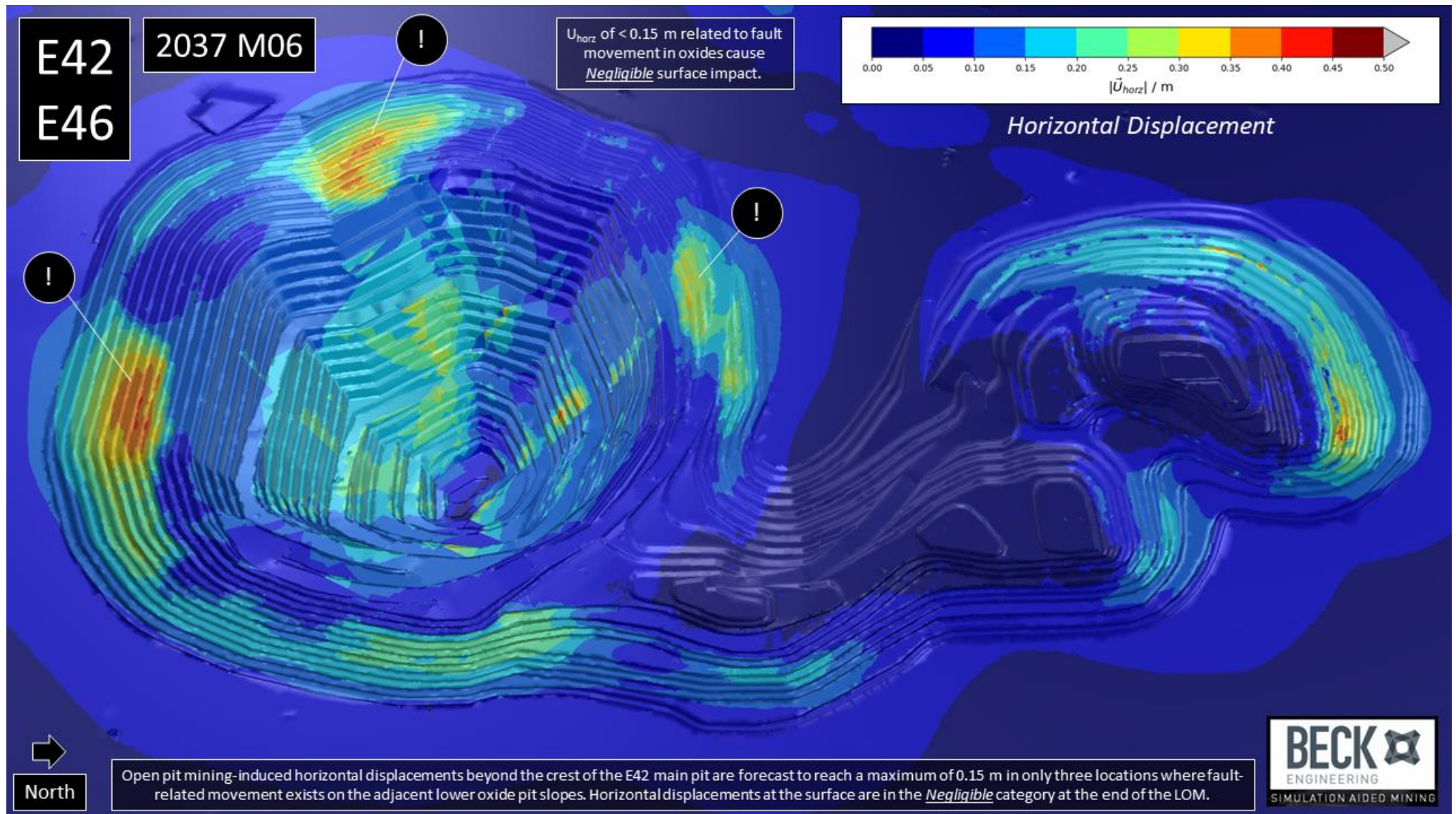


Figure 3-2 Forecast horizontal displacements of the E42, E46 & GR open pit slopes and surrounding natural surface topography (2037 M06).

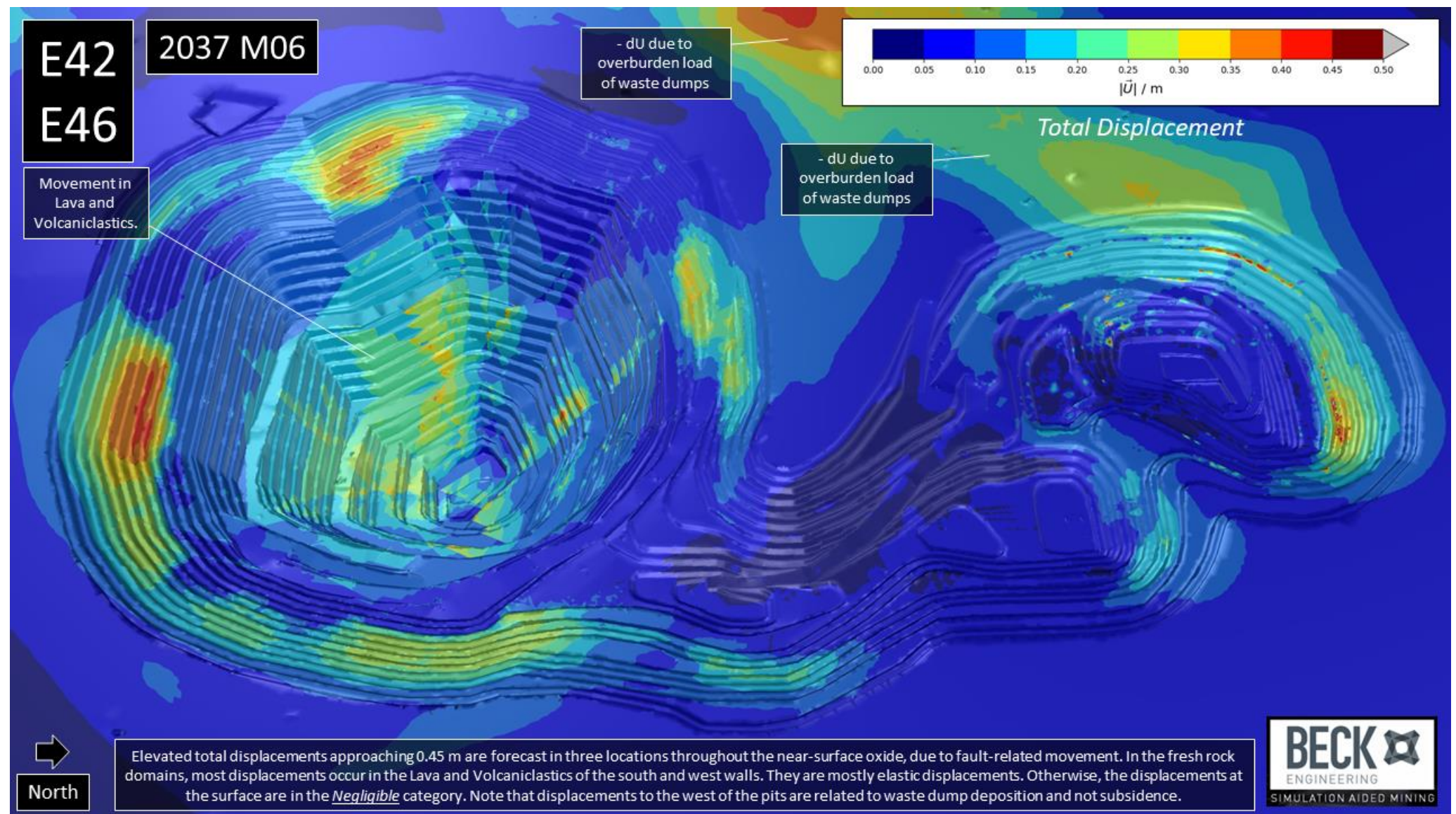


Figure 3-3 Forecast total displacements of the E42, E46 & GR open pit slopes and surrounding natural surface topography (2037 M06).

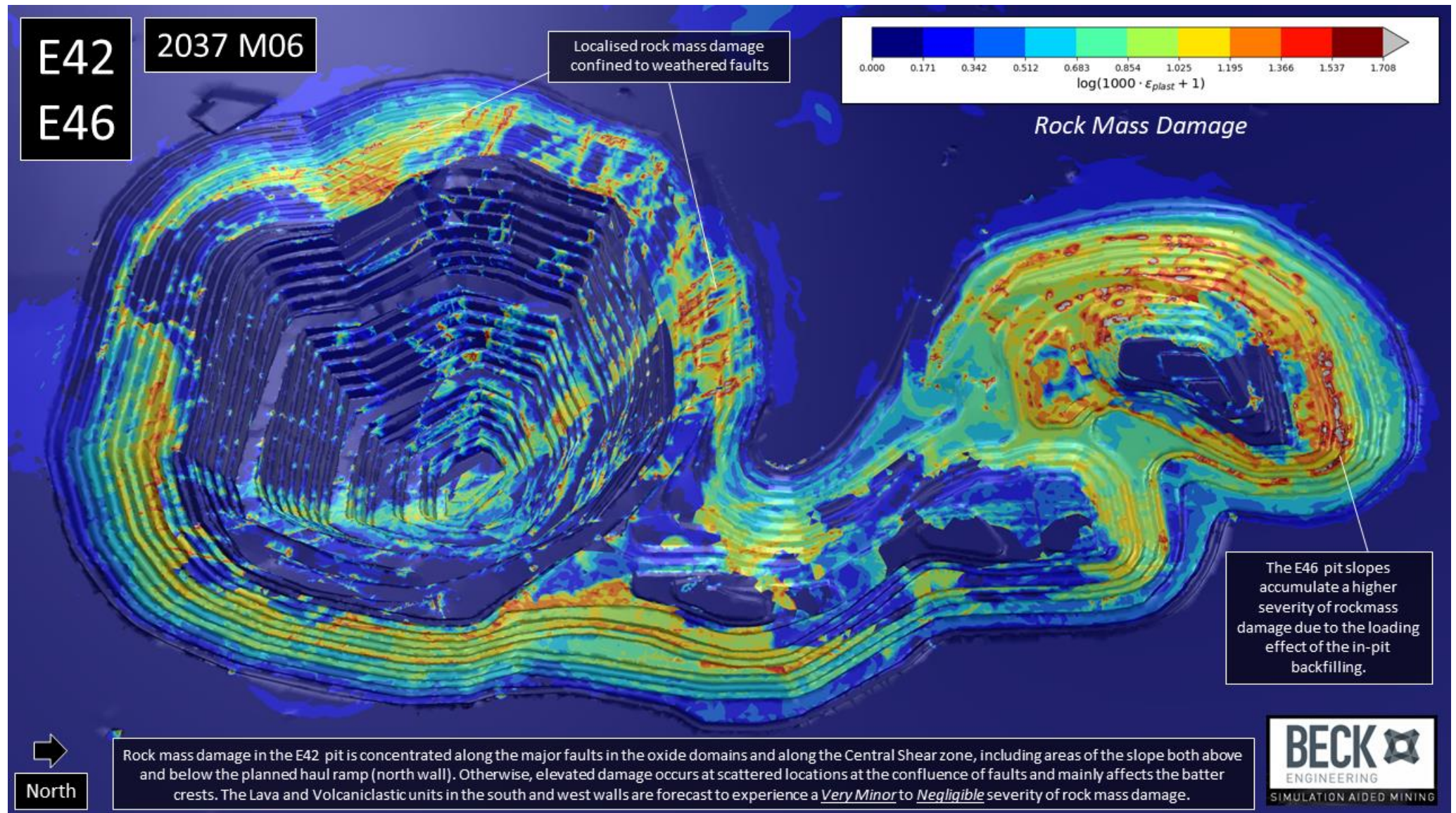


Figure 3-4 Forecast rockmass damage of the E42, E46 & GR open pit slopes and surrounding natural surface topography (2037 M06).

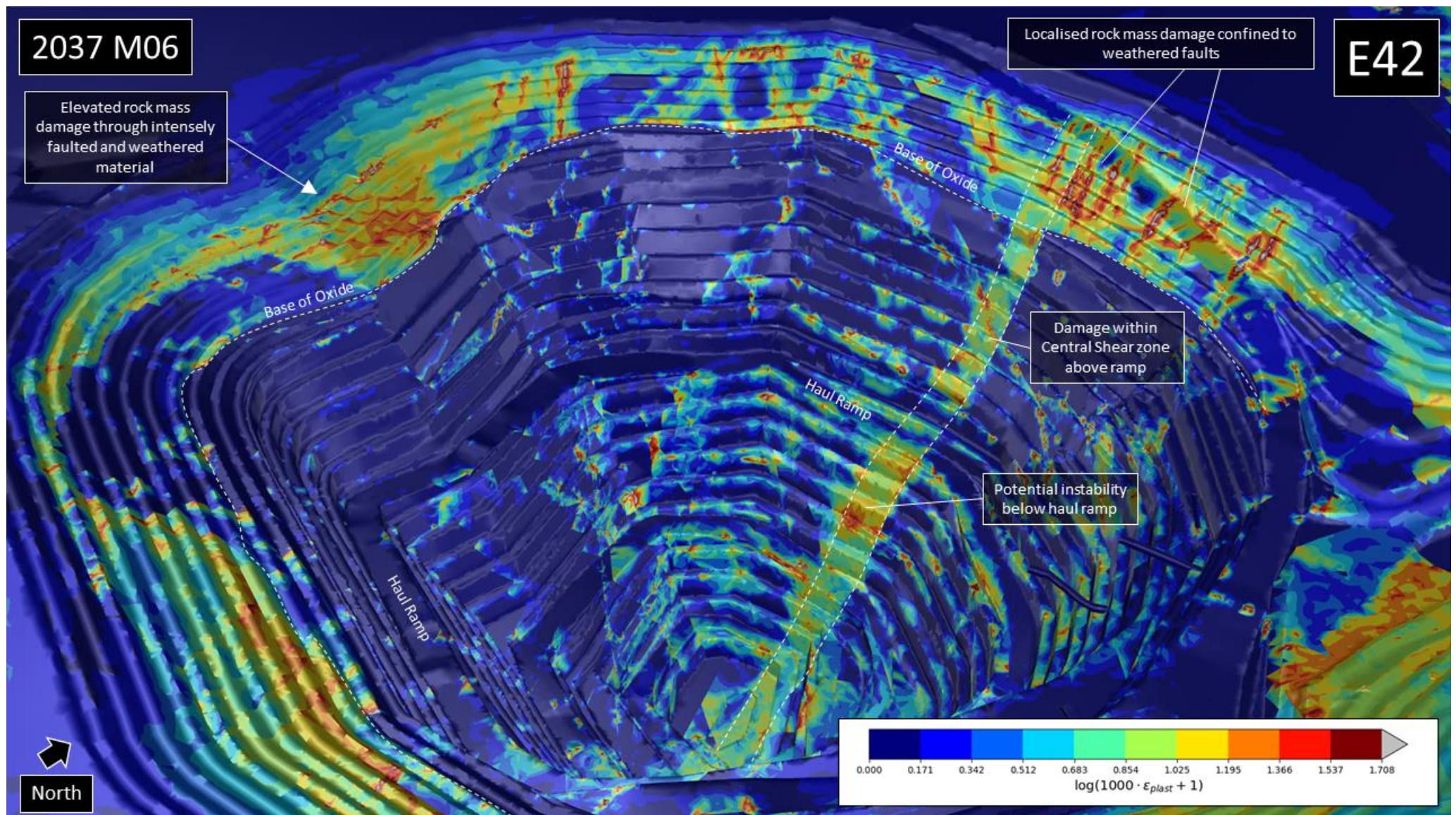


Figure 3-5 Rock mass damage forecasts for the E42 open pit showing elevated damage in the Central Shear and oxides (2037 M06).

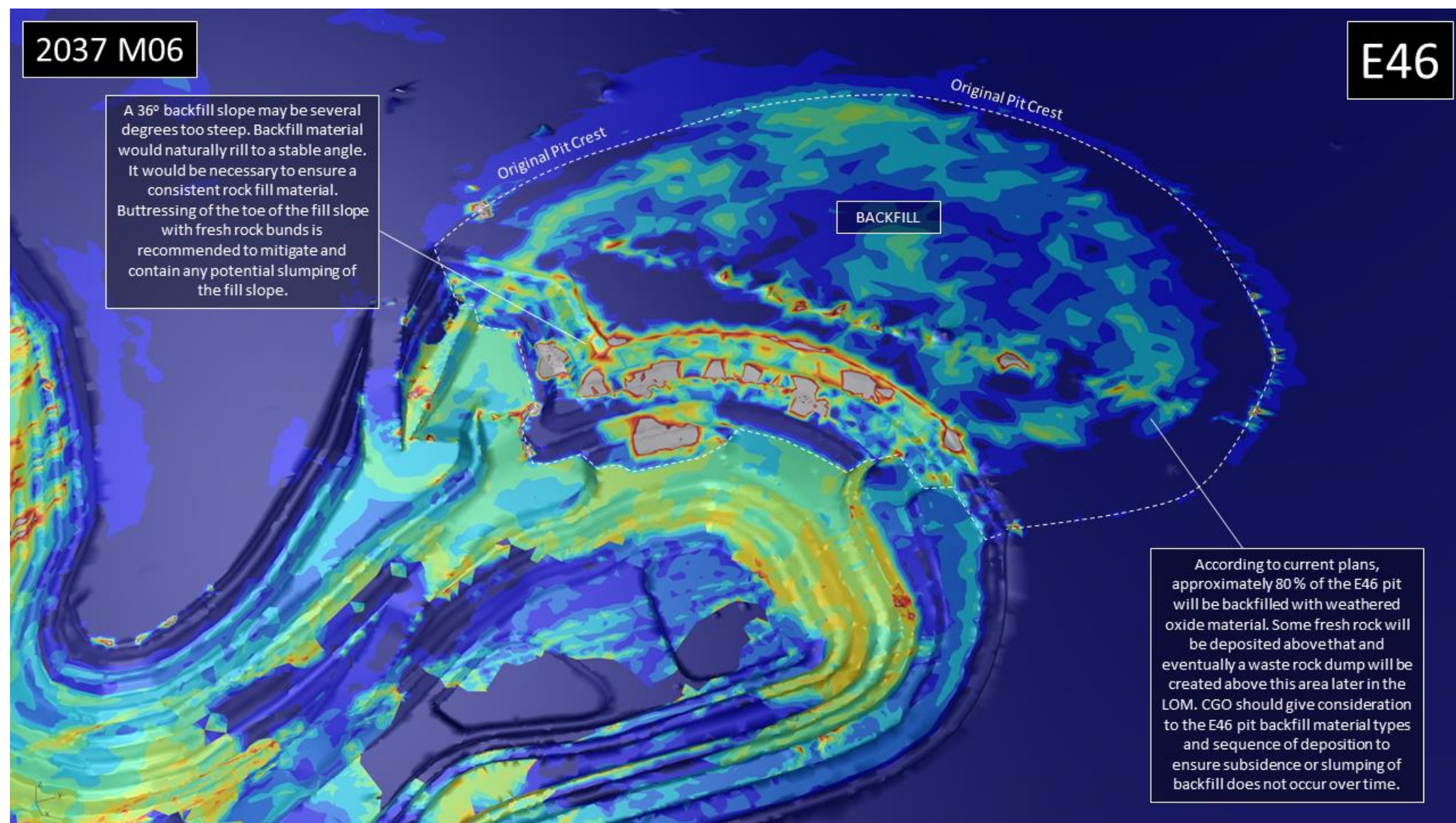


Figure 3-6 Rock mass damage forecasts for the E46 open pit after in-pit backfilling (2037 M06).

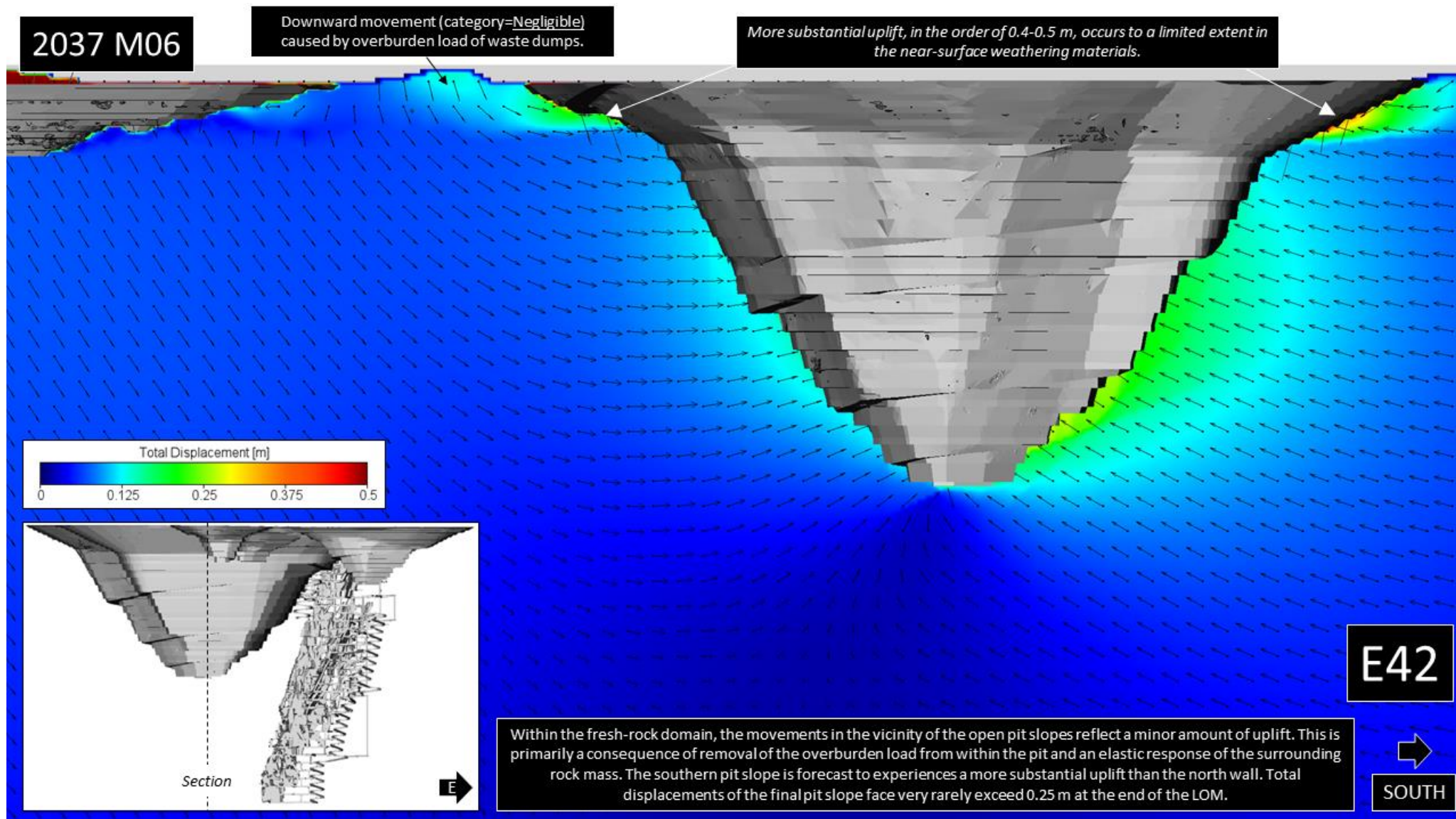


Figure 3-7 North-South long section showing forecast total displacements and directions in the E42 open pit slopes.

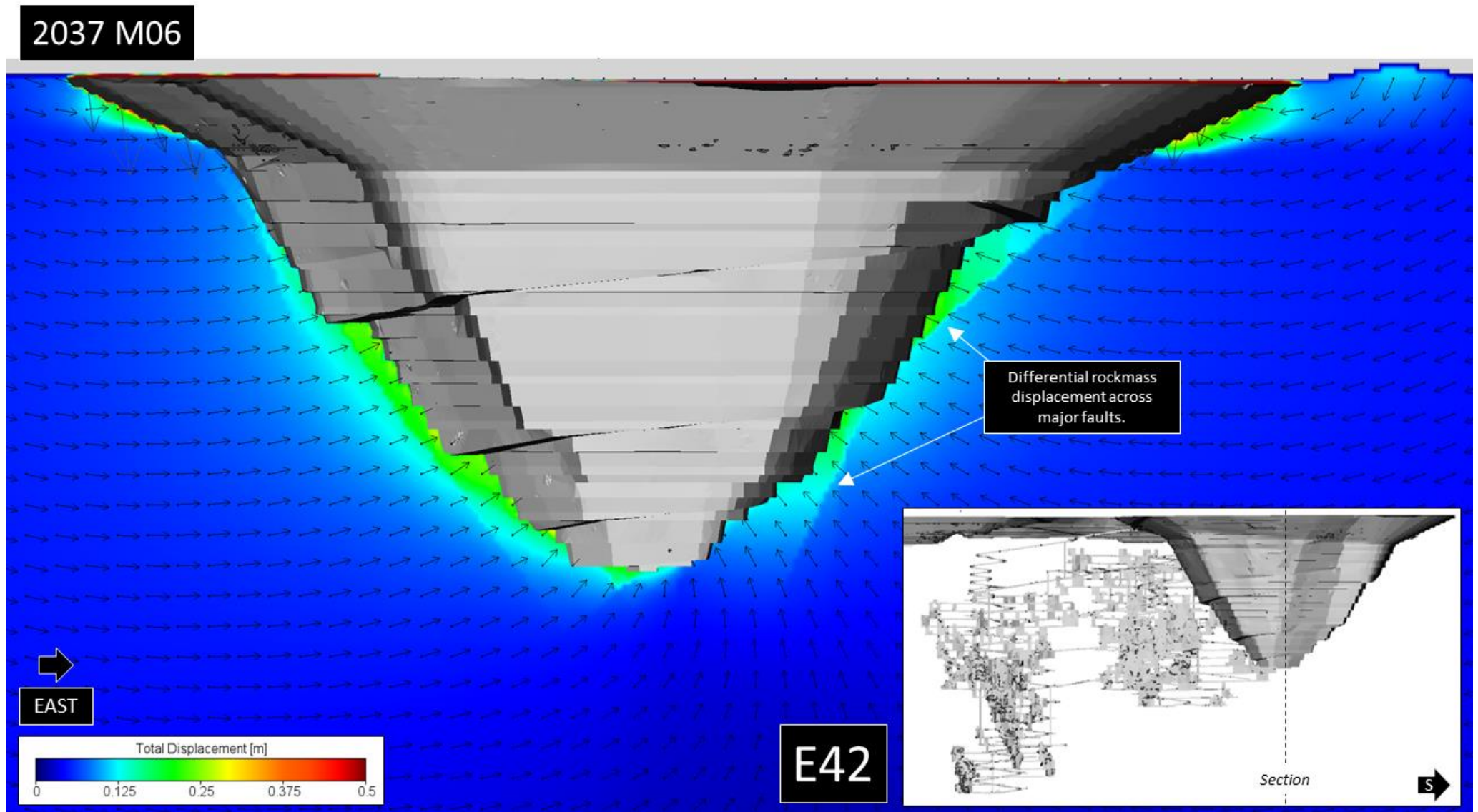


Figure 3-8 East-West cross section showing forecast total displacements and directions in the E42 open pit slopes.

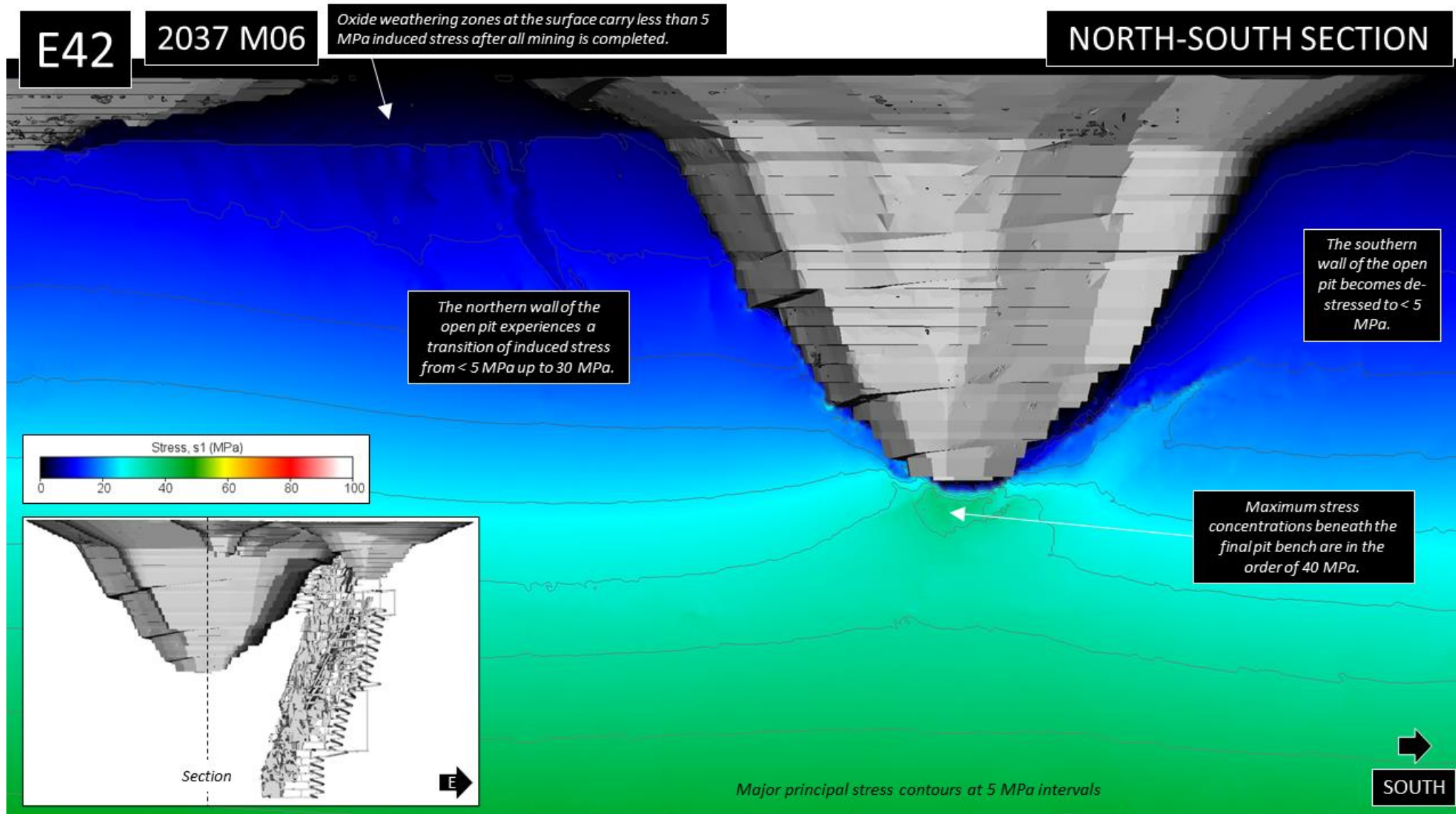


Figure 3-9 North-South long section showing induced major principal stress conditions in the E42 open pit slopes.

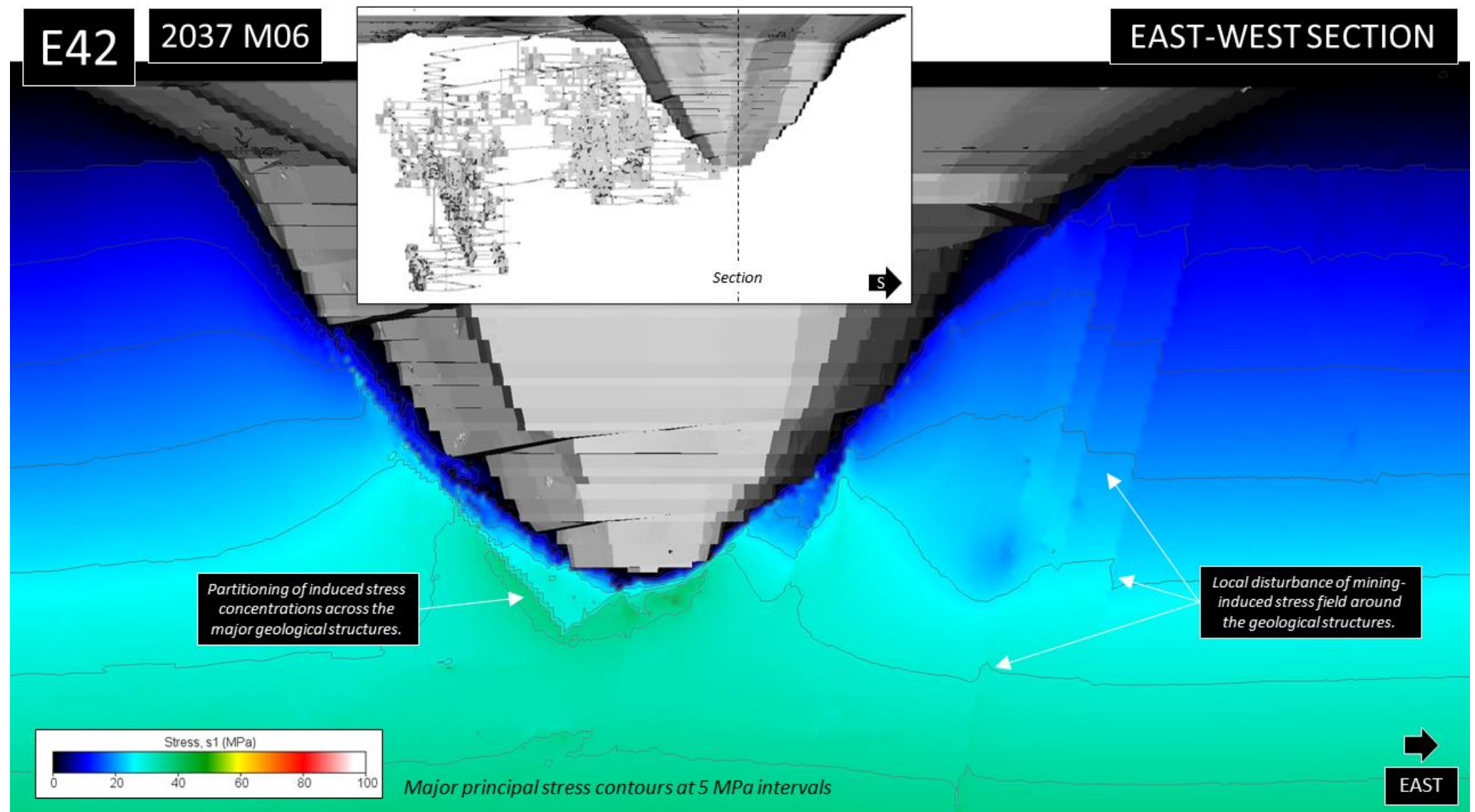


Figure 3-10 East-West cross section showing induced major principal stress conditions in the E42 open pit slopes.

3.3 E41 Open Pit

Selected images of the simulation forecasts for the rockmass response of the E41 open pit slopes and nearby surrounding surface topography at the conclusion of the life-of-mine plan in 2037 are presented in the following figures, as listed below.

- Figure 3-11 to Figure 3-13: Forecast vertical, horizontal and total displacements, respectively, of the E41 open pit and nearby natural surface topography at the end of the current mine plan,
- Figure 3-14: Rockmass damage forecast at the end of the mine plan.

The model results indicate:

- Mining of the E41 open pit is not forecast to generate vertical displacements exceeding 0.1 m anywhere beyond the physical limits of the pit itself. This magnitude of displacement is insufficient to cause visible subsidence effects or any permanent damage to the surface, such as tension cracking or ground depressions at the surface.
- Maximum horizontal displacements in the E41 slopes are forecast to approach 0.15 m in three locations within the Soft Oxide domain. This is a Negligible magnitude of displacement and primarily related to uplift of the slopes due to overburden removal, not subsidence or slope instability. Displacements of this nature are most evident in the eastern slopes around the Glennfiddich main fault. The horizontal displacements of the natural surface beyond the pit crest are < 0.05 m and can be considered Negligible and near-zero. This corresponds to elastic movement only and no adverse subsidence impact such as cracking should be expected in the nearby terrain as a result of the E41 mining activity.
- Total displacements of the E41 pit slopes approach 0.3 m within the Soft Oxides only. This is related to uplift of the slopes during overburden removal, not subsidence. Displacements in the Hard Oxide and Fresh rock domains are less than 0.05 m and can be regarded as Negligible. Total 3D displacements are forecast to be < 0.05 m for the vast majority of the surface beyond the pit crest, except for in the north, where some horizontal displacement (not subsidence) occurs through the pillar separating the E41 and E42 pits.
- Rock mass damage is mostly of a Minor to Moderate severity through some regions of the Soft Oxide domain, primarily around the fault structures. Some higher damage is forecast on the faults themselves, but this is highly localised and mostly associated with the east of the pit along the Glennfiddich fault, with the damage forecast within the haul ramp. The shallow overall slope angles there make slope instability unlikely. The damage is limited to the Soft Oxide zone, and to a lesser extent the Hard Oxide. Damage is forecast to be more likely on the Glennfiddich Main fault and also along the Cowal Shear below the ramp. The fresh rock benches show minimal damage and hence low instability potential.

In summary, the forecast displacements and rock mass damage indicate that the E41 pit is also expected to have a Negligible subsidence impact on the surrounding terrain and infrastructure.

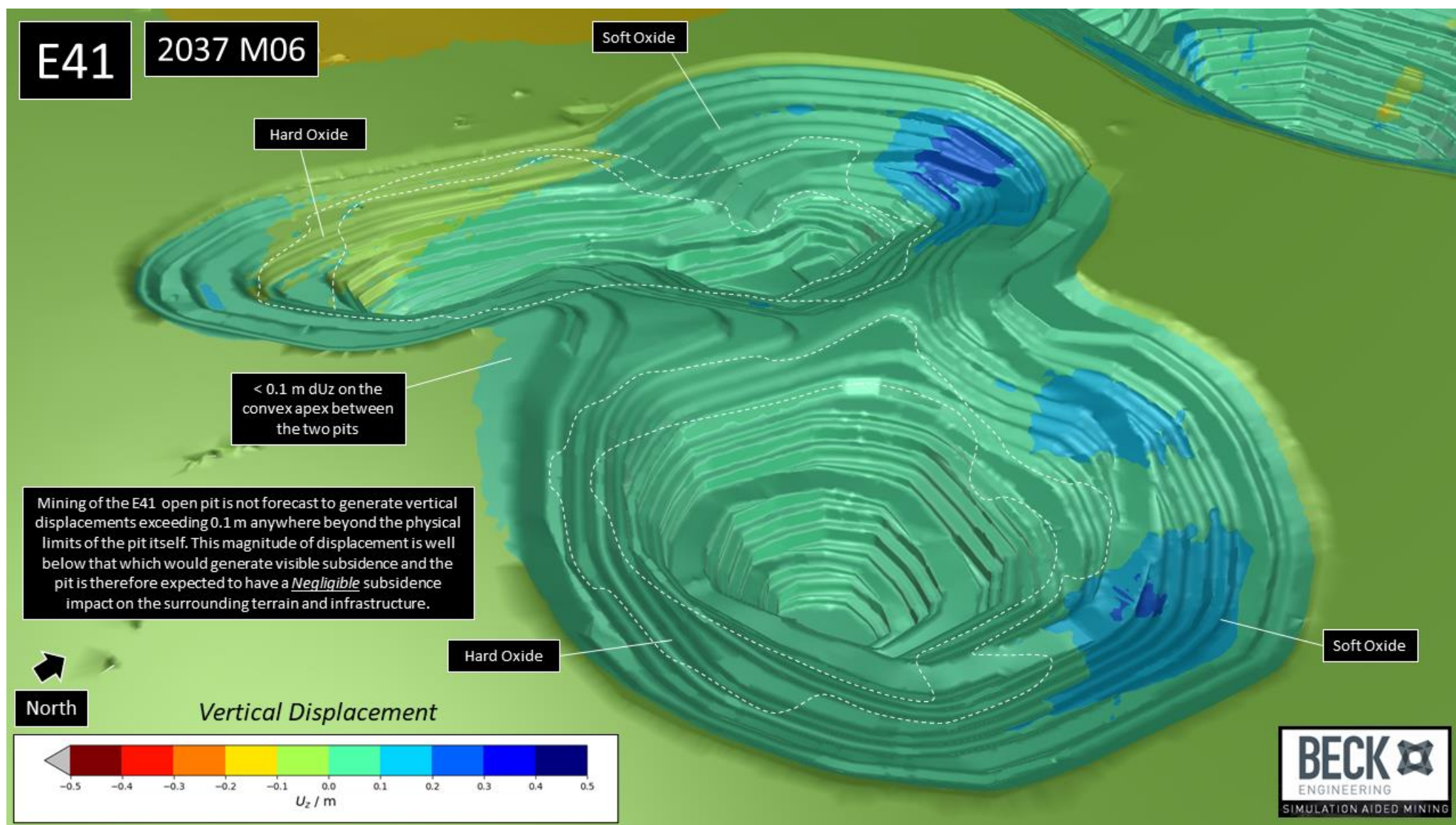


Figure 3-11 Forecast vertical displacements of the E41 open pit slopes and surrounding natural surface topography.

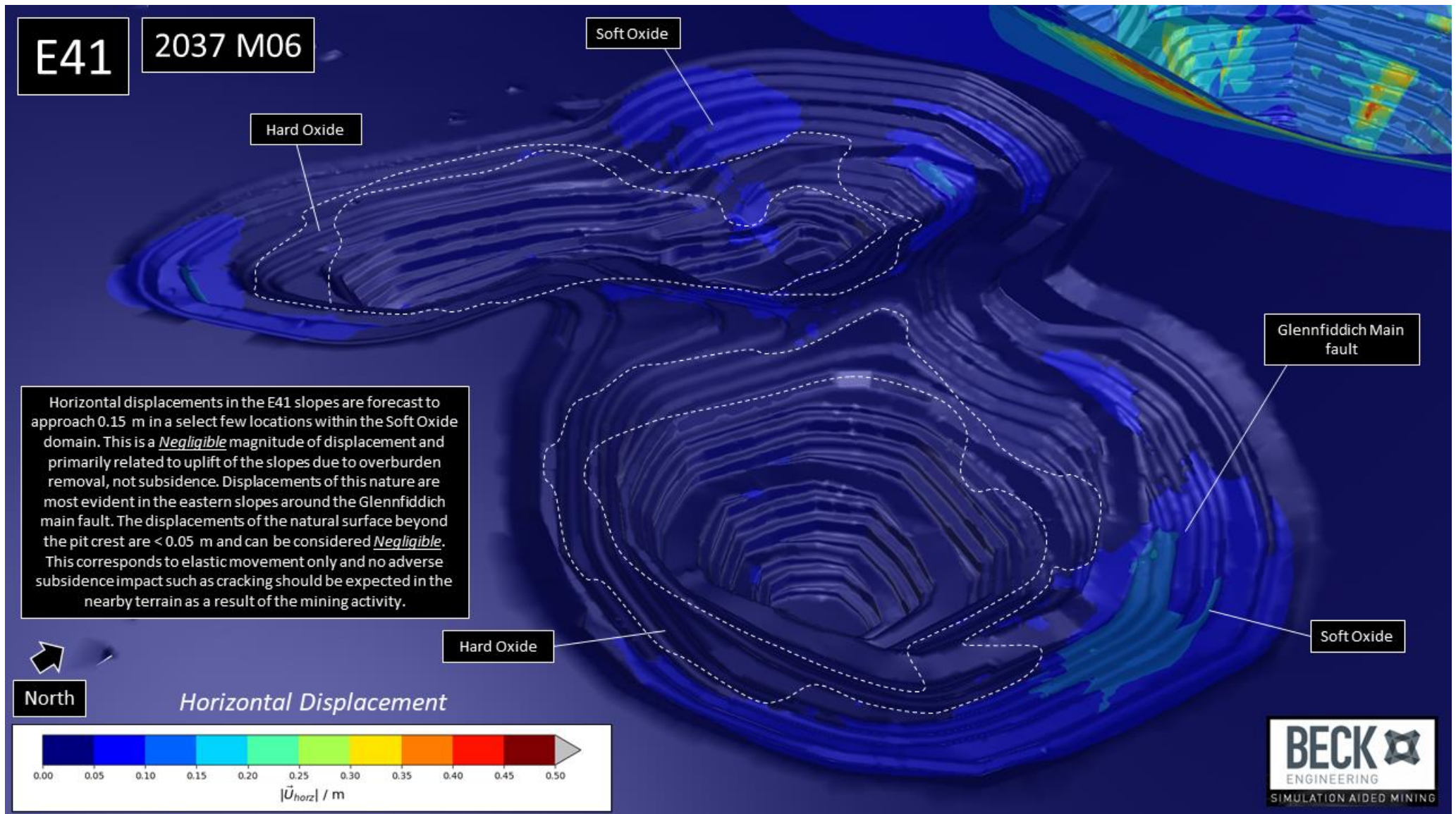


Figure 3-12 Forecast horizontal displacements of the E41 open pit slopes and surrounding natural surface topography.

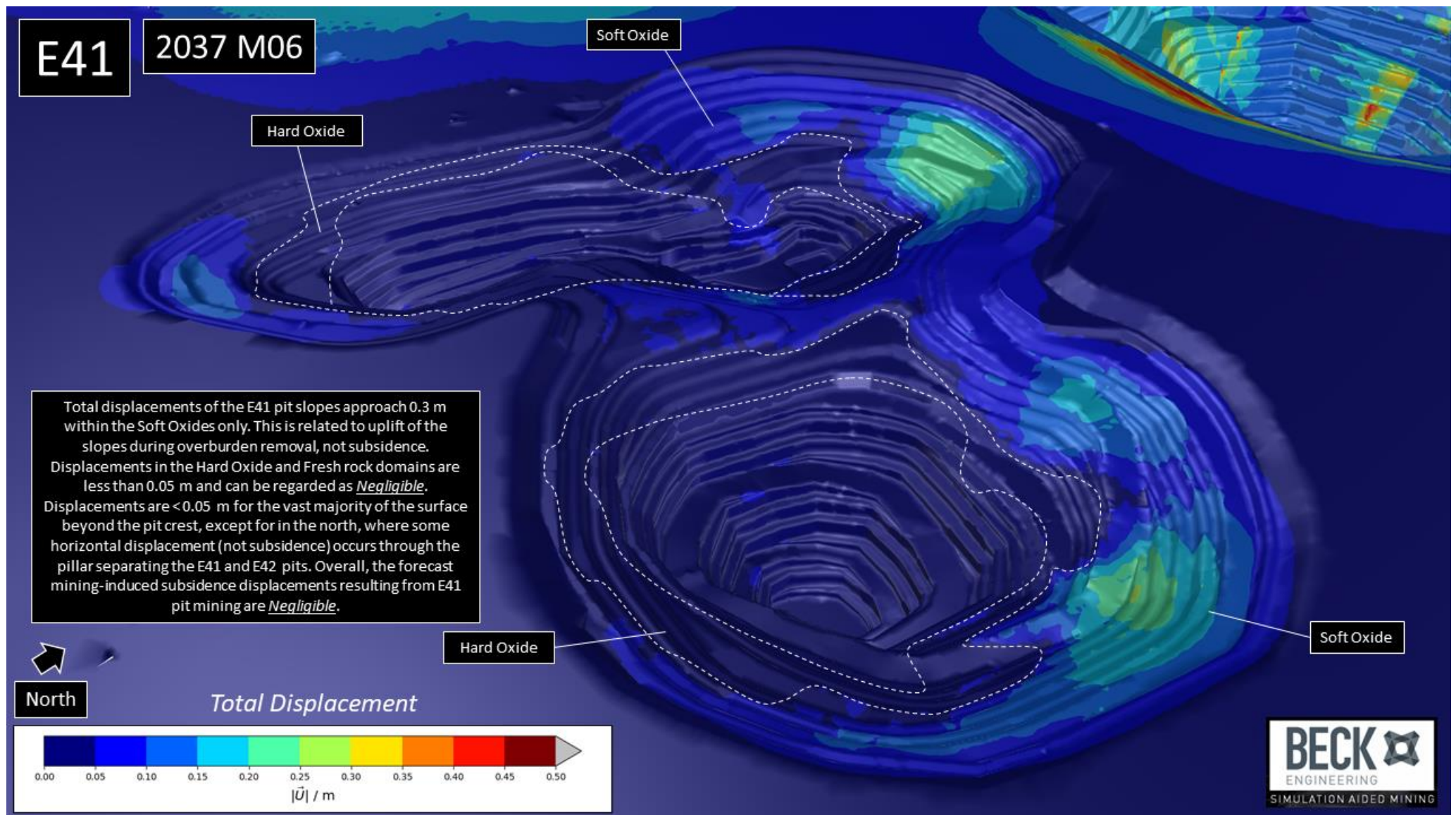


Figure 3-13 Forecast total displacements of the E41 open pit slopes and surrounding natural surface topography.

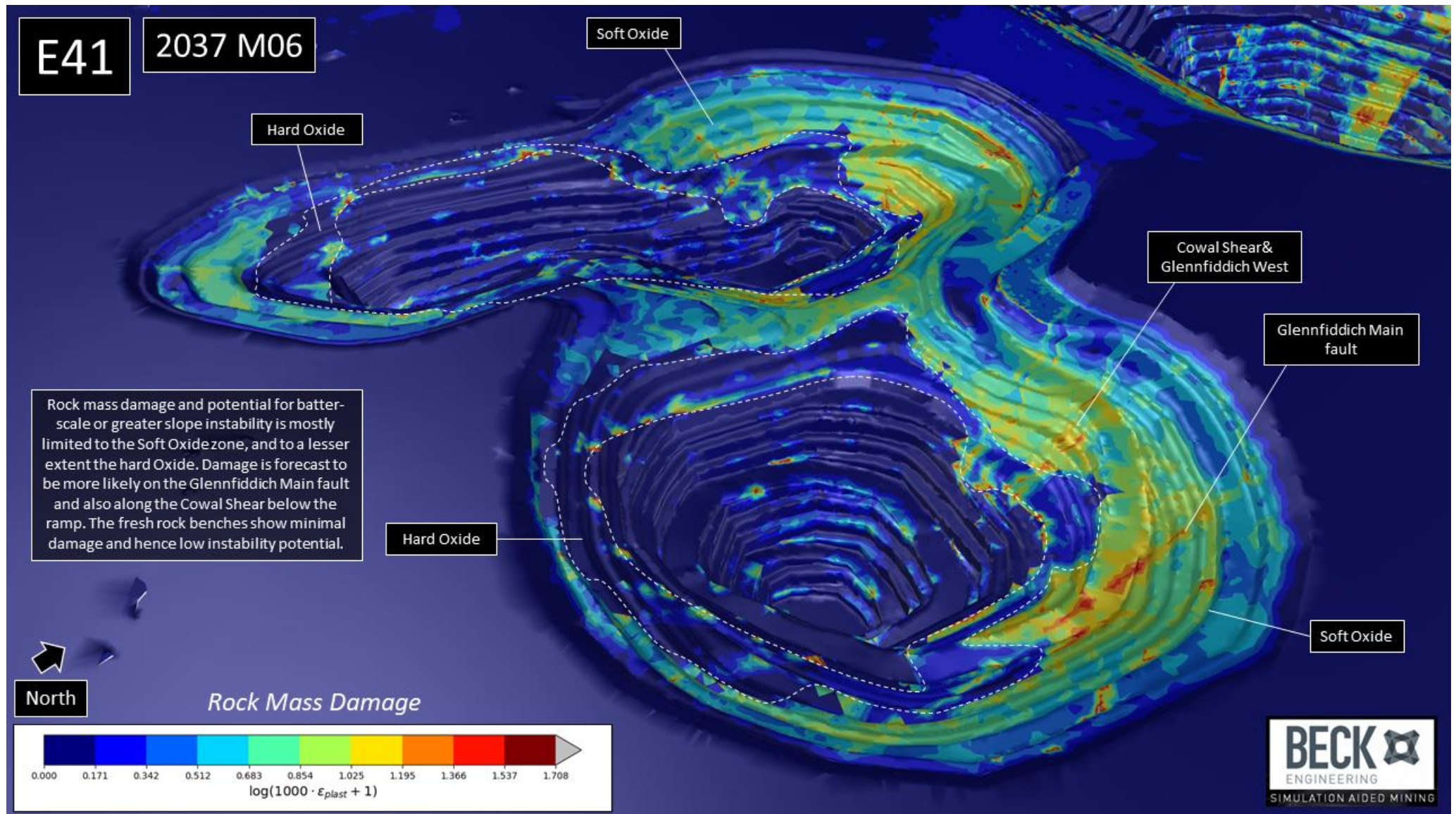


Figure 3-14 Forecast rockmass damage of the E41 open pit slopes and surrounding natural surface topography.

3.4 Lake Protection Bund & Other Infrastructure

Selected images of the simulation forecasts at the mine-scale, after completion of the mine plan, i.e. including the proposed future open pit mines, waste dumps, the final LPB, surface processing plant district and tailings storage facilities, are presented as follows:

- Figure 3-15 & Figure 3-16: Vertical and total displacements,
- Figure 3-17: Rock mass damage in the vicinity of the LPB,
- Figure 3-18 to Figure 3-21: Surface maps (various viewpoints and scales) showing contours of surface subsidence impact severity, as a function of horizontal strain and angular distortion, based on the assessment methodology proposed by Boscardin & Cording (1989), also known as the Harrison plot.

The main findings for the subsidence impact to the wider zone of near-mine infrastructure are:

- Vertical displacements beneath the final LPB are < 0.1 m at the end of the mine plan (Figure 3-15). The movements are elastic in nature and fall within the Negligible category of subsidence impact. Total displacements are forecast to be < 0.1 m below the northern half of the LPB and < 0.05 m below the southern half (Figure 3-16). These movements are also elastic and classed as Negligible. They remain well below the threshold where adverse subsidence impacts like surface tension cracking and ground depressions could occur. Rockmass damage beneath the entire LPB is forecast to be Negligible after completion of the mining (Figure 3-17).
- Vertical (downward) displacements of ~ 0.5 m and total displacements of a comparable magnitude are forecast for the natural surface terrain beneath the waste dumps. These displacements are caused by the overburden load of the tipped rock of the waste dumps, not open pit mining-induced subsidence. The zones of displacements > 0.1 m do not extend beyond the perimeter of the dumps.
- Negligible vertical and total displacements are forecast throughout the vast majority of the precinct of surface infrastructure, including the processing plant and associated infrastructure, ROM crusher, warehouses, ore stockpile cone, transformer stations and tailings storage dam walls etc.
- Assessment of the surface subsidence impact severity using the Boscardin & Cording (1989) approach indicates that impacts of a Slight nature or greater (see Section 2.9 for definitions) are confined to within the perimeter of the open pits (i.e. affecting the pit slopes) and including a small area of the pillar separating the E41 and E42 pits at the surface.
- A Very Slight subsidence impact is forecast to affect the rock mass directly beneath a minority of the ROM pad adjacent the western E42 pit crest. However, this impact affects the natural rock mass below the built-up rock fill of the ROM pad and visible subsidence effects like cracking in the ROM pad surface are highly unlikely. No adverse impacts to the ROM pad should be expected for this level of subsidence impact. The ROM crusher area is outside this zone of Very Slight impact and remains unaffected.
- Otherwise, the subsidence impact severity is forecast to be Negligible for the remainder of the natural surface.

In summary, the Lake Protection Bund and vast majority of the surface, including the processing infrastructure precinct, are forecast to experience a Negligible subsidence impact as a result of the proposed open pit mine plan. A Very Slight impact is forecast to affect a minority of the ROM Pad to the west of the final pit, but the effect is unlikely to present any visible subsidence damage or lead to any adverse consequences.

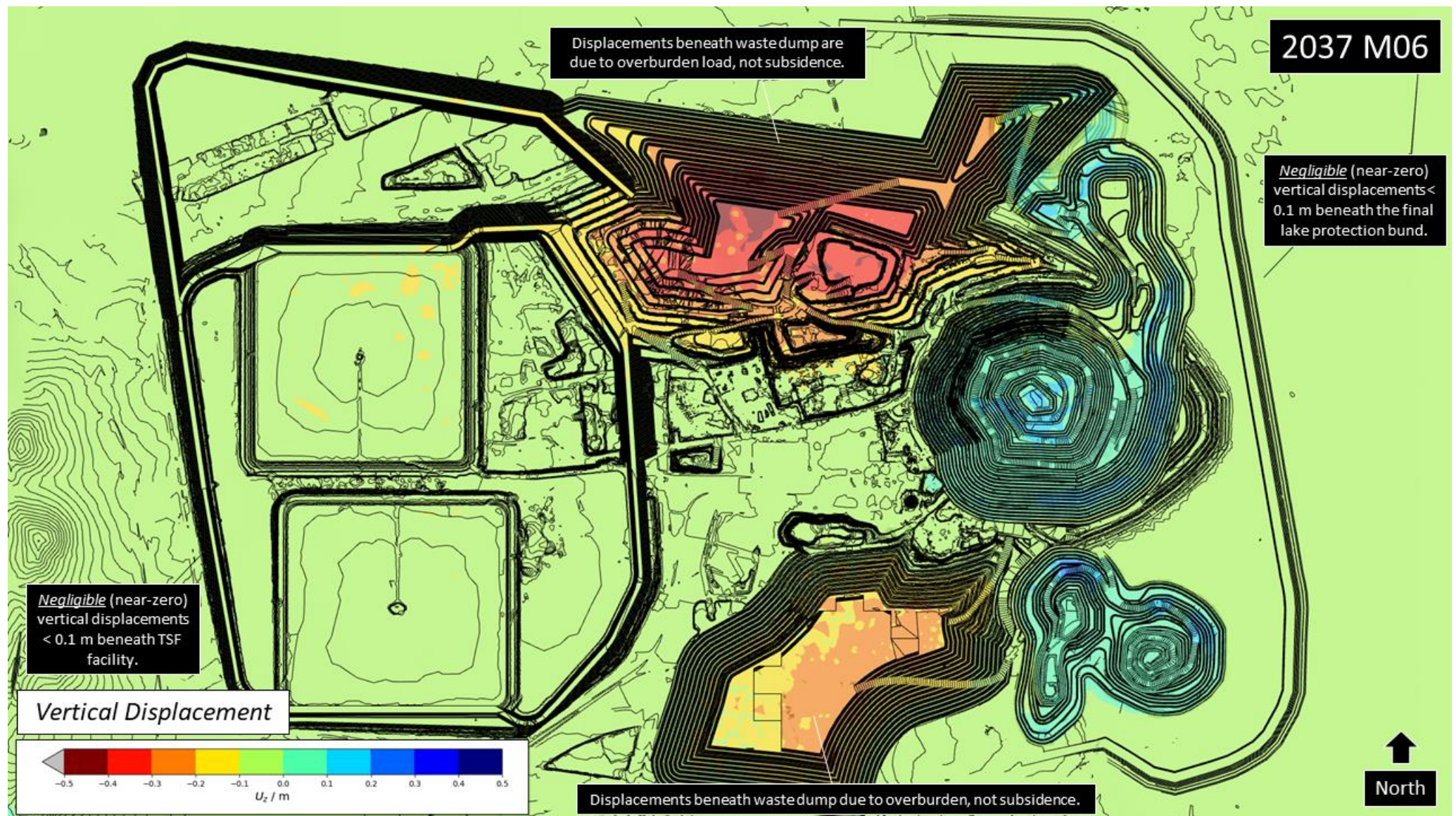


Figure 3-15 Mine-scale view of forecast vertical displacements (Y2037 M06).

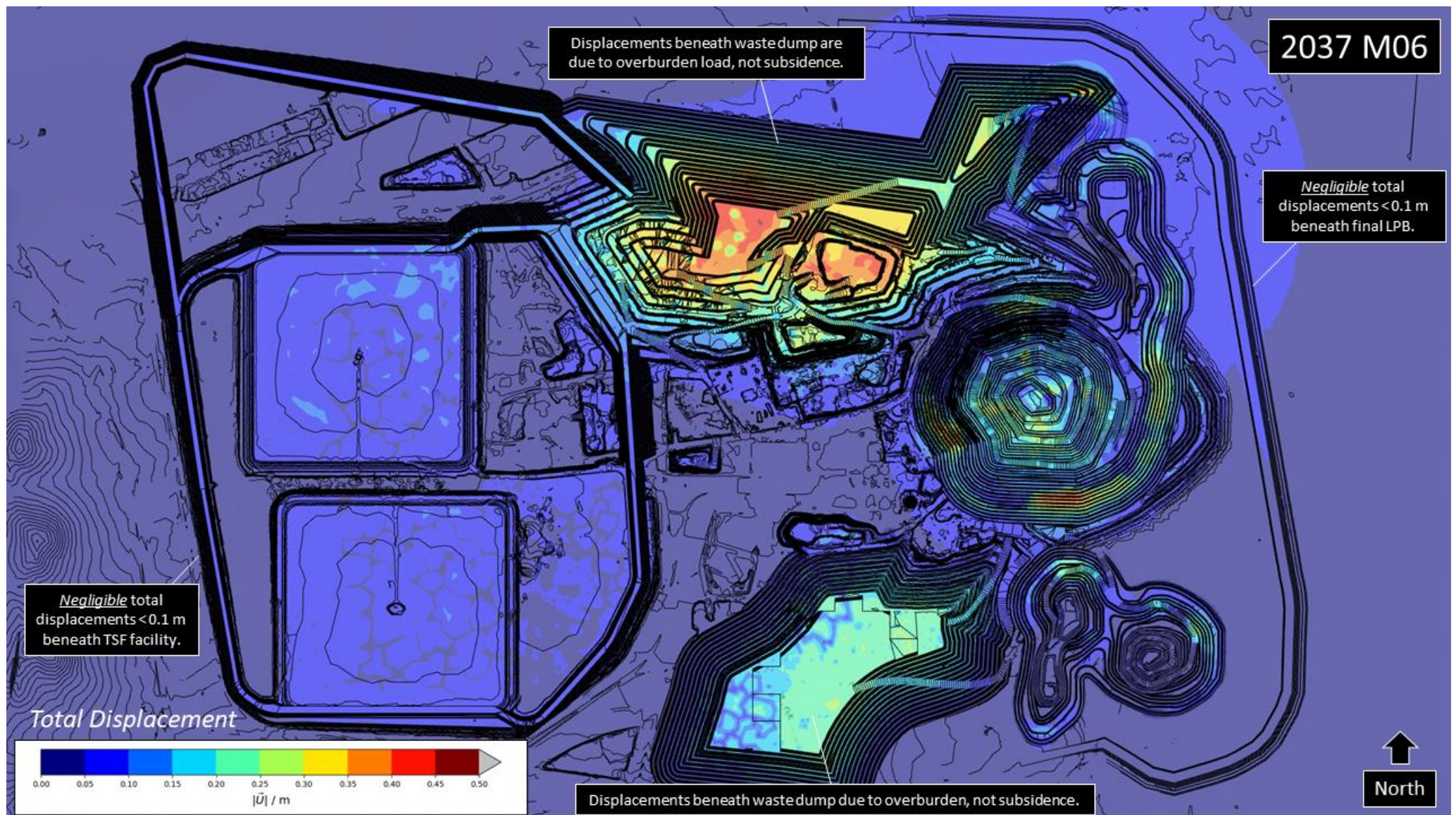


Figure 3-16 Mine-scale view of forecast total displacements (Y2037 M06).

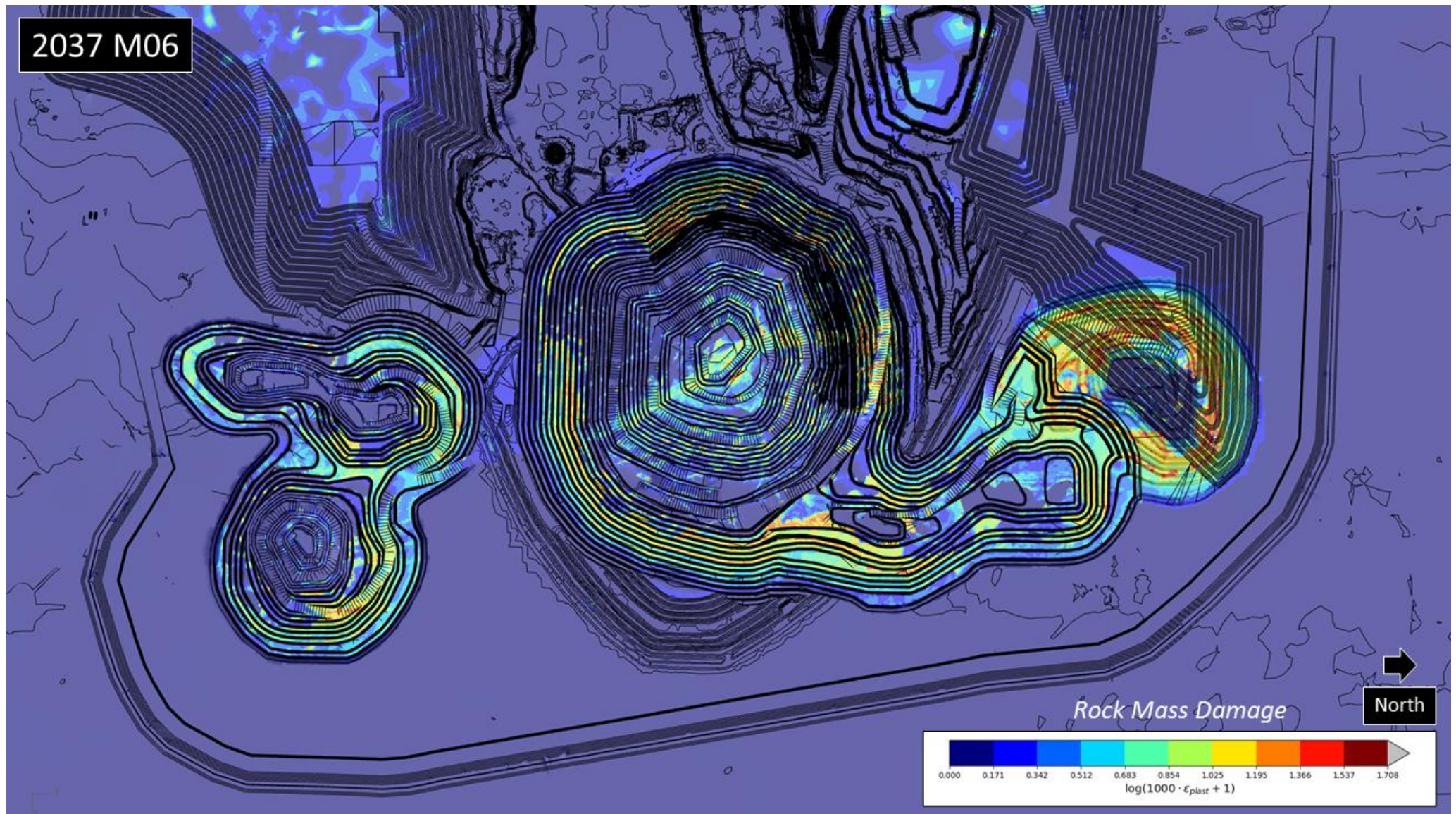


Figure 3-17 Rock mass damage showing impact of open pit mining to the Lake Protection Bund and nearby surface (2037 M06).

Horizontal Strain (ϵ_H) and Angular Distortion (β) (i.e. ratio of differential settlement of two points to their horizontal spacing) can have a significant impact on surface infrastructure, especially shaft headframes, chimney stacks, wide concrete foundations for vent fans, pipeline footings, roads etc.

A methodology for assessing the impact of subsidence on surface infrastructure is based on Boscardin & Cording (1989), also known as the Harrison Plot. This can be used to classify and assess the severity of the impact to critical assets located close to mining excavations like open pit slopes, underground caves or stoping blocks.

The plot is only applicable for surface infrastructure, not underground facilities. It is primarily formulated for rigid surface infrastructure, but can be used for other structures, like earth dams, as a high-level, first-pass subsidence impact assessment.

If a particular asset plots as Moderate impact or higher, BE suggest that an assessment of the horizontal strain & angular distortion tolerance limits should be conducted by a relevant structural expert.

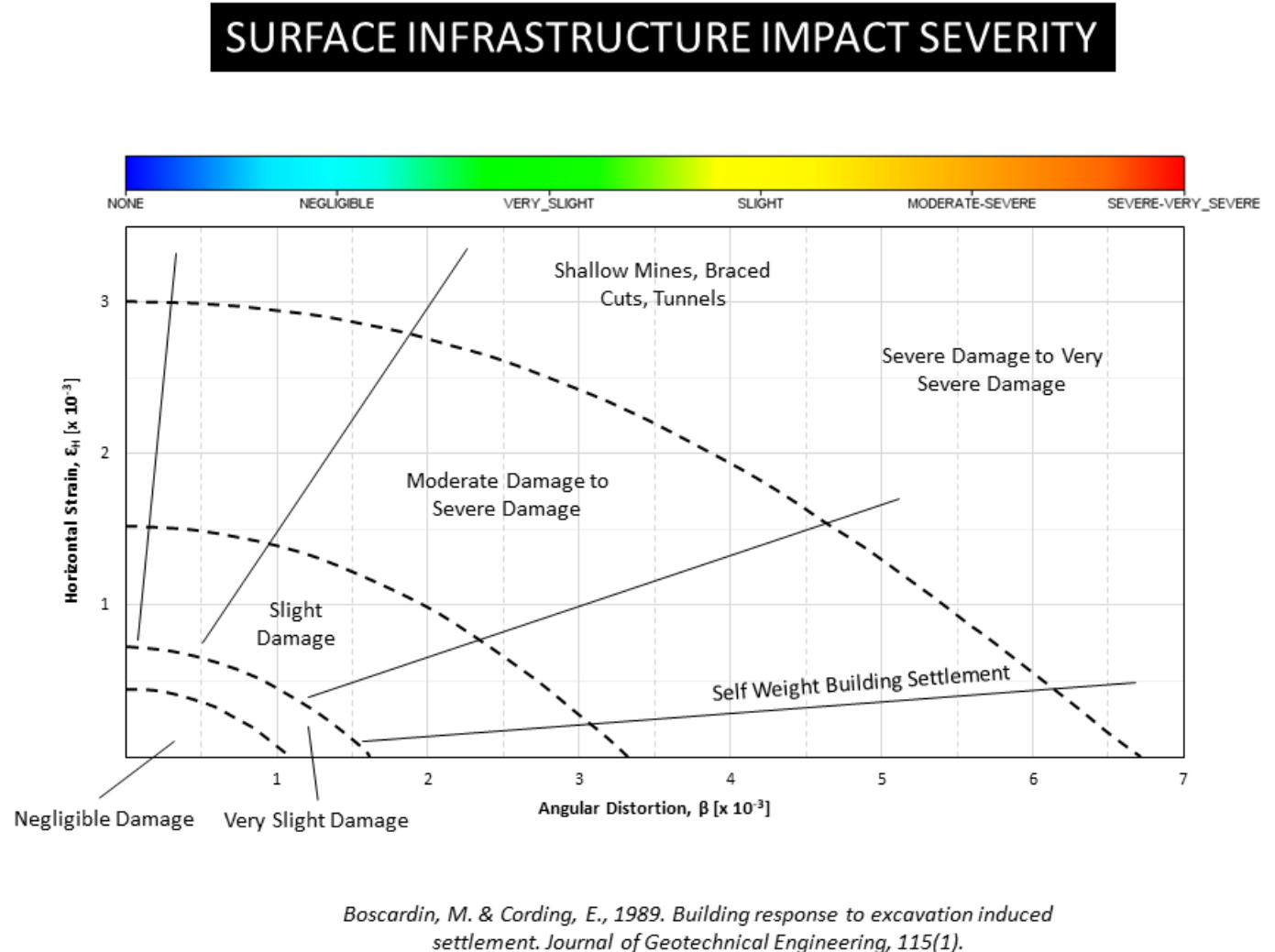


Figure 3-18 Classification system for the severity of surface subsidence based on Boscardin & Cording (1989).

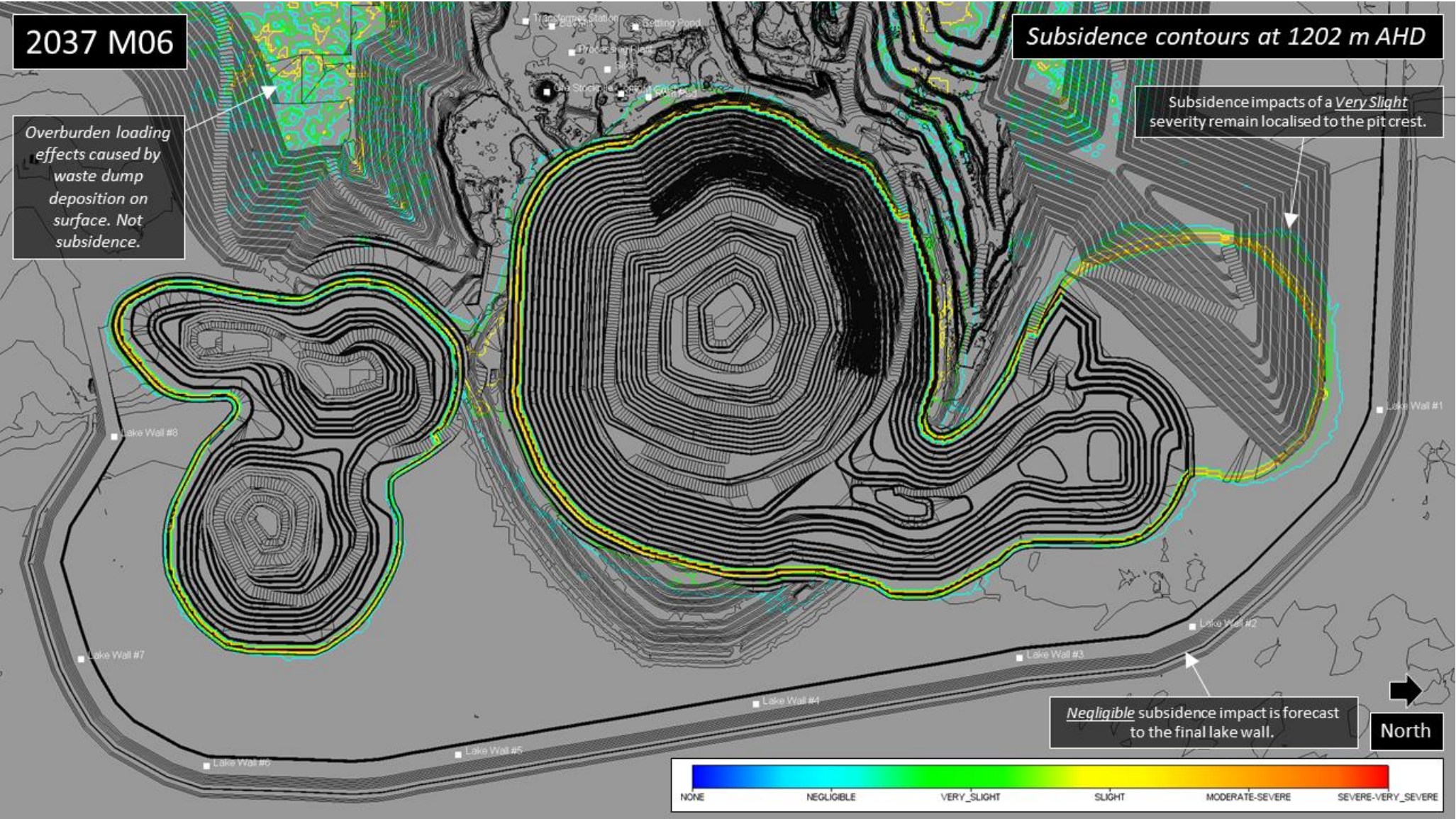


Figure 3-19 Contours of surface subsidence impact severity for the open pit district (top view).

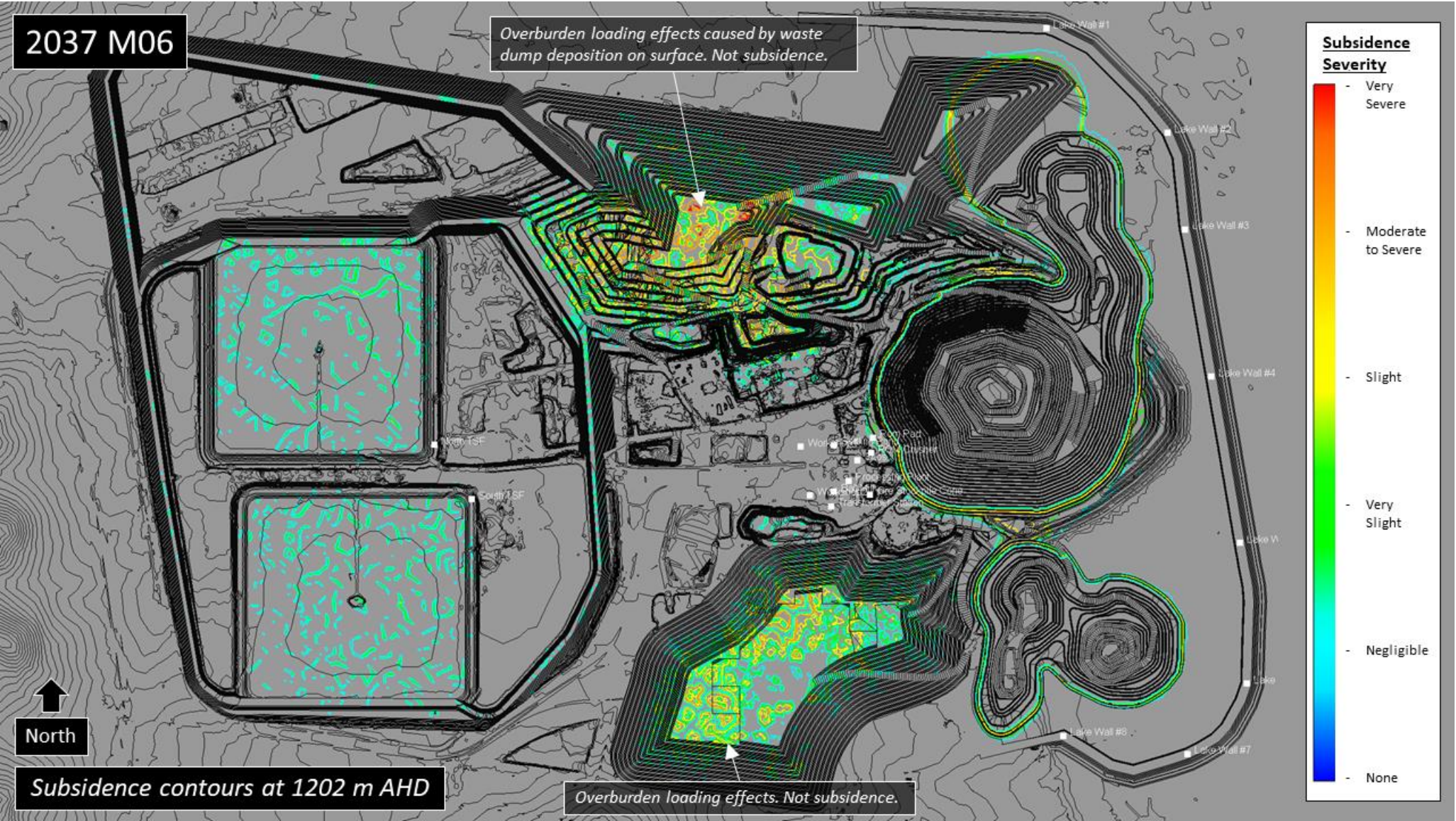


Figure 3-20 Contours of surface subsidence impact severity for CGO after completion of the proposed pit mining (global top view).

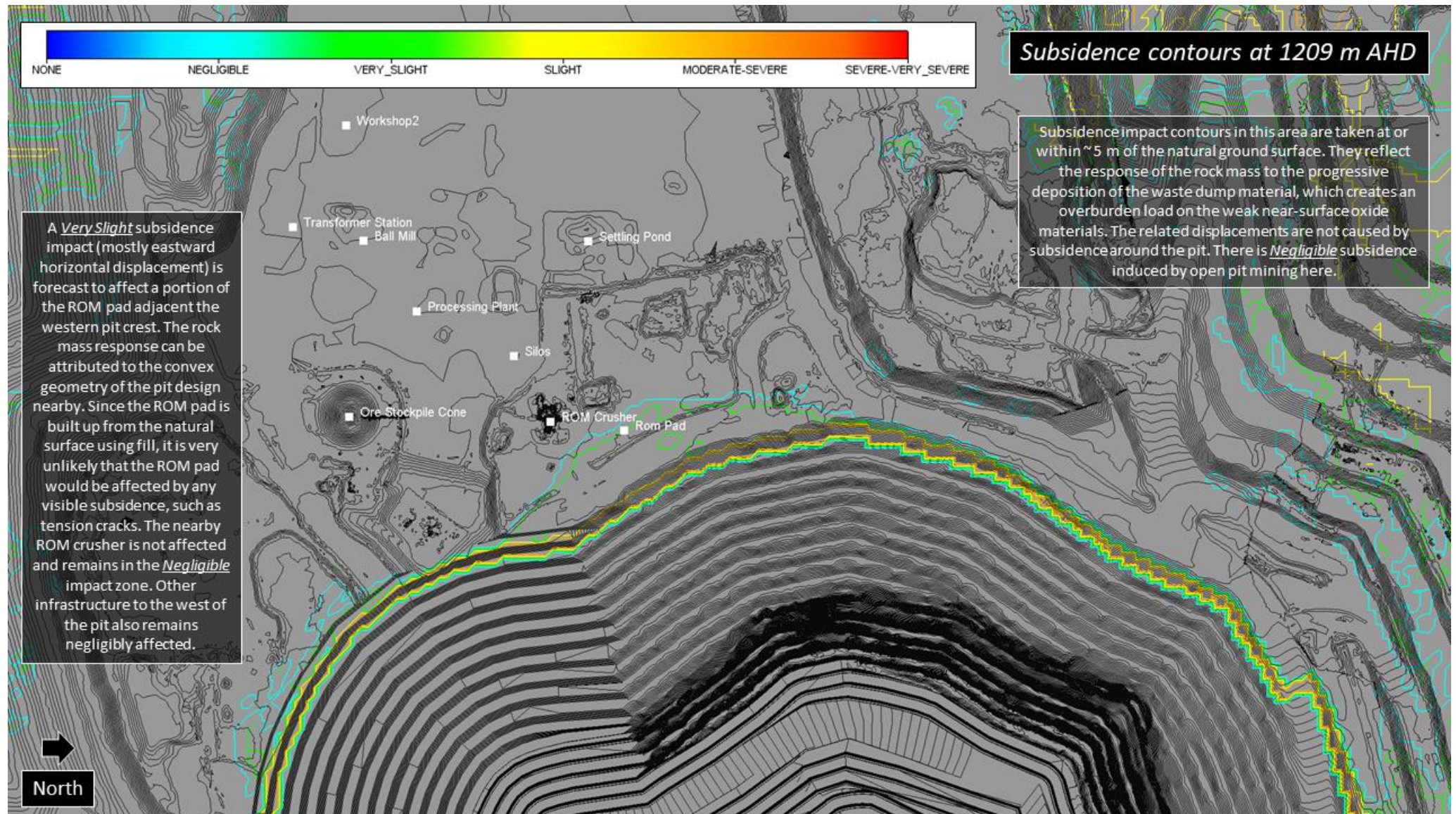


Figure 3-21 Contours of surface subsidence impact severity for the major surface plant adjacent the western pit crest (top view).

3.5 Open Pit / Underground Interaction

The E42, E46 and GR open pits are planned to be separated from the underground mine by a regional pillar of variable dimensions. At the narrowest point, which is close to surface and the 1060 level, the minimum distance of separation between the open pit and underground stopes is in the order of 35 m. At greater depths, the minimum distance of separation defining the pillar between the open pit and underground is in the order of 230 m.

A selection of model forecasts sampled through the regional pillar separating the future E42 open pit and underground mine are presented as follows below. All forecasts are at the completion of both open pit and underground mining (Y2037 M06).

- Figure 3-22: 3D volume render of rock mass damage (LogP),
- Figure 3-23: NE-SW oriented vertical section showing mining-induced major principal stress & contours,
- Figure 3-24: NW-SE oriented vertical section of total displacement with direction vectors,
- Figure 3-25: Isosurfaces of 100 mm and 200 mm total displacement.

In summary,

- There are no damage interactions forecast to occur between the open pits and underground mine at any time throughout the proposed mine plan, considering the mine-scale resolution of the numerical model.
- In order to ensure that small-scale mechanisms of instability and damage interaction between the underground mine and open pits do not occur, such as stope crown chimneying into the pit, which is below the forecast resolution of the model, BE's prior recommendations to EMM & Evolution made by Campbell, 2020, are reiterated. CGO should remain cognisant of, and comply with those recommendations.
- Above the Galway Splay #8 fault, induced σ_1 stress in the regional pillar separating the open pit and underground does not exceed 20 MPa. Below this fault and to the base of the proposed open pit, stresses within the regional pillar to the underground are in the range of 20-27 MPa.
- Total displacements within the regional pillar separating the open pit and underground are forecast to be < 0.1 m above the Galway Splay # 8 fault and < 0.05 m below it, with a general westward direction of movement through the bulk of the pillar.
- Rock mass within the 200 mm total displacement isosurface could be considered to have a *Slight* impact. Such areas are forecast to be very localised to the pit slopes. Rock mass inside or beyond the 100 mm displacement envelope, which includes the bulk of the regional pillar, can be classified as experiencing *Negligible* subsidence impact.

In summary, concurrent open pit and underground mining operations are forecast to have no adverse stability impact on one another, as no rock mass damage, elevated induced stress or adverse displacement effects are forecast to occur across the regional pillar separating the two mining precincts.

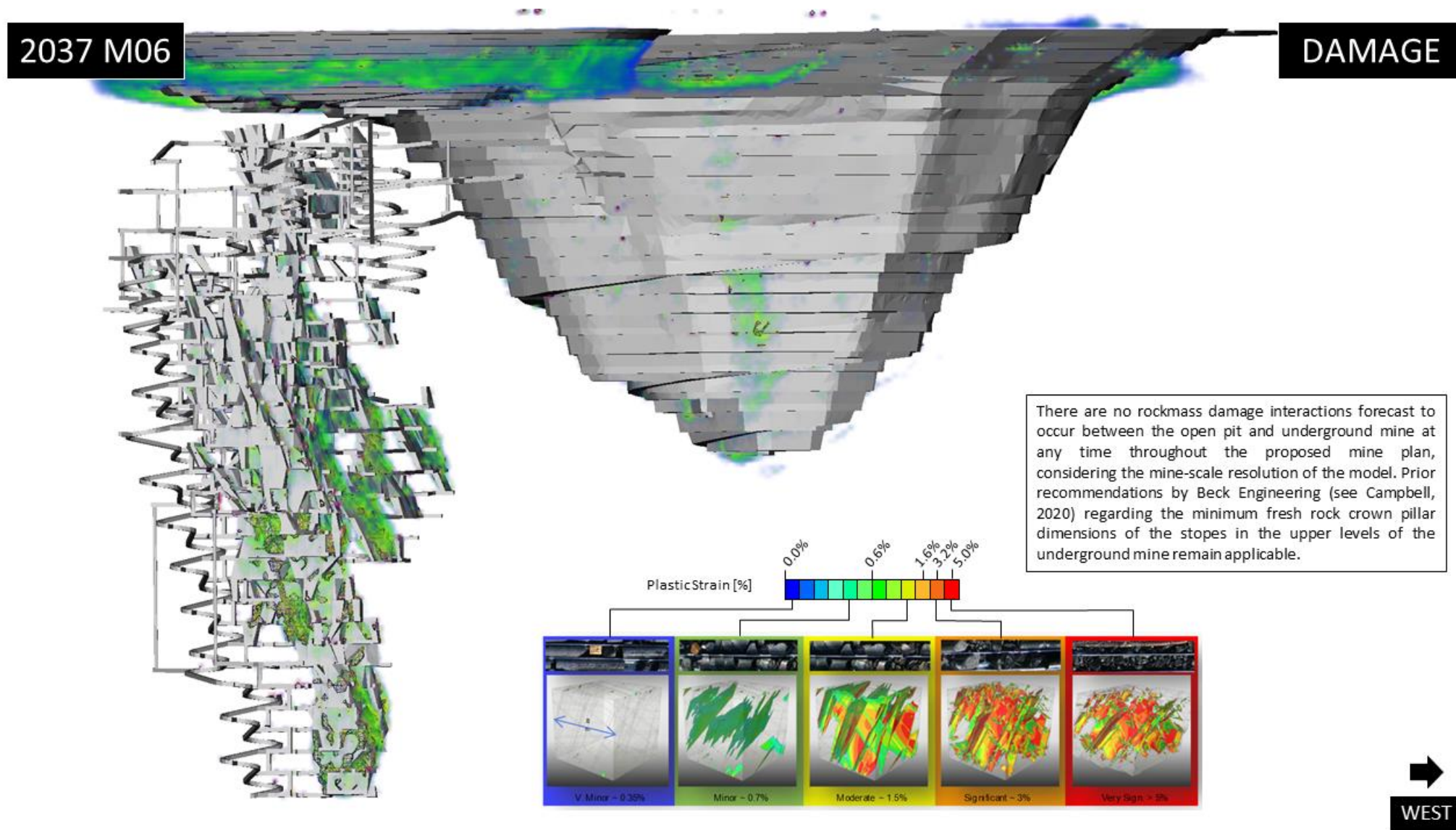


Figure 3-22 3D volume render of rockmass damage forecasts in the regional pillar separating the open pit and underground mine.

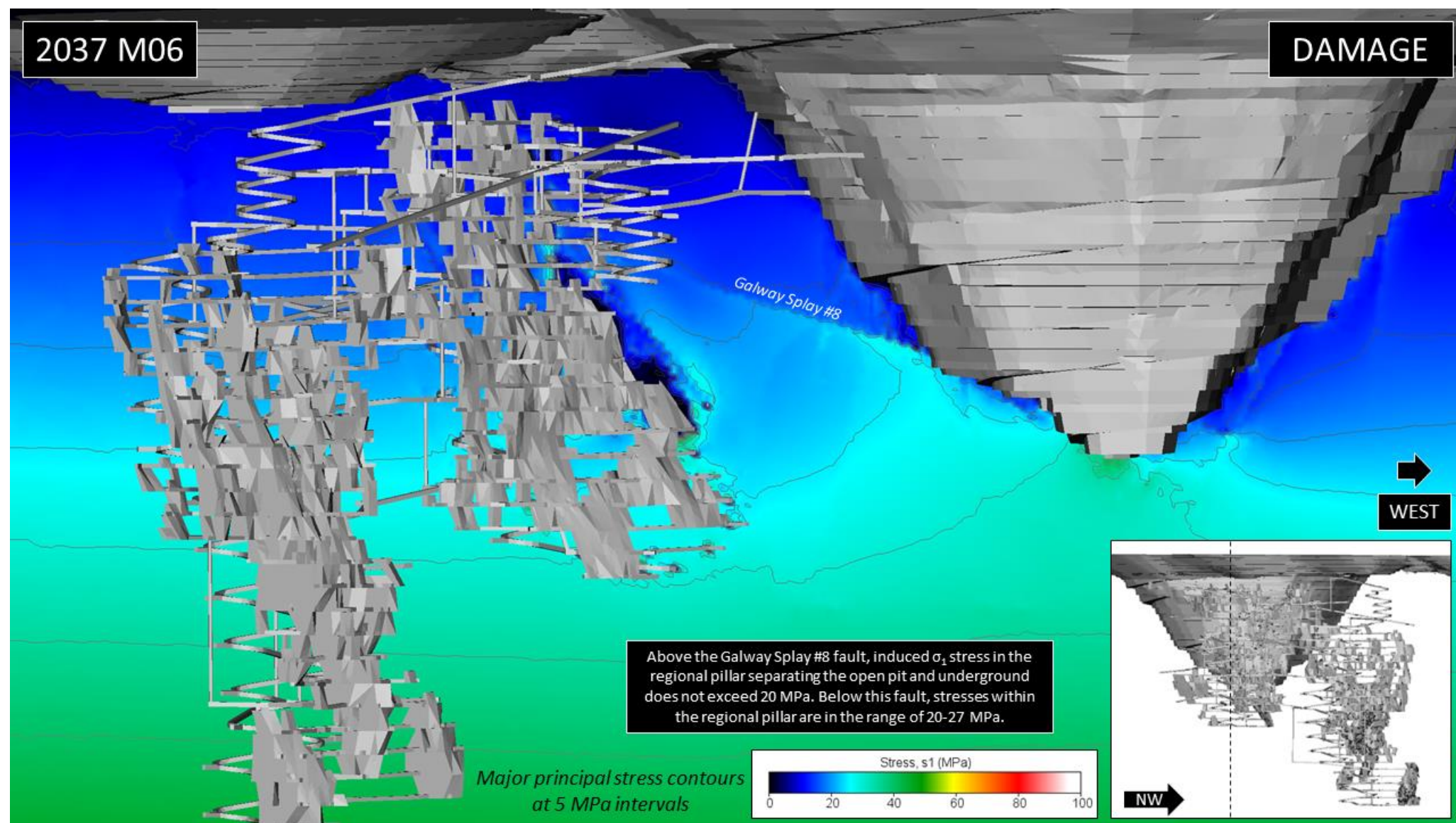


Figure 3-23 Northeast-Southwest oriented vertical section of forecast major principal stress concentrations in the regional pillar between the open pit and underground mine.

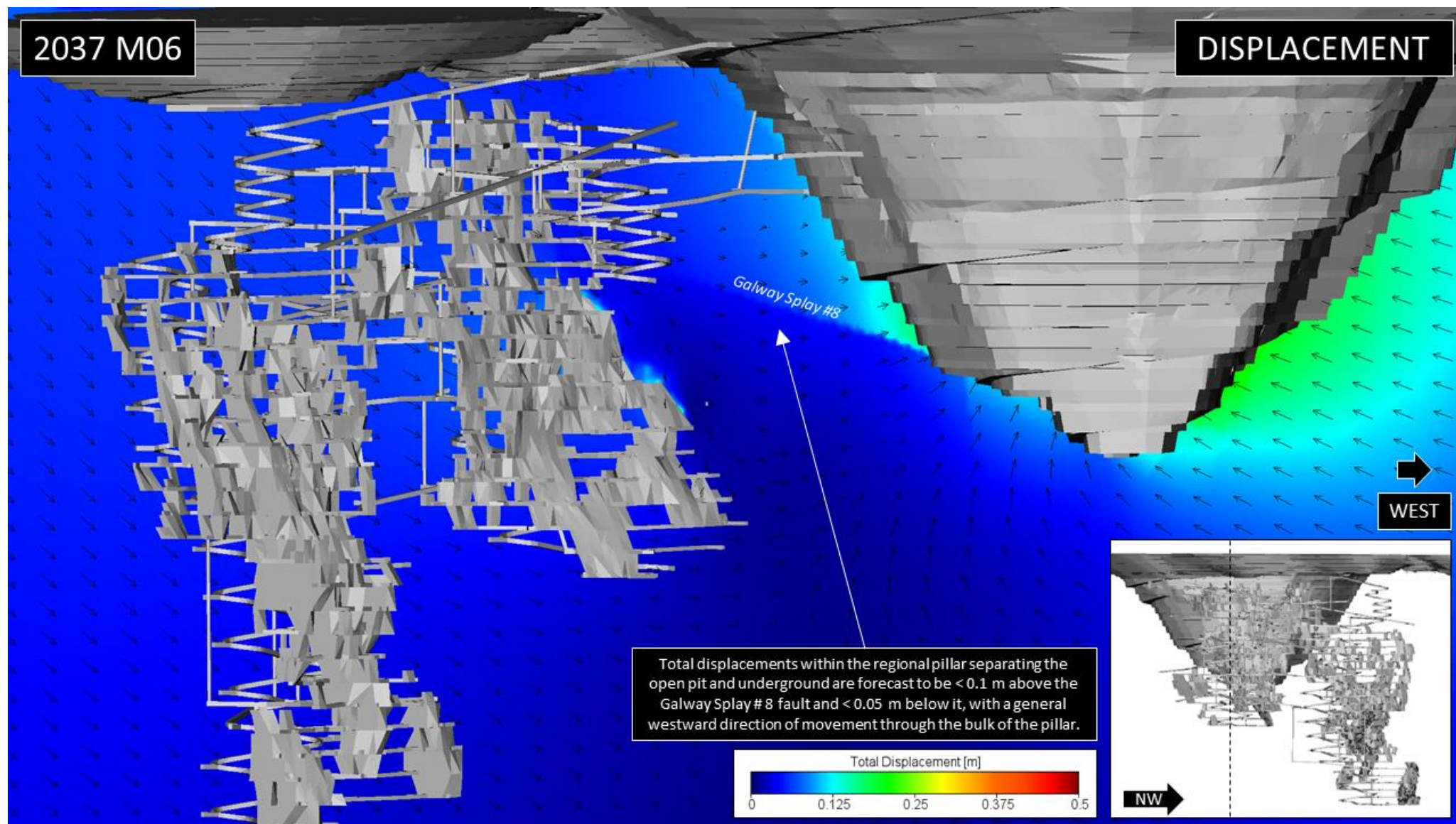


Figure 3-24 Northeast-Southwest oriented vertical section of forecast total displacement in the regional pillar between the open pit and underground mine.

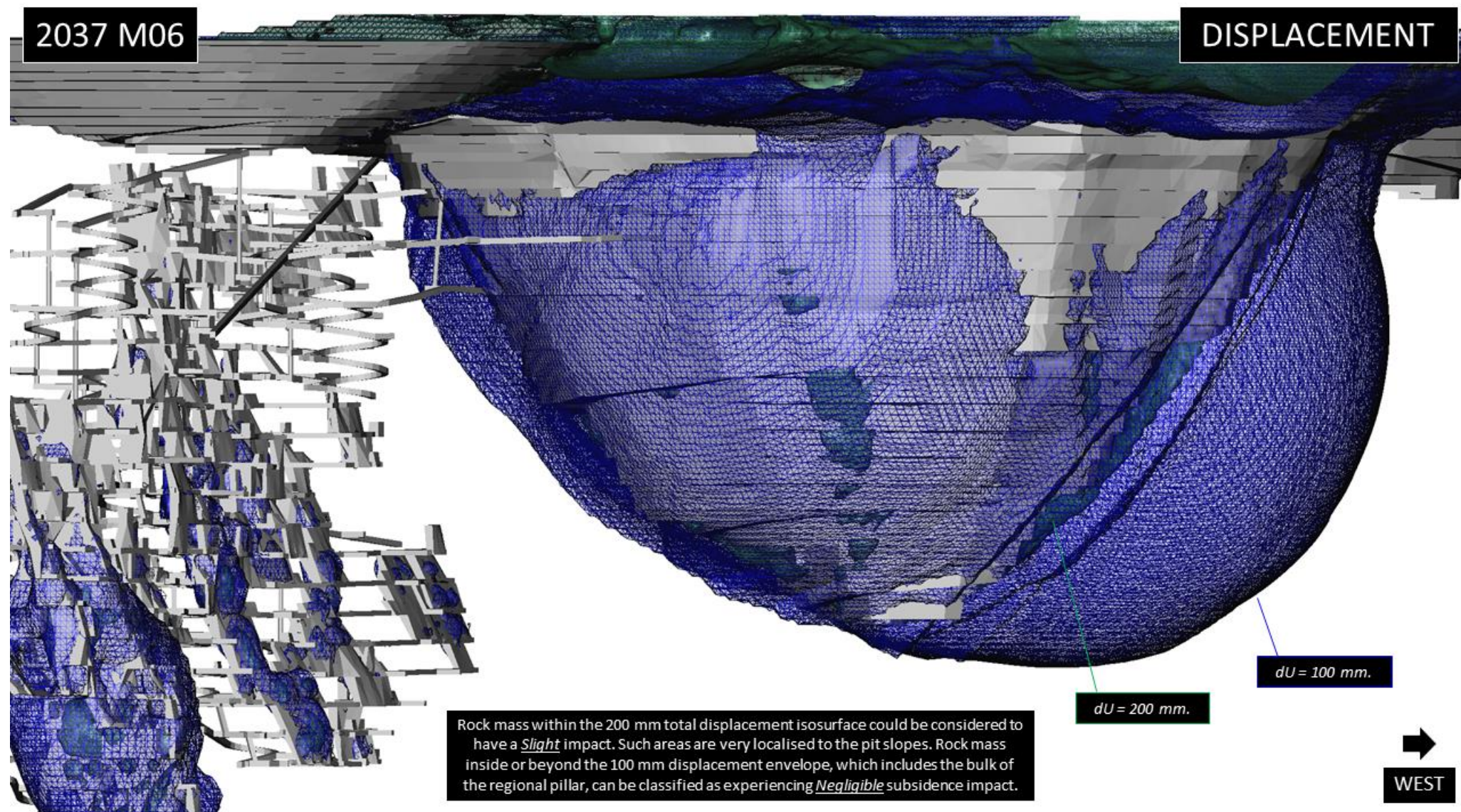


Figure 3-25 Isosurfaces of 100 mm and 200 mm total displacement surrounding the open pit and underground mines at the end of the LOM.

3.6 Asset Reports

The following asset reports presented in Figure 3-26 to Figure 3-38 summarise the forecast future trends in horizontal strain, plastic strain, total 3D displacement, angular distortion and subsidence impact classification (Harrison plot) for the natural surface topography underlying selected pieces of major infrastructure in the vicinity of the open pit mines. The charted data reflect the model forecasts sampled from the natural topography surface directly beneath the relevant asset (i.e. the original earth foundations). Table 3-1 provides the list of mining assets for which reports are provided. Additional reports for other assets not included on the list below are available from BE on request. Note: location maps in the asset reports display location coordinates in the FE model grid coordinate system (i.e. mine grid x:-86000,y:-36000,z:0)

Table 3-1 List of mine assets with detailed subsidence reports (precise locations in mine grid coordinates).

Asset Name	x	y	z
LPB #1	86382	38258	1200
LPB #2	87045	37689	1200
LPB #3	87142	37162	1200
LPB #4	87285	36357	1200
LPB #5	87441	35450	1200
LPB #6	87478	34682	1200
LPB #7	87153	34298	1200
LPB #8	86474	34397	1200
ROM Pad	85434	36025	1210
ROM Crusher	85424	35942	1210
Silos	85350	35900	1210
Ore Stockpile Cone	85419	35714	1210
Ball Mill	85220	35730	1205
Processing Plant	85300	35790	1210
D6 Pond	85220	35984	1205
Transformer Station	85205	35650	1210
Workshop	85040	35975	1210
Warehouse	85090	35710	1210
South TSF	83240	35688	1220
North TSF	83035	35985	1220

In summary:

- Based on the Boscardin & Cording (1989) subsidence impact severity classification method described in Section 2.9, all locations are forecast to experience a Negligible subsidence impact at the conclusion of the proposed mine plan in Y2037 M06.
- The model forecasts indicate that none of the listed mine assets would be affected or damaged as a direct result of open pit mining induced surface subsidence to the extent that an adverse environmental impact would occur, e.g. LPB failure, contaminant spill from surface plant etc.
- BE recommend that these asset reports be reviewed by an appropriate structural or civil engineering expert who is suitably qualified to confirm that the assets will remain within their design service limits, given the strains, displacements and angular distortions forecast by the numerical model.

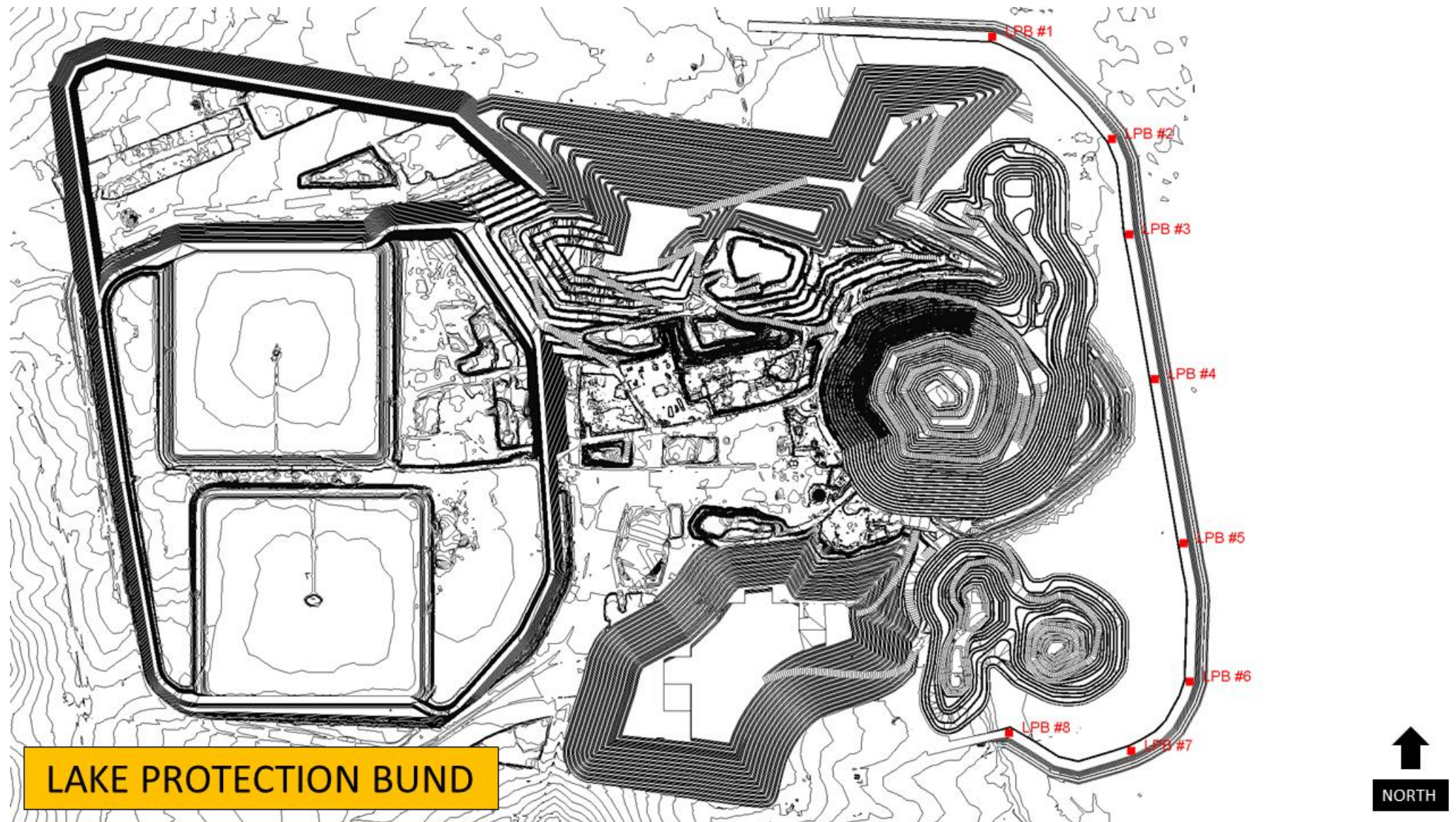


Figure 3-26 Location of asset subsidence reporting points for the Lake Protection Bund (LPB)

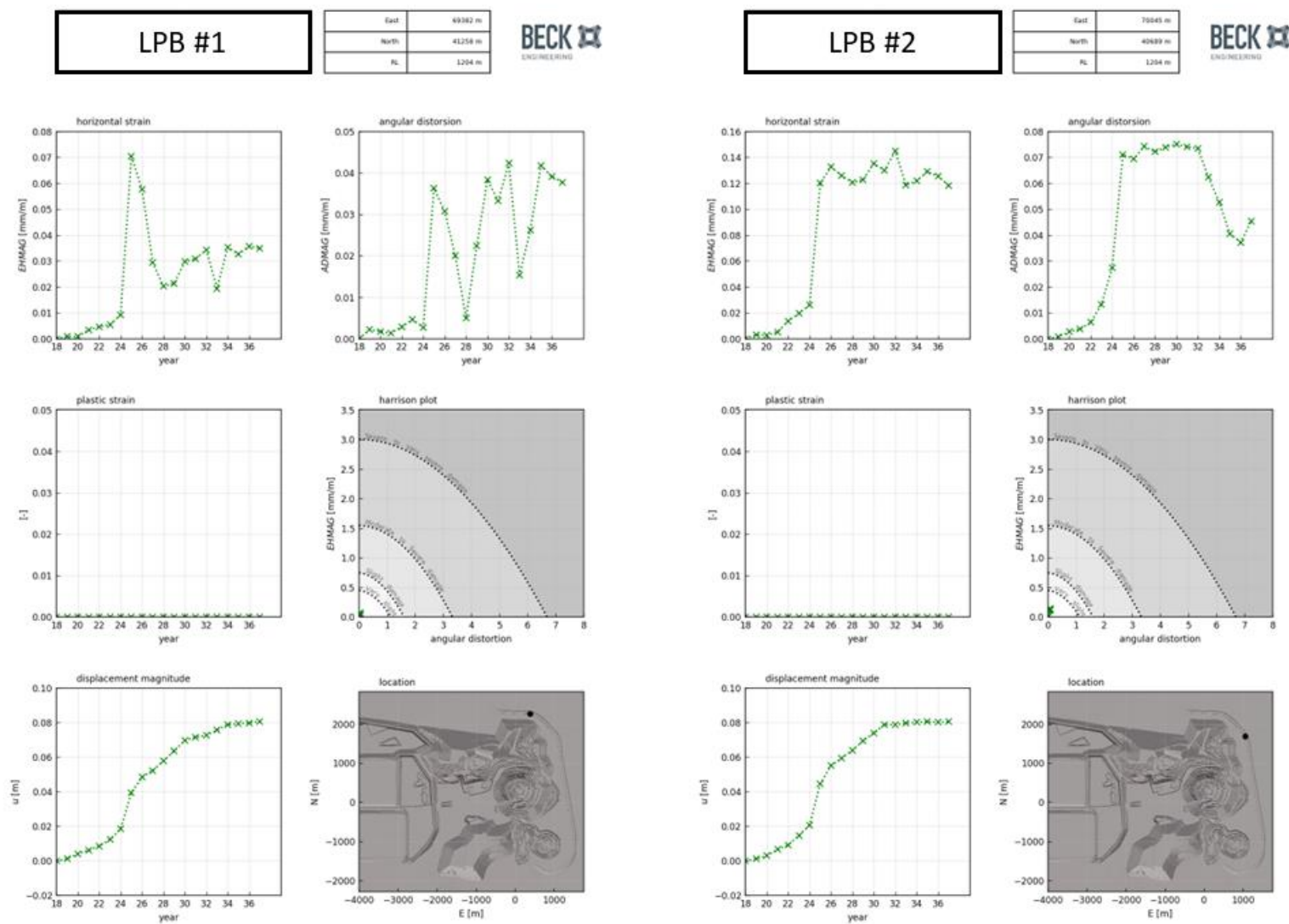


Figure 3-27 Subsidence reports for LPB #1 and #2 locations.

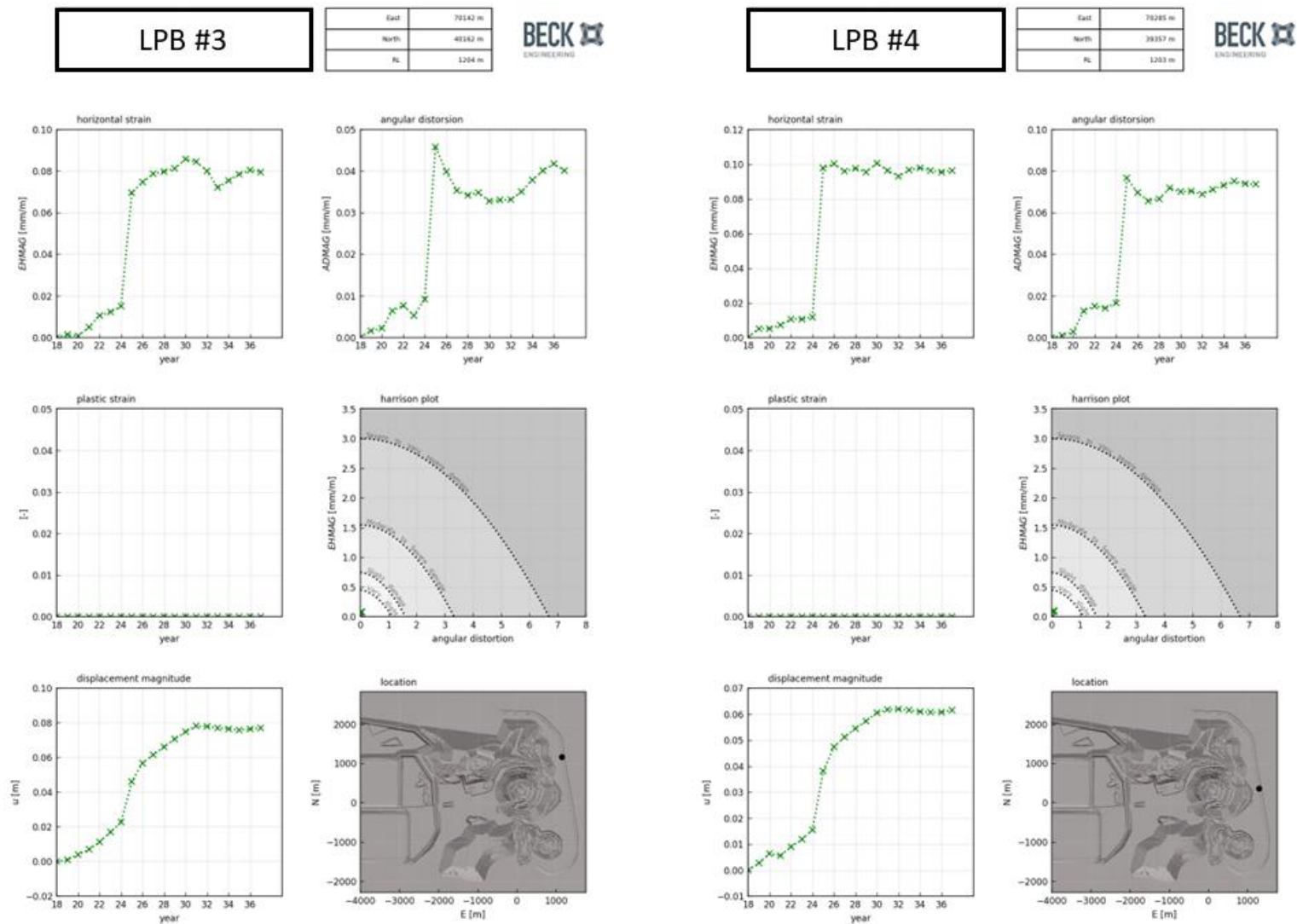


Figure 3-28 Subsidence reports for LPB #3 and #4 locations.

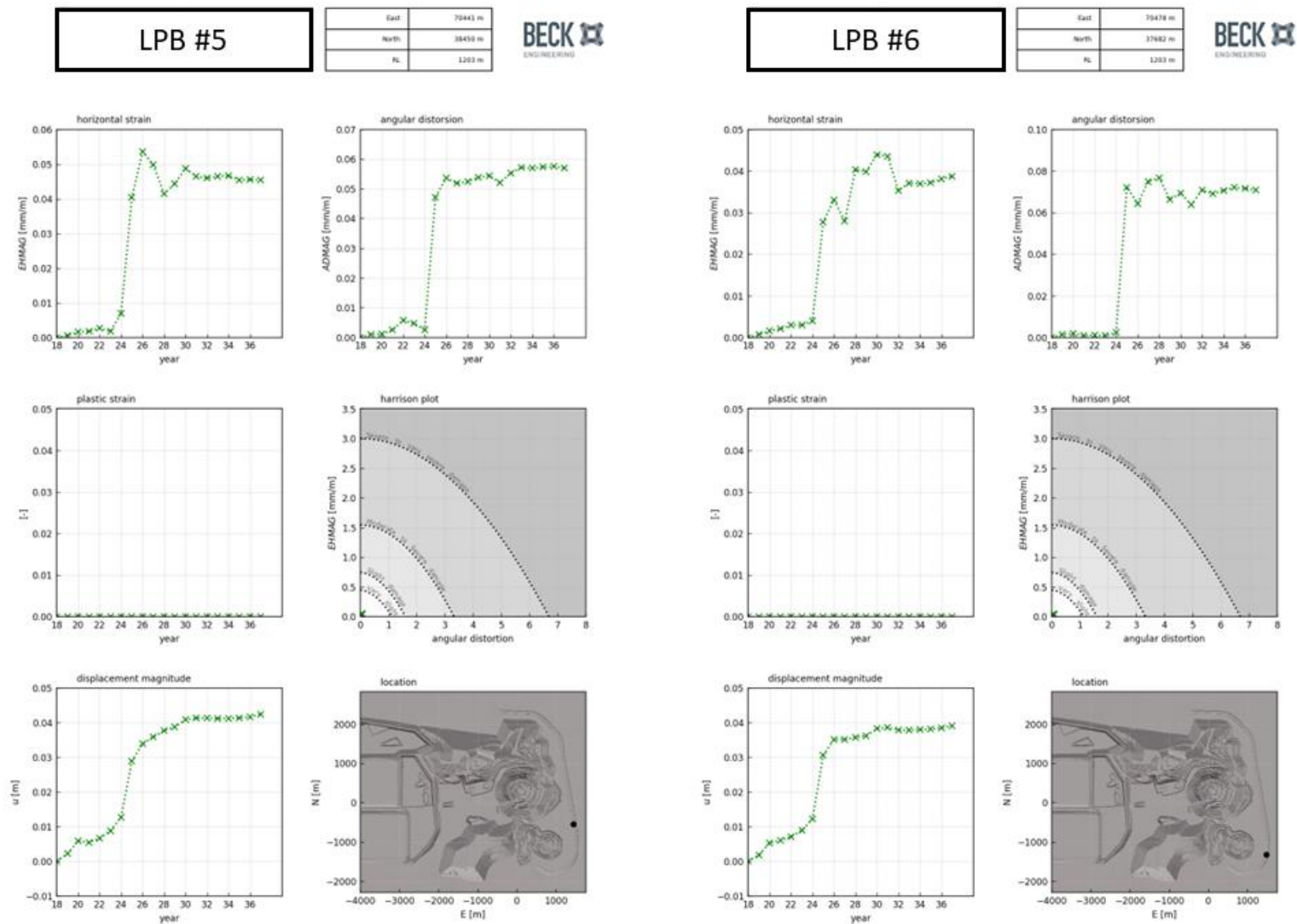


Figure 3-29 Subsidence reports for LPB #5 and #6 locations.

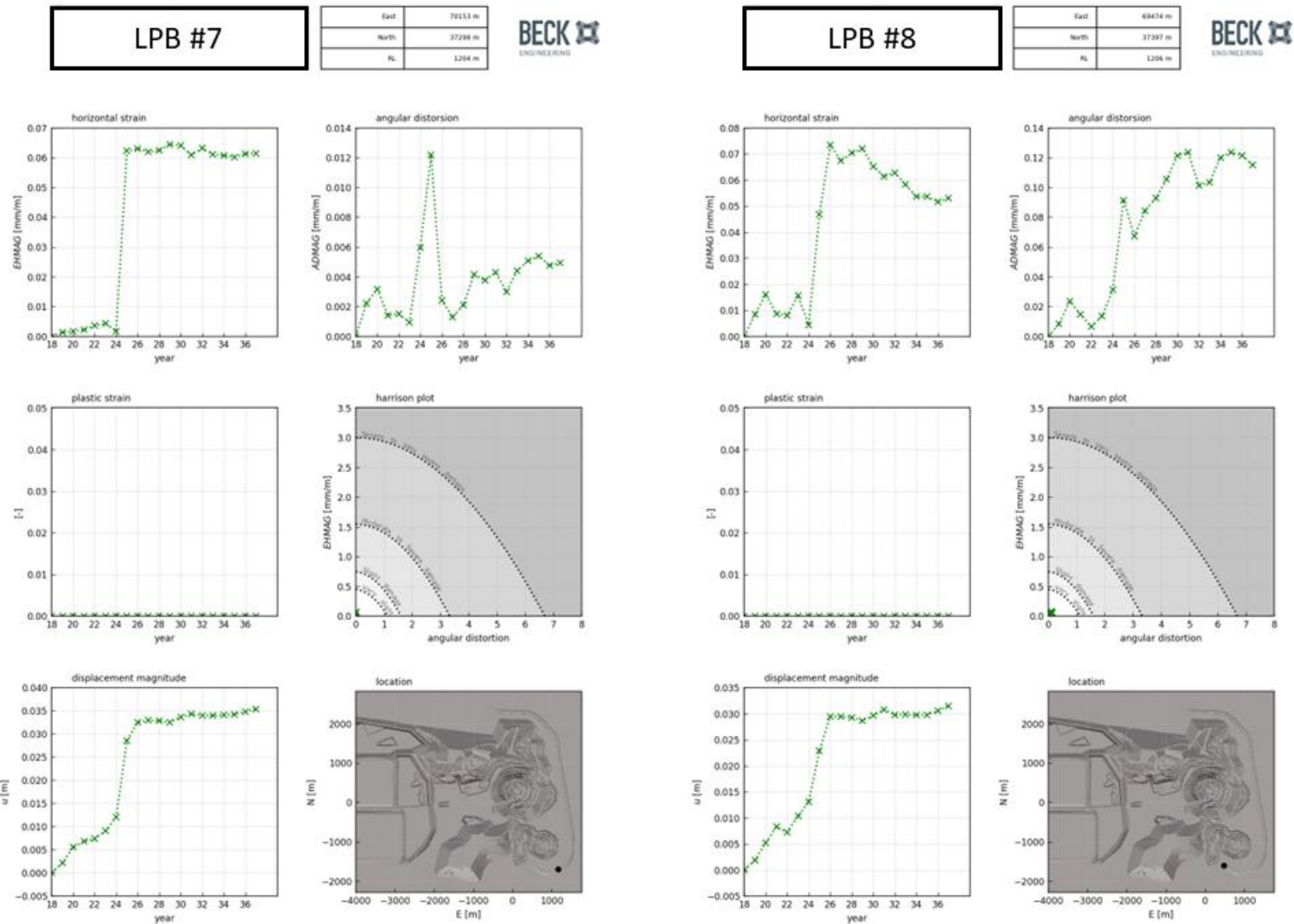
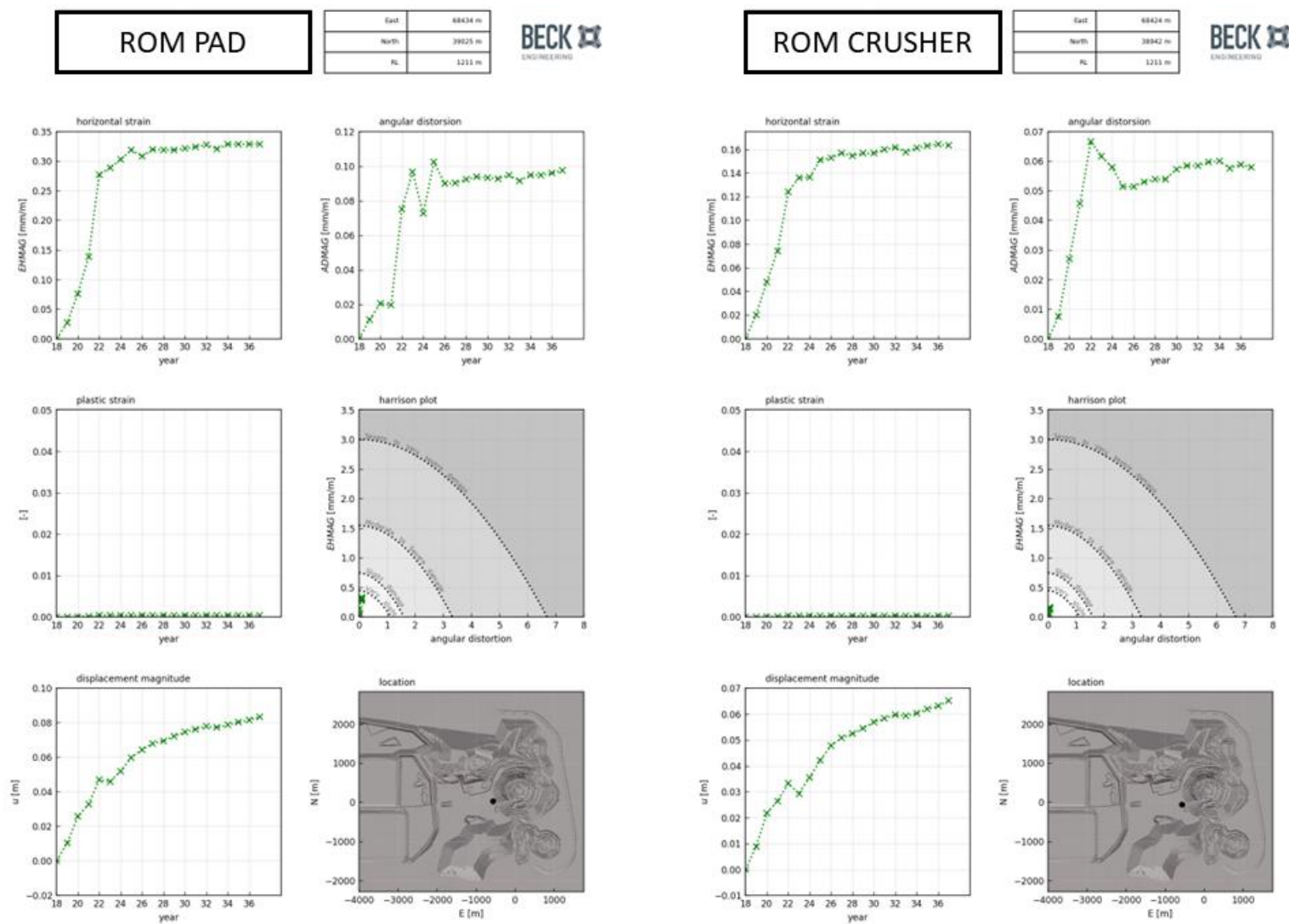


Figure 3-30 Subsidence reports for LPB #7 and #8 locations.



Figure 3-31 Location of asset subsidence reporting points for the processing plant & ROM precinct.



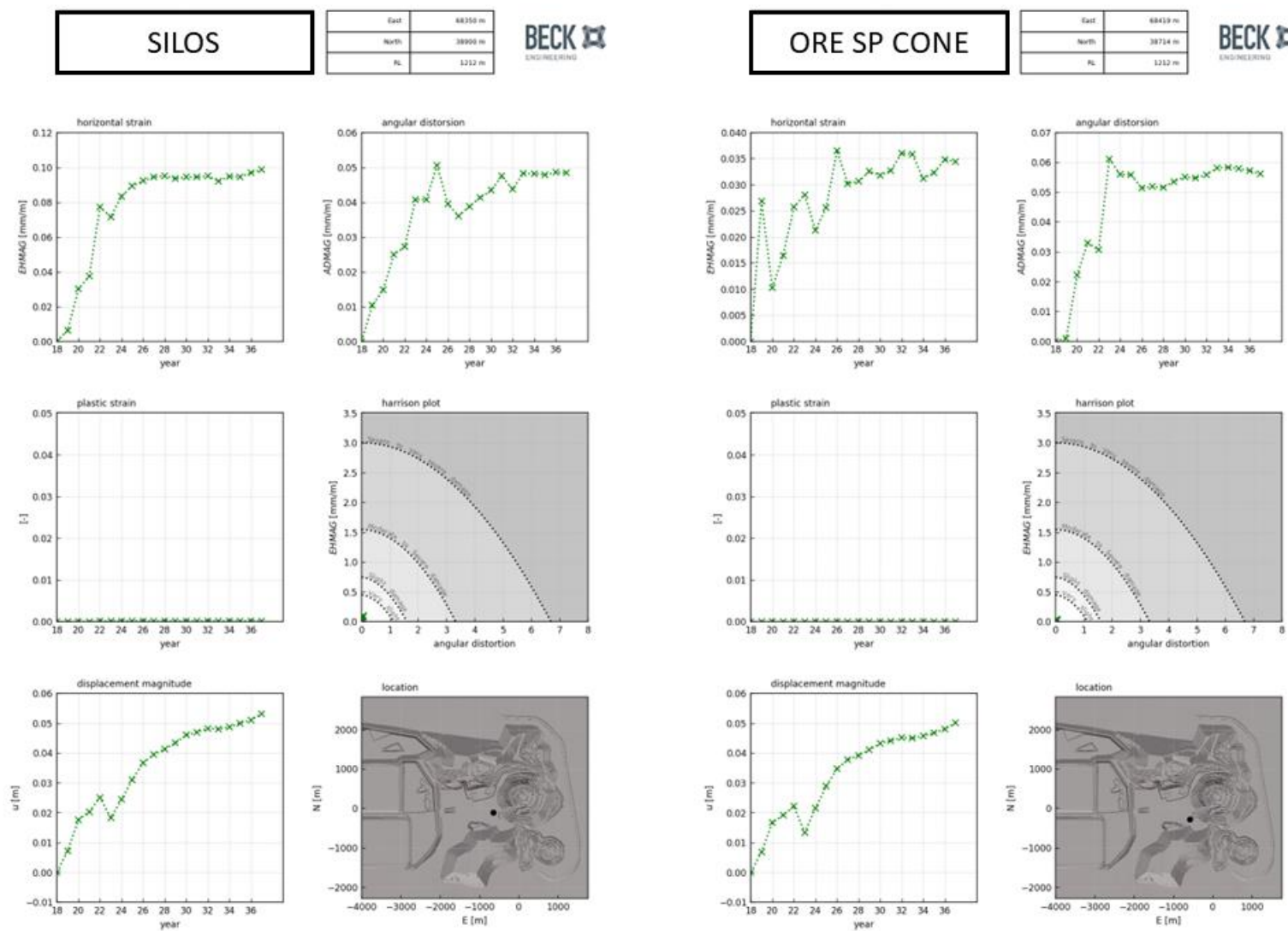


Figure 3-33 Subsidence reports for processing plant silos and ore stockpile cone.

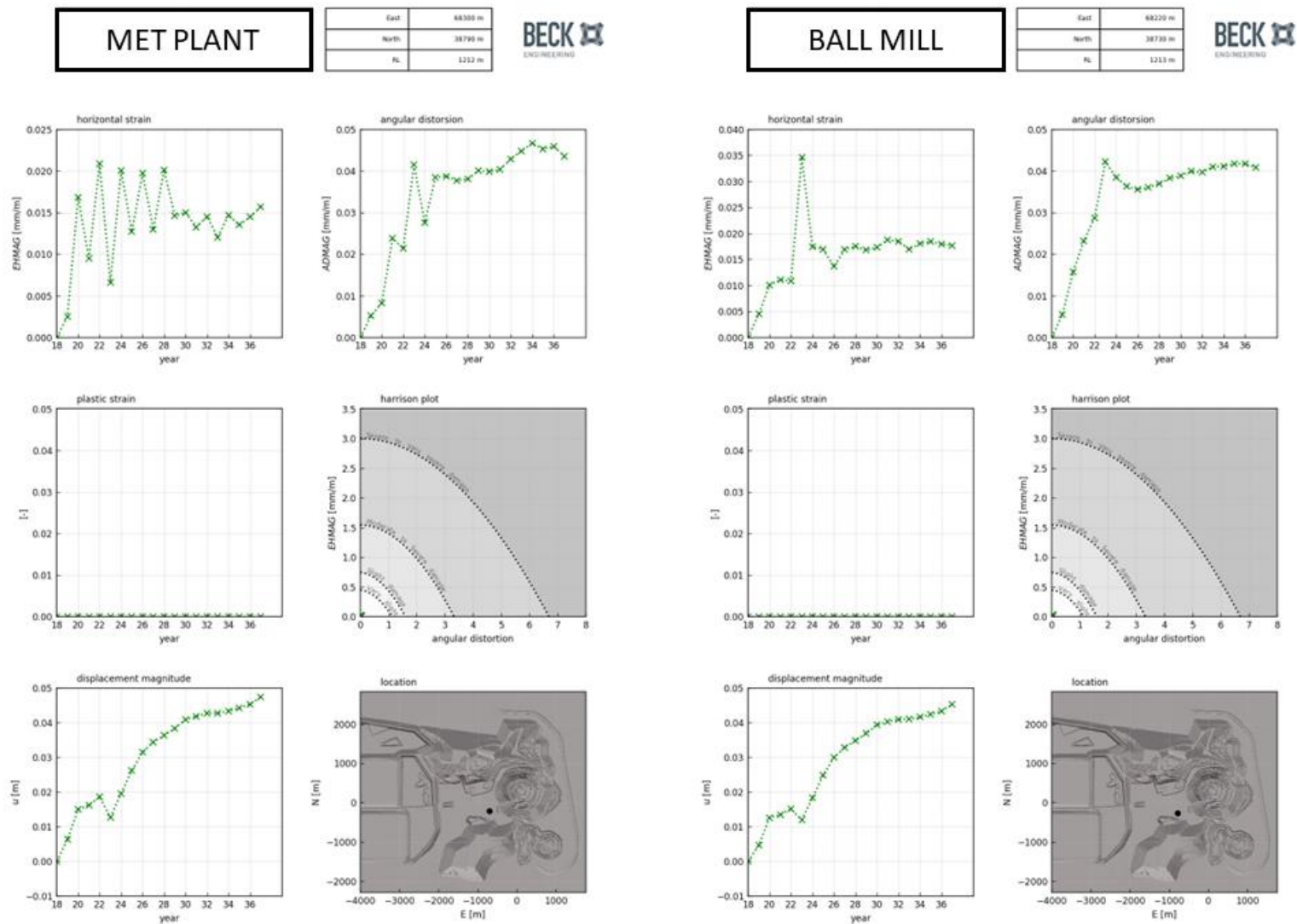


Figure 3-34 Subsidence reports for the metallurgy processing plant and ball mill.

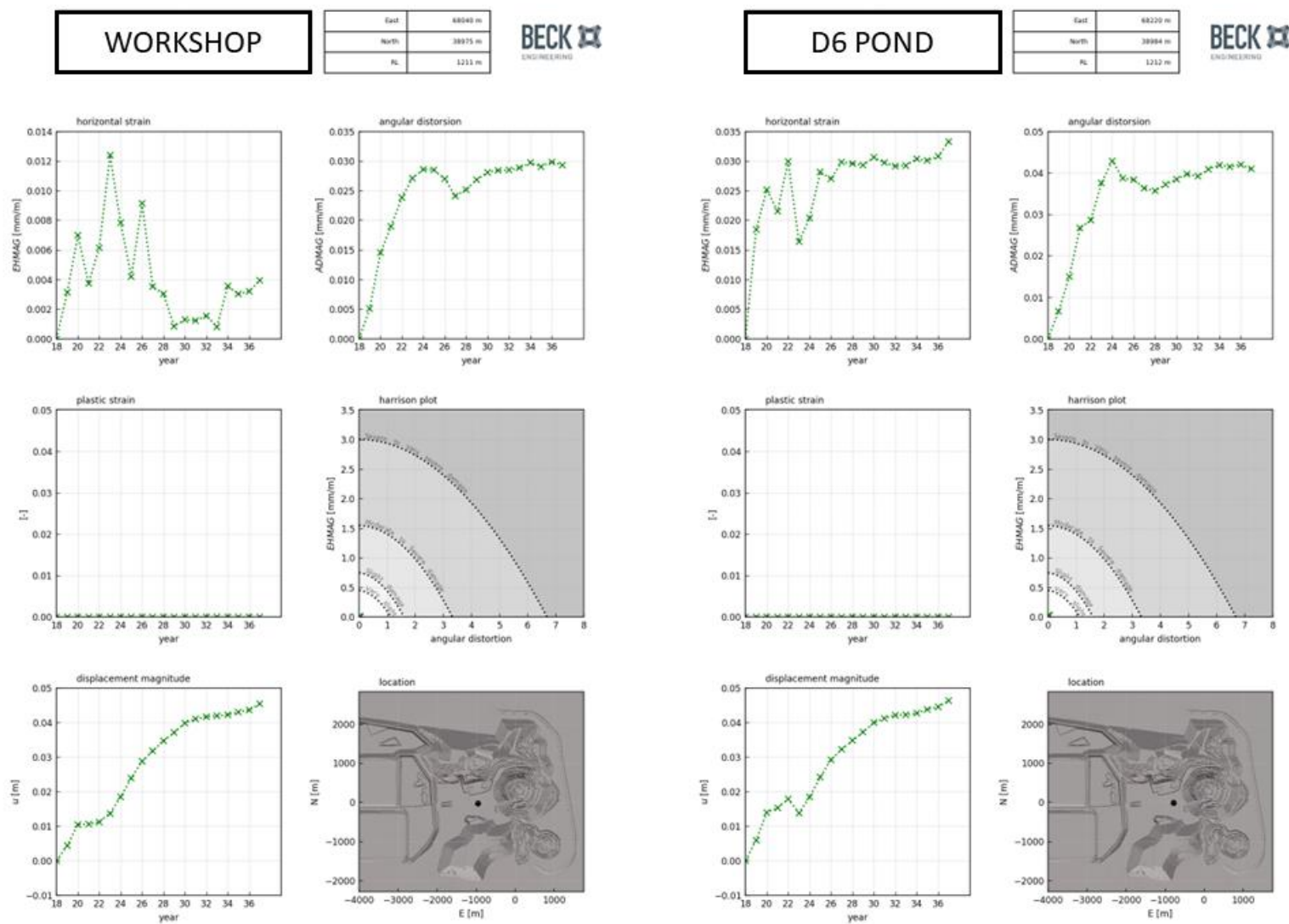


Figure 3-35 Subsidence reports for the workshop and D6 pond.

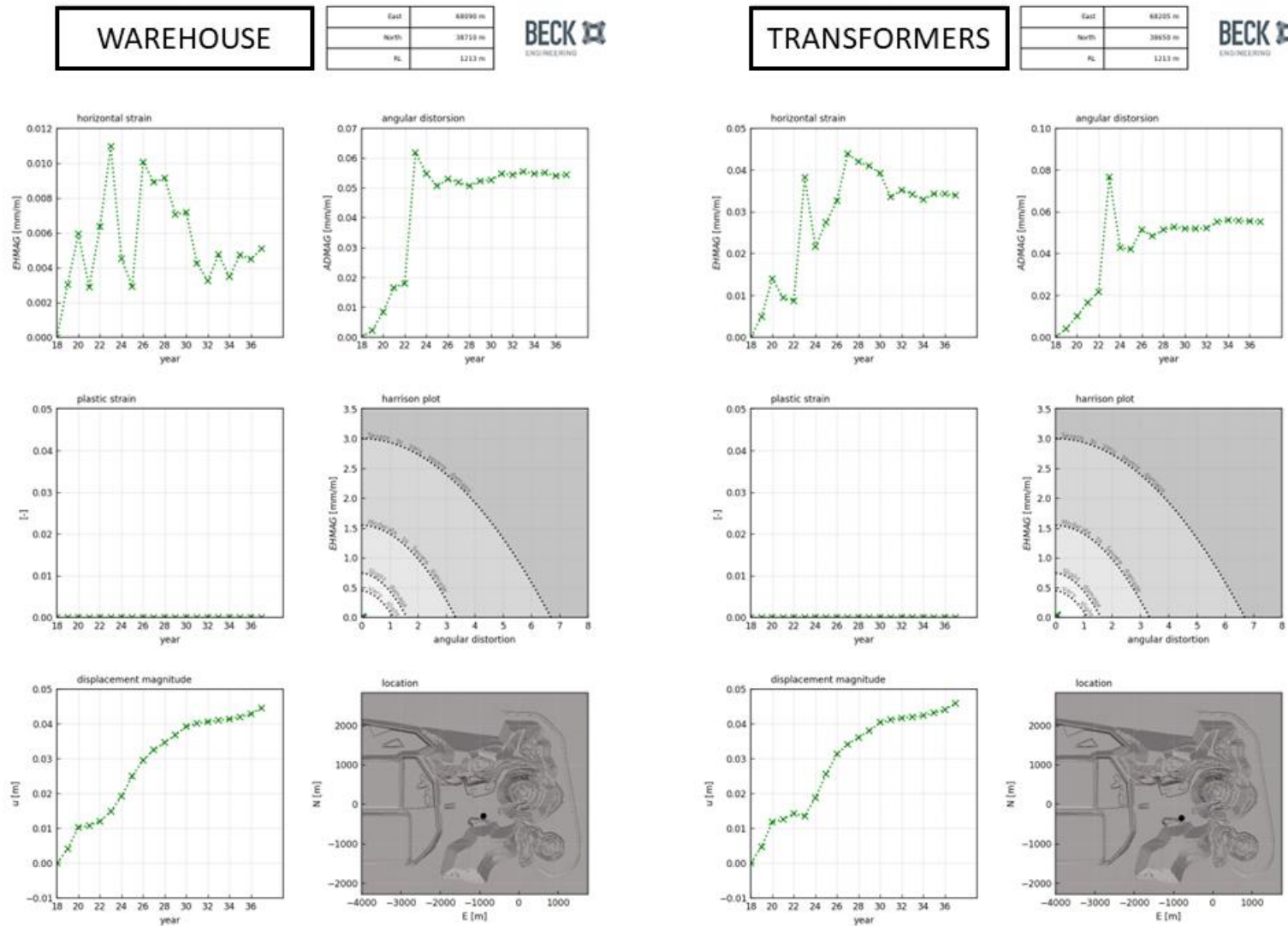


Figure 3-36 Subsidence reports for the main warehouse and surface transformer station.



Figure 3-37 Location of asset subsidence reporting points for the TSF dams.

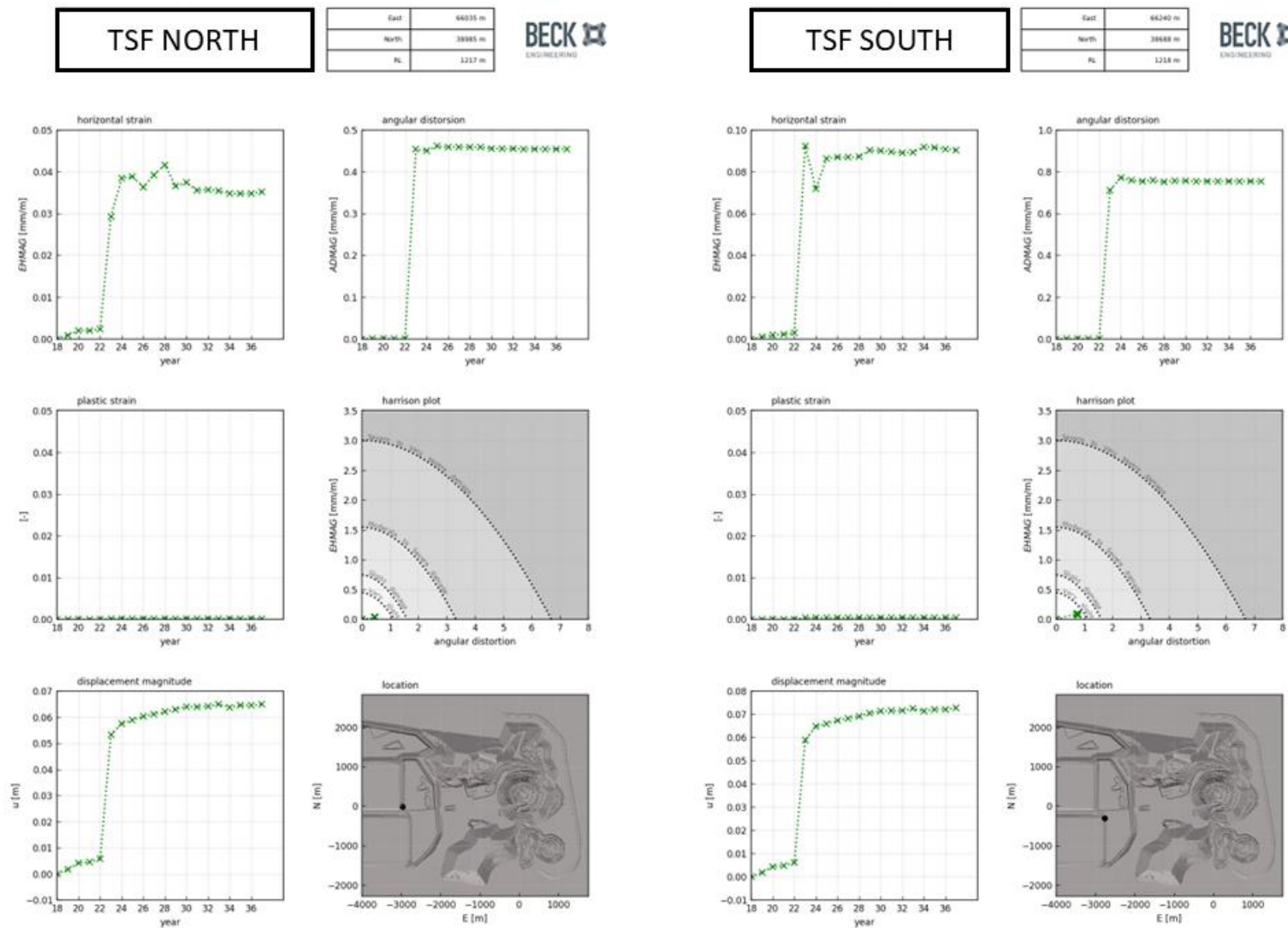


Figure 3-38 Subsidence reports for the north and south tailings storage facilities (closest points to the open pit).

3.7 Mining effect on groundwater conditions

The numerical simulation of the Lake Cowal Open Pit Expansion plan was hydro-mechanically coupled. This means that physical interactions between hydraulic and mechanical processes are considered within the discontinuum finite element model via coupling single-phase fluid flow formulations and discontinuous, strain-softening dilatant mechanical formulations. Characteristics of the local hydrogeological environment are included in the simulation, including the naturally evolving phreatic surface level as mining progresses, hydraulic conductivities of the lithologies and pore water pressure. The simulated hydrogeological characteristics of the rock mass contribute to the mechanical solutions of rock mass damage in the simulation and vice-versa. For example, pore water pressure influences the severity of rock mass damage over time, both within the rock mass continuum and within faults. Similarly, the hydraulic conductivity of the rock also changes within the simulation over time, as a function of the mining-induced rockmass fracturing.

- East-West vertical sections showing the typical simulation forecasts of hydraulic conductivity and flux before and after mining at Lake Cowal are presented in Figure 3-39 and Figure 3-40, respectively (looking south).
- The hydro-coupled simulation was run with the assumption that a constant 4 m water depth exists in Lake Cowal for the entire duration of the mine plan to 2037. This assumption is conservative.
- The model forecasts indicate that the majority of the rock mass between the mining excavations and Lake Cowal water body experiences minimal change in hydraulic conductivity or flux over the life-of-mine plan.
- There are some regions of forecast conductivity increase of up to 1.7×10^{-6} m/s within the oxide weathering domain in the immediate abutments of the open pit slopes. There are also conductivity increases in the order of 1.5×10^{-7} m/s forecast along some fault structures that also within close proximity to the open pit and/or underground workings in the upper eastern precinct of the mine (Figure 3-39). These structures are not persistent between the planned mining excavations and the lake, given the current geological understanding.
- Due to the draw-down of the phreatic surface in the vicinity of the mine, there is a forecast minor increase in the hydraulic flux from the lake towards the pit. By the end of mining in 2037 this increase in flux is in the order of 2×10^{-8} m/s (Figure 3-40).

In summary, the proposed open pit mine expansion plan is not forecast to cause any significant change in either hydraulic conductivity or flux between Lake Cowal and the mining excavations.

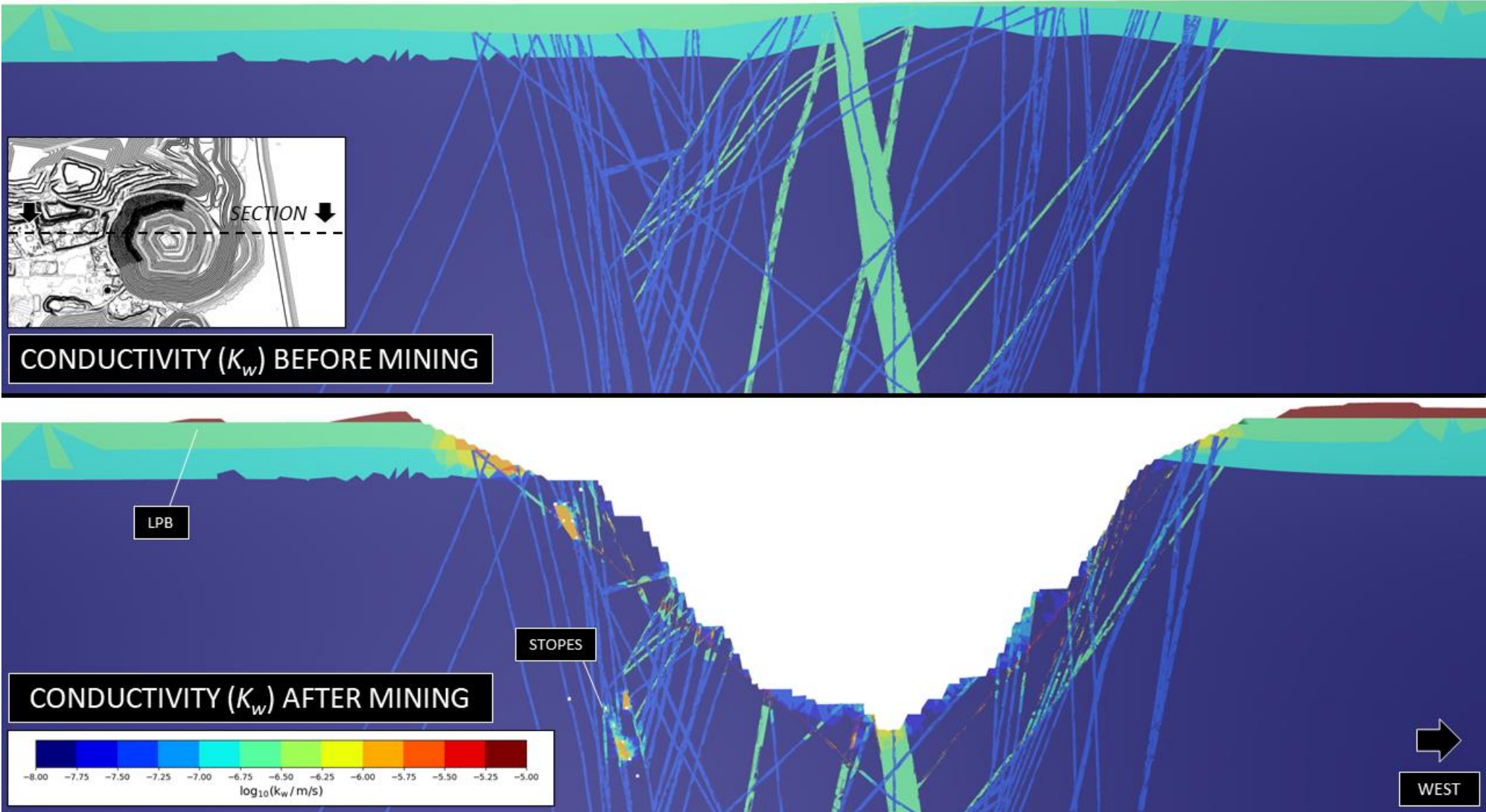


Figure 3-39 Forecast hydraulic conductivity between Lake Cowal and the orebodies before and after mining.

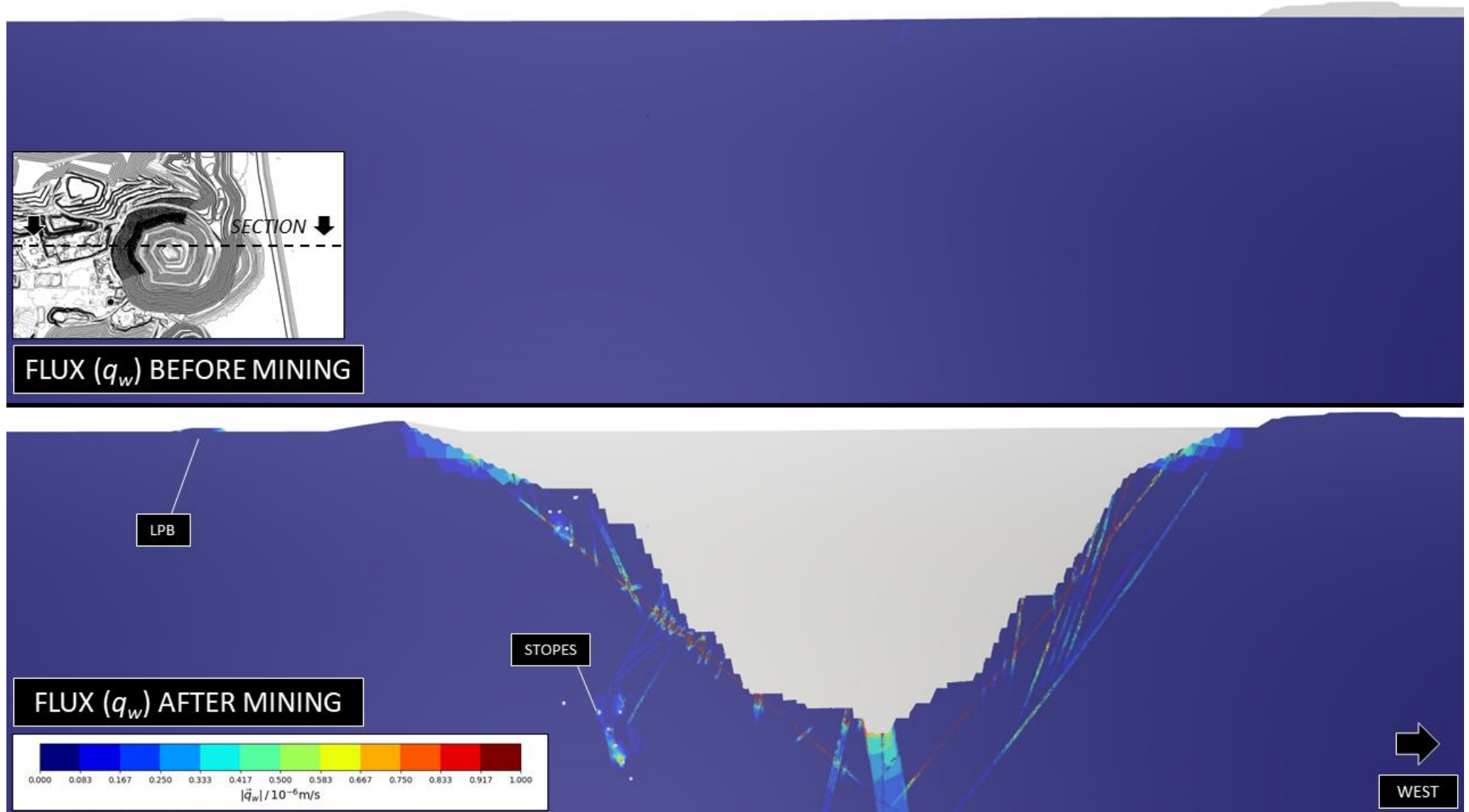


Figure 3-40 Forecast hydraulic flux between Lake Cowal and the orebodies before and after mining.

4 CONCLUSIONS, RECOMMENDATIONS & LIMITATIONS

Main findings

E42, E46 & GR Open Pits

- Vertical displacements of the original topography around the perimeter of the E42, E46 & GR open pits are forecast to be less than 0.1 m at the end of the mine plan (Y2037 M06). The direction of the forecast displacements of the pit walls is uplift. This is a typical response for large open pit mines as the overburden load is removed from the slopes over time.
- The forecast open pit mining-induced surface displacements and rockmass damage around the perimeter of the E42, E46 & GR open pits can be classified as Negligible and of a magnitude which would not present any visible evidence of disturbance to the natural topography or man-made features outside the pits. Displacements beyond the crest of the open pits are elastic in nature and near-zero. No plastic (i.e. permanent) rock mass damage is forecast beyond the crest of the pits at the natural surface level and therefore no visible surface cracking or other forms of visible damage are expected to occur.
- Rock mass damage of a Significant nature within the E42 pit is concentrated along the major faults in the oxide domains and along the Central Shear zone, including areas of the fresh rock slope both above and below the planned haul ramp in the north wall. The damage is not forecast to extend beyond the crest of the open pit and would therefore not affect surface terrain or infrastructure.
- The E46 pit slopes accumulate a higher severity of rockmass damage than the other open pits due to the slope loading effect of the E46 in-pit backfilling, which takes place during 2031/32. However, as the slopes are confined by that backfill, there would be no adverse subsidence or slope instability as a result.
- Potential for minor subsidence events in the E46 in-pit backfill material exists if weak oxides or other fine materials are deposited above coarser fragmentation backfill, such as fresh rock fill. This could occur if the overlying finer fill materials migrate through the coarser underlying fill over time, due to either water or gravity-driven vertical movement of the fines within the pore space of the coarse fill zones. These risks can be reliably avoided if a consistent source of backfill is utilised for the E46 in-pit backfilling campaign.
- The 36 degree final slope angle assumed for the E46 backfill slope may be too steep to achieve, as some damage is assumed in the model. However, in reality the tipped fill material would naturally rill to a stable slope angle.

E41 Open Pit

- Mining of the E41 open pit is not forecast to generate total displacements exceeding 0.1 m anywhere beyond the physical limits of the pit itself. The small magnitude elastic displacements at the surface are insufficient to cause visible subsidence effects or any permanent damage, such as tension cracking or ground depressions.
- Within the pit, maximum horizontal displacements of the slopes are forecast to approach 0.15 m in three locations within the Soft Oxide domain. This is a Negligible magnitude of displacement and primarily related to uplift of the slopes due to overburden removal, not subsidence or slope instability. Total displacements of the E41 pit slopes approach 0.3 m within the Soft Oxides only. This is also related to uplift of the slopes during overburden removal, not subsidence.
- There are total (i.e. 3D) displacements approaching 0.2 m to the immediate north of the E41 pit, through the permanent bridging pillar of rock that separates the E41 pit from the E42. These displacements are also classified as Negligible.

Lake Protection Bund & Other Infrastructure

- The final lake protection bund (LPB) and vast majority of the surface, including the processing infrastructure precinct, are forecast to experience a Negligible subsidence impact as a result of the proposed open pit mine plan. A Very Slight impact is forecast to affect a minority of the ROM Pad to the west of the final E42 pit, but the effect is unlikely to present as any visible subsidence damage or lead to any adverse consequences.
- Vertical displacements of the natural topographic surface of up to 0.5 m are forecast to occur during the deposition of the waste dumps (NWRD and SWRD) to the northwest and southwest of the open pits. These

displacements are caused by the overburden load applied to the weak and weathered cover sequence materials at the surface. They are not a result of open pit mining-induced subsidence. The displacements only affect the ground beneath the waste dumps and do not extend outwards to affect any nearby areas.

Effect of Mining on Groundwater Conditions

- The numerical simulation of the Lake Cowal mine plan was hydro-mechanically coupled. This means that groundwater characteristics of the local geological environment, such as the phreatic surface level, hydraulic conductivity and pore water pressure, and their effect on the rock mass, were included in the mechanical solutions of the simulation. The action of groundwater and pore water pressure within the model space influences the mining-induced rock mass damage. Similarly, the simulated hydraulic conductivity of the rock does change over time, as a function of the mining-induced rockmass fracturing.
- The model forecasts indicate that the majority of the rock mass between the mining excavations and Lake Cowal water body experiences minimal change in hydraulic conductivity or flux over the life-of-mine plan.
- There are some regions of forecast conductivity increase of up to 1.7×10^{-6} m/s within the oxide weathering domain in the immediate abutments of the open pit slopes. There are also conductivity increases in the order of 1.5×10^{-7} m/s forecast along some fault structures that are within close proximity to the open pit and/or underground workings in the upper eastern precinct of the mine. These structures are not persistent between the planned mining excavations and the lake, given the current geological understanding.
- Due to the draw-down of the phreatic surface in the vicinity of the mine, there is a forecast minor increase in the hydraulic flux from the lake towards the pit. By the end of mining in 2037 this increase in flux is forecast to be in the order of 2×10^{-8} m/s.
- Overall, the proposed open pit mine expansion plan is not forecast to cause any significant change in either hydraulic conductivity or flux between Lake Cowal and the mining excavations.

Main geotechnical risks

- The main geotechnical risk affecting surface subsidence and relating to open pit mining is a large-scale instability of the pit slope which either undermines or causes displacement of the surface terrain. Such an event is likely to be either a circular failure through the near-surface weathered rock material or else structurally controlled. In the worst case, the affected area would be unlikely to extend more than several tens of metres from the pit crest limits at the time. The mine already has a detailed structural model, which includes many major faults through the open pit precinct and these have been included in the numerical simulation. The existing geology knowledge and simulation results, which indicate that the pit crest region will remain stable, both reduce the probability of an unforeseen slope instability event occurring. Further structural data collection, interpretation and model updates are recommended to be conducted on an ongoing basis during mine planning and operations.

Recommendations

- Engage a qualified structural or civil engineer to review the following detailed subsidence forecasts for all pieces of major mining-related infrastructure, including but not limited to the final LPB, major plant in the processing precinct and tailings storage facilities etc, in order to confirm that the forecast strains, displacements and angular distortions do not exceed the service limits of any assets.
- Review and where necessary update the underground mine design to ensure that no stopes are excavated beneath the open pit with a fresh rock crown pillar height of less than 20-30 m (i.e. maintain a minimum stope width to fresh rock crown pillar ratio of 1:2). Where any non-compliant stopes do exist in the mine plan, remove them. BE re-iterate the recommendations made previously by Campbell (2020) in relation to subsidence interactions between the underground and open pit vicinity.
- When backfilling the E46 open pit, consider the fill material types used and the sequence of the deposition in order to avoid creation of voids within the fill, which might lead to subsidence over time. Ideally, fill material(s) with minimal porosity should be used to backfill the E46 pit.
- In order to mitigate and contain any potential slumping of the E46 final backfill slope, it is recommended to construct fresh rock bunds at the toe of the slope.

- Continue and expand the open pit slope displacement and groundwater monitoring activities at the mine in order to record trends as the open pit increases in size and to periodically evaluate those trends against the numerical model forecasts. Valuable future data collection programs would include some or all of the following: pit slope radar, prism monitoring, INSAR displacement surveys of the entire mining lease, GPS survey stations around the pit crest and critical/valuable assets, piezometers in the local bore network to record groundwater elevation changes etc.
- Continue to collect and interpret rock mass characterisation data from the open pit and underground mining domains, especially regarding the strength properties of the various lithologies as well as the location, orientation and characteristics of the geological structures (i.e. mine scale faults, shears, intermediate scale faults and small scale joint sets). Use this information to inform future slope stability and hydrogeology assessments.

Limitations

In addition to the normal resolution limits associated with the current finite element model, the main limitations of this project are:

- The current understanding of rockmass strength and its' spatial variability, which affects forecasts of damage.
- The resolution and accuracy of the structural model, including the large and intermediate scale discontinuities which may affect the performance of the excavations.
- Knowledge of the hydrogeological characteristics of the Lake Cowal site, including conductivity and storativity parameters of the orebody, nearby host rock and faults, the location and characteristics of local aquifers and aquitard structures, and also the nature of the groundwater sources and sinks, such as inflow/outflow rates.

Enquiries

Please direct further enquiries to the undersigned.



Christopher Drover

PhD MEngSc BE (Hons) BSc

Principal Engineer, Mining & Rock Mechanics

5 REFERENCES

- Best, R., 2008. *Cowal Gold Mine - Pit Dewatering Assessment*, Technical Report to Barrick: Coffey Geotechnics, Sydney, Australia.
- Bird, F. & Hulls, I., 2020. *Cowal Gold Mine Stress Testing Summary*, Technical report to Evolution Mining Ltd: Mining One Consultants, Melbourne, Victoria.
- Boscardin, M. & Cording, E., 1989. Building response to excavation-induced settlement. *Journal of Geotechnical Engineering*, 115(1).
- Campbell, A., 2020. *Geotechnical assessment of surface impacts for proposed underground mining at Lake Cowal*, Technical report to EMM & Evolution: Beck Engineering, Brisbane, Australia.
- Flatten, A., Reusch, F. & Beck, D., 2016. *The application of hydromechanical mine-scale modelling for large block caving operations*. Proceedings of the Seventh International Conference & Exhibition on Mass Mining, Sydney, NSW, 9-11 May 2016, pp. 341-347.
- Lee, M., Mollison, L., Campbell, A. & Litterbach, N., 2010. *Rock Stresses in the Australian Continental Tectonic Plate - Variability and Controls*. 11th IAEG Congress - Geologically Active New Zealand, September 2010.

6 APPENDIX A - LRX CONSTITUTIVE FRAMEWORK

6.1 Constitutive model and physical composition

6.1.1 The LR2 constitutive framework

The Levkovitch-Reusch 2 (LR2) constitutive framework is a package of tools that describe the stress-strain behaviour of rockmasses and structures. The main features of LR2 are:

- The continuum regions of the rockmass are modelled as strain-softening dilatant materials. This means that as strain increases the material softens, weakens and dilates. All parameters can vary at different rates with respect to strain changes, and this allows approximation of complex stress-strain behaviour of real rockmasses. A generalisation of the Hoek-Brown yield criterion (Hoek et al. 2002) was used for the continuous regions of the rockmass, as described below.
- The behaviour of explicit discontinuities is approximated using cohesive elements. These elements are used because they can capture the mechanical response of thin structures at large deformations, which normal tetrahedral finite elements cannot achieve effectively. Cohesive elements allow simulation of the discrete behaviour associated with structures and can be used to construct a rockmass model compromising continuum regions separated by discontinuities. The structures are free to dislocate, dilate and degrade.
- Small scale structures can be represented in detailed models explicitly as cohesive elements, or ubiquitously by smearing the effects of the joints within the continuum parts of the rockmass.
- Tetrahedral higher-order elements are used for the discretization of the model geometry. These are considered essential for FE models where large gradients of displacements and damage are expected.
- The LR2 framework includes provision for hydromechanical coupling when necessary, which means that the material constitutive equations (governing mechanical behaviour) are solved at the same time as the equations governing fluid flow in porous media (Darcy's equation), or solved in sequential or staggered incremental schemes, depending on the problem. This means that the modelling framework can capture the effects of pore water pressure on the strength of the rock (as may be caused by groundwater percolation through the rockmass itself).
- Seismic potential can be assessed by considering the modelled rate of energy release (RER), which is the maximum instantaneous rate of energy release within a unit volume during a model frame. RER can be correlated with seismic potential and has been successfully applied to forecast seismic potential in several projects. This requires calibration using seismic data for quantitative evaluations of seismic potential.

Model outputs include displacement, stress, strain and pore water pressure fields, where the presence of pore-water pressure is implemented. Plastic strain, reported as the plastic strain tensor or as scalar equivalent plastic strain measure, represents the amount of plastic rockmass deformation after yield. The plastic strain can be interpreted as rockmass damage and usually correlates well with most engineers' visual interpretation and intuitive understanding of rockmass damage. BE's damage scale is based on plastic strain (see further below how modelled rockmass damage can be interpreted).

6.2 Constitutive model for the continuum parts

The relation between stress, strain, strength and degradation is described by the constitutive model. Generally, constitutive models consist of 3 main parts:

- (i) a stress dependent yield criterion,
- (ii) a plastic strain potential, which describes how the material will deform as a consequence of changes in stress due to damage and
- (iii) a description of how stress and strain are related.

In the LR2 framework, a generic yield criterion is used that can approximate almost any common rock mechanics yield criterion. In BE models, Hoek-Brown is applied as the base case for most problems.

The starting point for the generic criterion that can approximate Hoek Brown, Mohr coulomb or other criteria is the Menetrey/Willam strength criterion (1), described by the following function.

$$\left[\frac{q}{\sigma_{ci}}\right]^2 + m \left[\frac{1}{3} \frac{q}{\sigma_{ci}} R(\theta, e) - \frac{p}{\sigma_{ci}}\right] - s = 0 \quad \text{A.1 1}$$

The material constants s and m are the measures of the cohesive and frictional strength, and σ_{ci} represents the uniaxial compressive strength of intact rock. Further,

$$p = -\frac{1}{3} \mathbf{I} \cdot \boldsymbol{\sigma} \text{ is the hydrostatic pressure,}$$

$$q = \sqrt{\frac{3}{2} \mathbf{S} \cdot \mathbf{S}} \text{ is the Mises equivalent stress and}$$

$$r = \left[\frac{9}{2} \mathbf{S} \cdot (\mathbf{S} \mathbf{S}) \right]^{1/3} \text{ is the third stress invariant}$$

with \mathbf{S} being the deviatoric part of the Cauchy stress $\boldsymbol{\sigma}$. The dependence on the third invariant is introduced via the convex elliptic function in the deviatoric stress plane

$$R(\theta, e) = \frac{4(1-e^2) \cos^2 \theta + (2e-1)^2}{2(1-e^2) \cos \theta + (2e-1) \sqrt{4(1-e^2) \cos^2 \theta + 5e^2 - 4e}} \quad \text{A.1 2}$$

Here, the variable θ , defined via $\cos 3\theta = (r/q)^3$, is the deviatoric polar angle (also known as Lode angle) and the material constant e is the deviatoric eccentricity that describes the "out-of-roundedness" of the deviatoric trace of the function $R(\theta, e)$ in terms of the ratio between the Mises stress along the extension meridian ($\theta = 0$) and the compression meridian ($\theta = \pi/3$). For $\theta = 0$ and $\theta = \pi/3$ the function becomes $1/e$ and 1 respectively. The convexity of $R(\theta, e)$ requires that $0.5 \leq e \leq 1$.

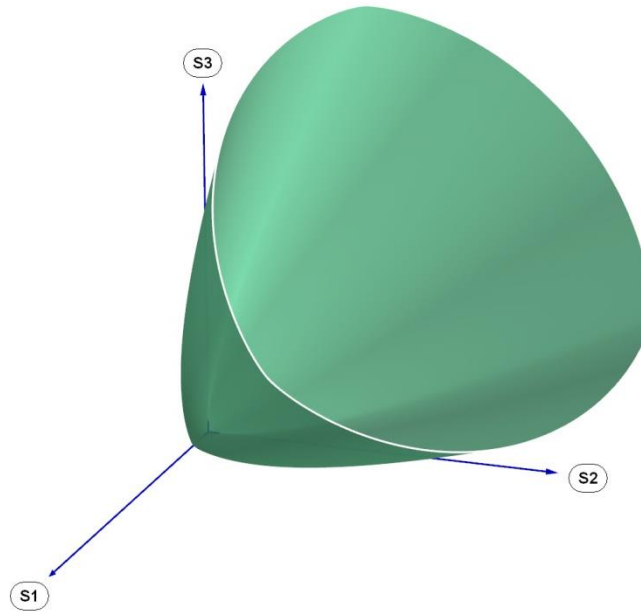


Figure A.1 1: Three dimensional representation of the Menetrey/Willam failure surface in the principal stress space

In the case of $e = 0.5$ the Menetrey/Willam failure function represents a circumscribed approximation of the Hoek-Brown (2) strength criterion

$$\left(\frac{\sigma_1 - \sigma_3}{\sigma_{ci}}\right)^2 + m \frac{\sigma_3}{\sigma_{ci}} - s = 0, \quad \text{A.1 3}$$

where σ_1 and σ_3 are the major and minor principal stresses at failure. In order to recognize the similarity between both criteria we rewrite the principal stresses representation using the relation between the stress invariants and the principal stresses

$$\sigma_1 = -p + \frac{2}{3}q \cos \theta \text{ and } \sigma_3 = -p + \frac{2}{3}q \cos \left(\theta + \frac{2}{3}\pi \right).$$

Inserting the upper expressions for the principal stresses into [3] one obtains the Hoek/Brown strength criterion in terms of the stress invariants

$$\left[\frac{2}{\sqrt{3}} \frac{q}{\sigma_{ci}} \sin \left(\theta + \frac{\pi}{3} \right) \right]^2 + m \left[\frac{2}{3} \frac{q}{\sigma_{ci}} \cos \theta - \frac{p}{\sigma_{ci}} \right] - s = 0. \quad \text{A.1 4}$$

Setting $e = 0.5$ results in an exact match between both criteria at the extension and compression meridians. For $\theta = 0$ and $\theta = \pi/3$ both expressions are reduced respectively to

$$\left[\frac{q}{\sigma_{ci}} \right]^2 + m \left[\frac{2}{3} \frac{q}{\sigma_{ci}} - \frac{p}{\sigma_{ci}} \right] - s = 0 \quad \text{A.1 5}$$

$$\left[\frac{q}{\sigma_{ci}} \right]^2 + m \left[\frac{1}{3} \frac{q}{\sigma_{ci}} - \frac{p}{\sigma_{ci}} \right] - s = 0. \quad \text{A.1 6}$$

Thus, for $e = 0.5$ the Menetrey/Willam criterion can be considered as a circumscribed approximation of the Hoek/Brown function (Fig.A.1 2).

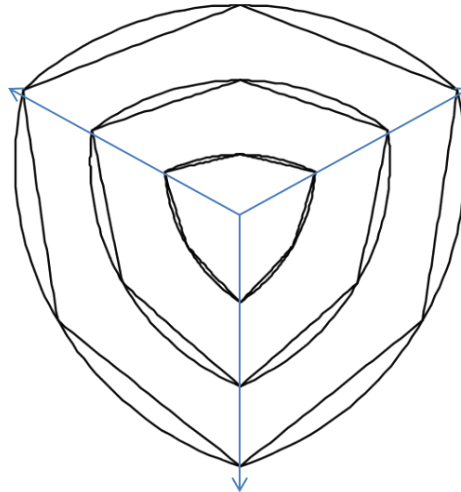


Figure A.1 2: Comparison between the Deviatoric traces of the Menetrey/Willam failure model (smooth curves) and the 1980 Hoek-Brown criteria at three levels of confinement in the principal stress space

In contrast to the Hoek/Brown model that doesn't account for the intermediate principal stress, the dependence on σ_2 in the case of the Menetrey/Willam criterion [1] is governed by the eccentricity parameter e . Increasing eccentricity values cause a higher dependence on σ_2 with the deviatoric trace of the Menetrey/Willam model approaching a circle (Fig A.1-3).

Thus, the Menetrey/Willam model possesses a material parameter that can be adjusted to match the true triaxial failure data if this is required.

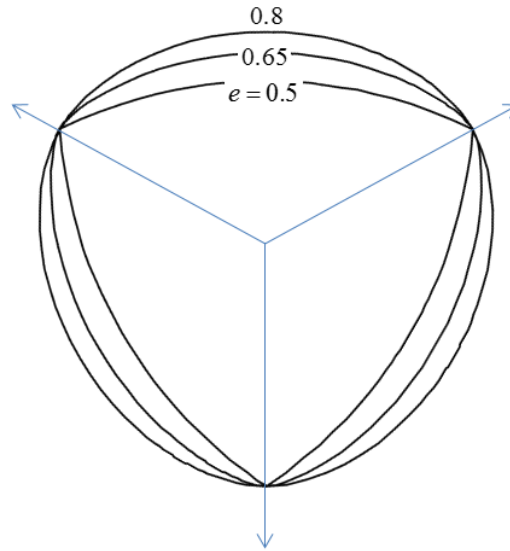


Figure A.1 3: Deviatoric traces of the Menetrey/Willam failure function for three different eccentricity values.

In 1992 the original Hoek/Brown criterion was extended (3) by an additional parameter a to the following form

$$\left(\frac{\sigma_1 - \sigma_3}{\sigma_{ci}}\right)^{\frac{1}{a}} + m \frac{\sigma_3}{\sigma_{ci}} - s = 0, \quad \text{A.1 7}$$

that allows to change the curvature of the failure envelope, particularly in the very low normal stress range to account for very low or zero tensile strength in heavily jointed or very poor rockmasses. A corresponding extension of the Menetrey/Willam model takes the form

$$\left[\frac{q}{\sigma_{ci}}\right]^{\frac{1}{a}} + m \left[\frac{1}{3} \frac{q}{\sigma_{ci}} R(\theta, e) - \frac{p}{\sigma_{ci}}\right] - s = 0, \quad \text{A.1 8}$$

which is the failure criterion in the framework of the LR2 model.

Accordingly, the above failure function [7] can be considered as a circumscribed approximation of the 1992 Hoek/Brown (3) criterion.

The plastic strain potential is given by the relation:

$$\mathbf{D}_p = \dot{\lambda} \frac{\partial G}{\partial \boldsymbol{\sigma}}, \quad \text{A.1 9}$$

where $\dot{\lambda}$ is the magnitude of the plastic strain increment and G is the flow potential

$$G = \sigma_{ci} \left[\frac{q}{\sigma_{ci}}\right]^{\frac{1}{a}} + \frac{1}{3} m q R(\theta, e) - d_g p. \quad \text{A.1 10}$$

Here, d_g is the dilation parameter in the bulk. If the flow potential differs from the yield function the flow rule is non-associative which is the case for most geotechnical materials.

The model is implemented in such a way that all the strength parameters as well as the dilation and the Elastic modulus can be prescribed as piecewise linear functions of the equivalent plastic strain which is the accumulated deviatoric plastic strain

$$p_{eq}^{dev} = \int_0^t \left(\dot{\lambda} \left\| \left(\frac{\partial G}{\partial \boldsymbol{\sigma}} \right)^{dev} \right\| \right) dt \quad \text{A.1 11}$$

to account for the stress-strain behaviour of the rock type, i.e. s , m_b , d_g and the Youngs modulus are piecewise linear functions of p_{eq}^{dev} . $\|\mathbf{A}\|$ is the norm of a tensor \mathbf{A} and $(\mathbf{A})^{dev}$ the deviatoric part of a tensor \mathbf{A} .

6.3 Representation of explicit structure

The behaviour of explicit discontinuities is approximated using cohesive elements (formulation COH3D6 in ABAQUS). These elements are used because they can capture the mechanical response of thin structures at large strains, which normal tetrahedral finite elements cannot achieve effectively. Cohesive elements allow simulation of the discrete behaviour associated with structures and can be used to construct a rockmass model compromising continuum regions separated by discontinuities. The structures are free to dislocate, dilate and degrade. The constitutive behaviour of the cohesive elements can be defined using the LR2 continuum-based constitutive model, or a constitutive model specified directly in terms of traction versus separation with Coulomb yield criterion with cohesion.

The first approach is typically used to model layers of finite thickness, while the second approach is useful in applications for discontinuities of zero thickness such as fractures. Both models have the LR2 feature of elastic-plastic material behaviour in such a way that all the strength parameters as well as the dilation and the Elastic modulus can be prescribed as piecewise linear functions of accumulated plastic strain or the accumulated fault slip.

Discontinuities modelled with continuum LR2 material behaviour have the same set of material properties as LR2 bulk materials (s. chapter A.1.2 Constitutive model for the continuum parts).

The main feature of the traction-separation fault behaviour is the onset of the fault slip is described by the following cohesive-frictional criterion

$$\tau - p_n \tan \beta - c = 0 \quad \text{A.1 12}$$

with c and β being the fault cohesion and friction angle, respectively. Further, τ is the magnitude of the shear stress resolved onto the fault plane and p_n the normal stress acting across the fault. The kinematic of the fault slip deformation is described by the plastic strain rate

$$\mathbf{D}_p = \dot{\gamma} [\text{sym}(\mathbf{s} \otimes \mathbf{n}) + \tan \psi \mathbf{n} \otimes \mathbf{n}] \quad \text{A.1 13}$$

with $\dot{\gamma}$ being the fault slip rate and ψ the fault dilation angle. Further, \mathbf{n} is the unit normal vector of the fault plane (i.e. the orientation of the finite element) and \mathbf{s} the unit vector into the direction of the resolved shear stress. The constitutive fault parameters c , β and ψ are prescribed as piecewise linear functions of the accumulated fault slip γ . The required parameter to define the mechanical behaviour of a traction-separation cohesive section are:

Table A.1 1: Material properties for traction-separation cohesive sections

D	Constitutive thickness	These parameters are a function of the accumulated fault slip.
ρ [kg/m ³]	Density	
E [GPa]	Elastic modulus	
ν	Poisson's ratio	
d	Dilation	
s	Fault cohesion	
a	Fault friction angle	

6.4 Extension for the case of transversal isotropy

The isotropic LR2 framework is extended for the case of transversal isotropy using the theory of liner stress transformation. The main assumption in this theory is that the anisotropic yield function of the actual stress $\boldsymbol{\sigma}$ is equivalent to an isotropic yield function of the linear transformed stress $\boldsymbol{\sigma}^*$

$$f_{aniso}(\boldsymbol{\sigma}) = f_{iso}(\boldsymbol{\sigma}^*) \quad \text{A.1 14}$$

With this approach the usage of an arbitrary isotropic yield function is possible.

The linear stress transformation:

$$\boldsymbol{\sigma}^* = \mathbf{L}\boldsymbol{\sigma} \quad \text{A.1 15}$$

is performed via a fully symmetric 4th order tensor \mathbf{L} that has to satisfy the material symmetry conditions (similar to the elastic stiffness tensor). It is also called the stress weighting tensor. Depending on the material anisotropy type it has different number of independent material constants.

Rock with a population of parallel weakness planes or cracks can be considered as transverse isotropic. With x_3 axis being the symmetry axis and written in the material symmetry frame (Fig A.1-4),

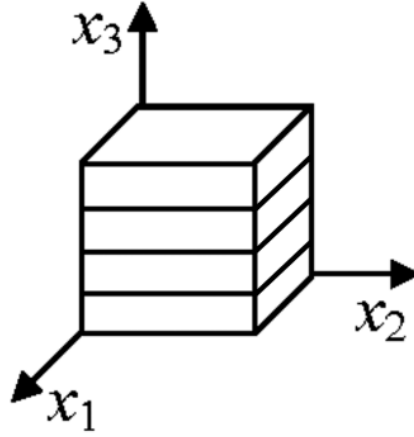


Figure A.1 4: Material symmetry frame of a transverse isotropic material.

\mathbf{L} has the following form:

$$\mathbf{L} = \begin{pmatrix} n & 0 & 0 & 0 & 0 & 0 \\ 0 & n & 0 & 0 & 0 & 0 \\ 0 & 0 & 1 & 0 & 0 & 0 \\ 0 & 0 & 0 & n & 0 & 0 \\ 0 & 0 & 0 & 0 & s & 0 \\ 0 & 0 & 0 & 0 & 0 & s \end{pmatrix} \quad \text{A.1 16}$$

with only two independent material constants n and s .

To extend the LR2 framework for the case of transverse isotropy, the actual stress in the equation [8] is replaced by the stress transformed via [16]

$$\boldsymbol{\sigma}^* = \mathbf{L}\boldsymbol{\sigma} = \begin{pmatrix} \sigma_{11}n \\ \sigma_{22}n \\ \sigma_{33} \\ \sigma_{12}n \\ \sigma_{23}s \\ \sigma_{13}s \end{pmatrix} \quad \text{A.1 17}$$

The meaning of the anisotropy constants s and n becomes clear if the yield function is analysed for the case of pure shear loading parallel to the cracks and of uniaxial compressive loading parallel to the cracks, respectively.

In the case of pure shear loading parallel to the cracks the yield condition reads:

$$f_{iso}(\mathbf{L}\boldsymbol{\sigma}) = f_{iso}(\sigma_{13}s) = 0$$

and $\sigma_{13}s = CS_{iso}$ follows. Accordingly, parameter s represents the reduction factor of the cohesive strength with respect to the isotropic case if shear loading is applied parallel to the cracks.

For the case of uniaxial compressive loading parallel to the cracks (loading direction x_1 or x_2)) the yield criterion reads

$$f_{iso}(\mathbf{L}\boldsymbol{\sigma}) = f_{iso}(\sigma_{11}n) = 0$$

and $\sigma_{11}n = UCS_{iso}$ follows. Accordingly, parameter n represents the reduction factor of the uniaxial compressive strength with respect to the isotropic case if the uniaxial compressive load is applied parallel to the cracks. If compressive load is applied in x_3 direction $\sigma_{33} = UCS_{iso}$ follows which means that the uniaxial compressive strength perpendicular to the cracks is not influenced by them.

For an arbitrary direction of the uniaxial compressive load with respect to the material symmetry frame the stress weighting tensor \mathbf{L} has to be transformed into the loading coordinate system. As a result, the simple diagonal shape is

lost and the components of the transformed stress tensor $\sigma^* = L\sigma$ attains shear components that depends also on constant s . Accordingly, the uniaxial compressive strength for such a transverse isotropic material depends on both anisotropy constants.

The pictures below show the dependence of UCS from the rotation angle of the load axis relative to x_3 axis for load direction varying from 0° (perpendicular to the cracks) to 90° (parallel to the cracks) for different combinations of s and n values.

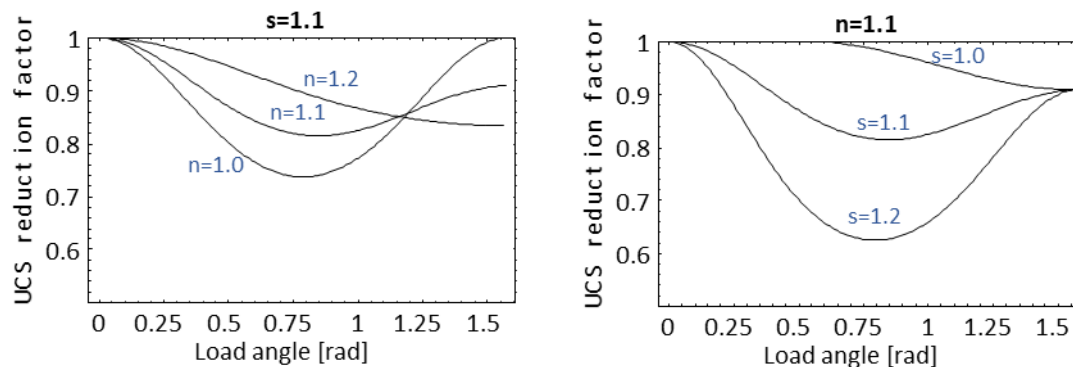


Figure A.1 5: Influence of the loading direction on UCS for different combinations of n and s values.

6.5 Model parameter to determine rock strength

The application of the constitutive model for a particular rock type or the mechanical behaviour of a discontinuity requires the determination of a set of model parameters. One common approach is to determine the model parameter with help of the GSI (geological strength index) system (see (3) and (4) for the application) and the value m_i (frictional strength of the intact rockmass). This allows an initial determination of elastic properties E and ν , the frictional strength of the broken rock m_b and the cohesive strength s as well as the dilation.

Table A.1 2: Material properties for continuum LR2 material.

UCS [MPa]	Uniaxial Compressive Strength	
GSI	Geological Strength Index	
m_i	Frictional strength of intact rock	
D	Damage parameter (Hoek-Brown)	
ρ [kg/m ³]	Plastic strain	
m_b	HB parameter for frictional strength of broken rock	These parameters are a piecewise linear function of the accumulated plastic strain.
E [GPa]	Elastic modulus	
ν	Poisson's ration	
d	Dilation	
s	cohesive strength parameter	
a	strength parameter	

A set of these parameters describes the onset of yielding for a rock type. To describe the post-yield behaviour of stress-strain relation of the rock the implementation of the constitutive model allows an arbitrary number of characteristic points to describe the stress-strain curve of the material. An example for the documentation of material properties is provided in the next figure:

COWAL GOLD OPERATIONS: SURFACE SUBSIDENCE ASSESSMENT FOR OPEN PIT EXPANSION

Material property set: M12																							
Material	Code	UCS	Density	k	Peak							Transitional					Residual						
					mb	s	a	e	d	Eb	v	PS_start	mb	s	d	Eb	v	PS_start	mb	s	d	Eb	v
		(MPa)	(kg/m ³)	(m/s)						(GPa)					(GPa)					(GPa)			
Quartz andesite	QAND	90	2,700	1E-09	1.27	1.23E-03	0.503	0.6	0.079	8.71	0.25	0.5%	1.27	1.23E-03	0.079	8.71	0.25	1.5%	0.59	1.50E-04	0.018	1.67	0.25
Younger andesite	YAND	24	2,700	1E-08	0.55	1.25E-04	0.521	0.6	0.034	1.37	0.25	0.5%	0.55	1.25E-04	0.034	1.37	0.25	1.5%	0.37	4.16E-05	0.011	0.29	0.25
Undifferentiated ignimbrite	UDIG	60	2,700	1E-04	3.09	2.22E-03	0.505	0.6	0.193	5.81	0.25	0.5%	3.09	2.22E-03	0.193	5.81	0.25	1.5%	1.52	2.46E-04	0.048	1.86	0.25
Welded ignimbrite	WEIG	90	2,700	1E-08	4.19	3.87E-03	0.505	0.6	0.262	9.49	0.25	0.5%	4.19	3.87E-03	0.262	9.49	0.25	1.5%	1.91	3.35E-04	0.060	2.67	0.25
Unwelded sandy ignimbrite	UWIG	24	2,700	1E-04	4.07	1.17E-02	0.502	0.6	0.255	8.71	0.25	0.5%	4.07	1.17E-02	0.255	8.71	0.25	1.5%	1.45	4.68E-04	0.045	1.64	0.25
Lake sediments	LSED	2.4	1,900	1E-04	0.21	2.40E-04	0.530	0.6	0.013	0.37	0.25	0.5%	0.21	2.40E-04	0.013	0.37	0.25	1.5%	0.17	1.38E-04	0.005	0.28	0.25
Surface sediments	SSED	2.4	1,900	1E-04	0.21	2.40E-04	0.530	0.6	0.013	0.37	0.25	0.5%	0.21	2.40E-04	0.013	0.37	0.25	1.5%	0.17	1.38E-04	0.005	0.28	0.25
Alluvium	ALLU	12	1,700	1E-04	2.01	3.87E-03	0.505	0.6	0.126	3.46	0.25	0.5%	2.01	3.87E-03	0.126	3.46	0.25	1.5%	0.82	2.40E-04	0.026	0.82	0.25
Tuff	TUFF	12	1,700	1E-04	2.18	3.87E-03	0.505	0.6	0.136	3.46	0.25	0.5%	2.18	3.87E-03	0.136	3.46	0.25	1.5%	0.89	2.40E-04	0.028	0.82	0.25
Blue Shear	BLUE	2.4	2,100	1E-08	2.45	7.30E-04	0.515	0.6	0.153	0.65	0.25	0.5%	2.45	7.30E-04	0.153	0.65	0.25	1.5%	1.44	1.38E-04	0.045	0.28	0.25
Mineralised structures	QTVN	60	2,700	1E-04	0.65	1.97E-04	0.516	0.6	0.040	2.20	0.25	0.5%	0.65	1.97E-04	0.040	2.20	0.25	1.5%	0.31	3.04E-05	0.010	0.15	0.25
Other cohesive elements	COH1	2.4	2,700	Note 1	1.20	1.38E-04	1.000	0.6	0.075	0.50	0.25	0.5%	1.20	1.38E-04	0.075	0.50	0.25	1.5%	0.87	1.38E-04	0.027	0.50	0.25
Quartz andesite 2	QAND2	78	2,700	1E-09	1.11	8.55E-04	0.505	0.6	0.069	6.92	0.25	0.5%	1.11	8.55E-04	0.069	6.92	0.25	1.5%	0.51	1.50E-04	0.016	1.67	0.25
Quartz andesite 3	QAND3	66	2,700	1E-09	0.65	1.97E-04	0.515	0.6	0.040	2.20	0.25	0.5%	0.55	1.25E-04	0.034	1.37	0.25	1.5%	0.39	5.00E-05	0.012	0.40	0.25
Milking Cow		Elastic	Note 2	Note 3						0.05	0.25												
Backfill		Elastic	2,160	1E-04						0.05	0.25												
Underground voids		Elastic								1E-04	0.25												

- Notes
- 1: Different k for cohesive elements not applied in this simulation.
 - 2: Density within the Milking Cow assumed to be the same as original rock.
 - 3: k within the Milking Cow assumed to be 1E-3 of k in original rock.

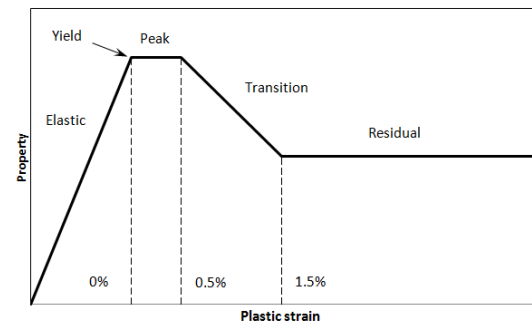


Figure A.1 6: Example for documentation of material properties of the LR2 framework.

6.6 Modelling softening behaviour

The image below shows frequently used idealizations for the softening behaviour of the rock materials. (P) denotes the peak strength material, (T) indicates the onset of softening and (R) examples for the residual strength level.

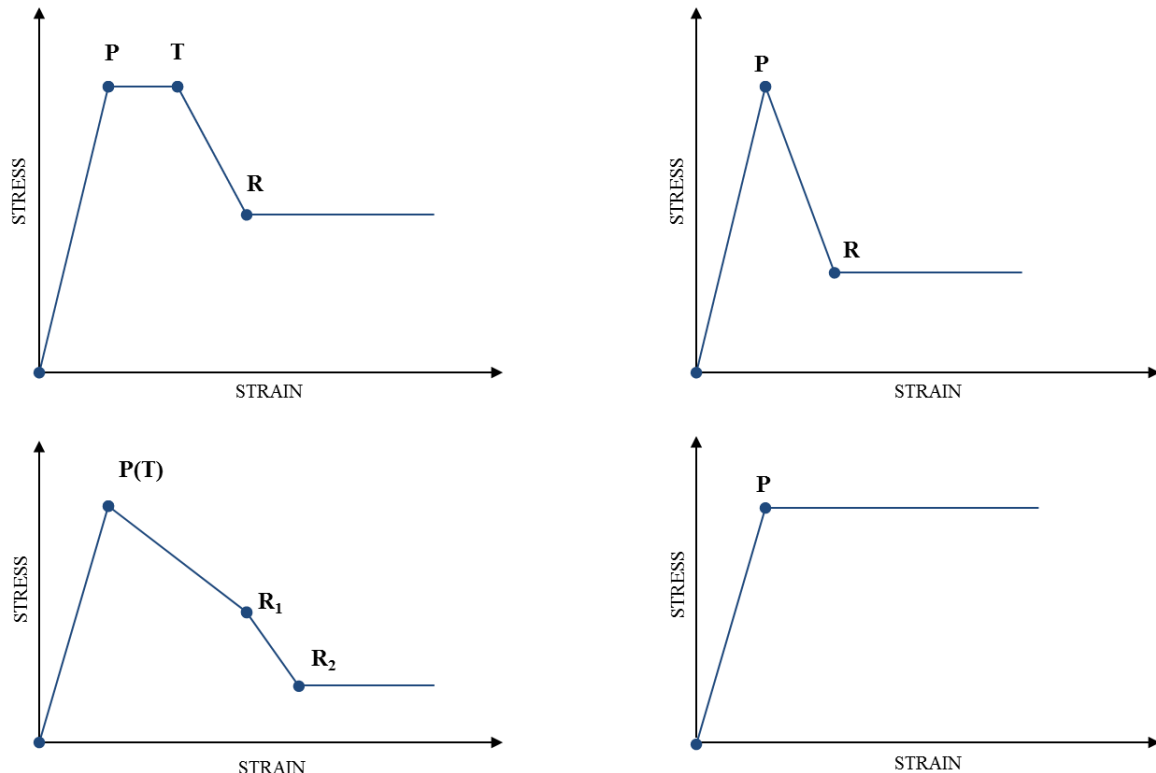


Figure A.1 7: Idealizations for the softening behaviour of the rock materials. (P) denotes the peak strength material, (T) indicates the onset of softening and (R) examples for the residual strength level.

In the LR2 framework the softening behaviour is introduced in such a way that all the strength parameters as well as the dilation and the Elastic modulus can be prescribed as piecewise linear functions of accumulated plastic strain to account for the stress-strain behaviour of the rock type, i.e. d_g , s and m_b and the Young's modulus can evolve independently according to the available laboratory data or available description of the deformation and damage behaviour rockmass.

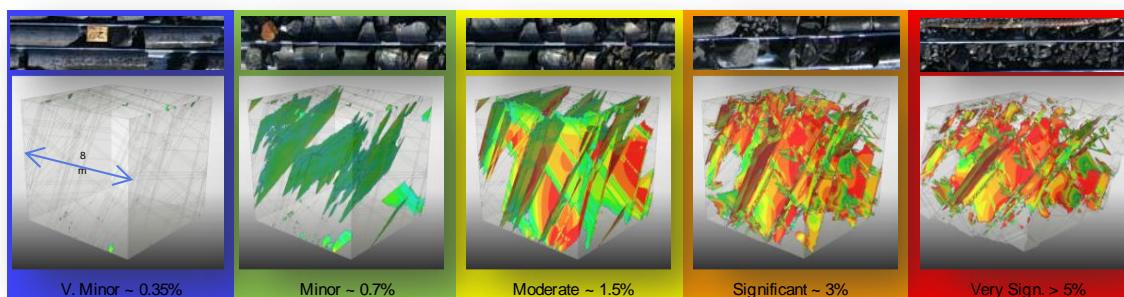
6.7 The common damage scale

As a purely phenomenological model the constitutive equations do not incorporate a damage variable that allows the direct quantification of the damage state of the rock.

For non-linear elastic-plastic models as used in the LR2 framework the rockmass damage is related to the amount of accumulated equivalent plastic strain, which is the amount of permanent (irreversible) rockmass deformation after yield. The table below shows a possible correlation of plastic strain values with the damage state of the rock. The specific correlation of plastic strain levels with damage states is often referred to as the "common damage scale (CSD)", which can vary depending of the softening behaviour of the investigated rock.

Table A.1 8: Correlation of plastic strain values with the damage state of the rock.

Plastic strain	Damage state	Observed behaviour
>5%	Very significant	Gross distortion and comminution.
~3%	Significant	Extensive fracturing of intact rock.
~1.5%	Moderate	Constant load leads to increasing deformation.
~0.7%	Minor	No significant decrease in strength or stiffness.
<0.35%	None to very minor	Undisturbed in situ conditions.



6.8 Assessing seismic potential with RER

The mining of excavations in rock re-distributes stress and causes damage to the rockmass and discontinuities. The resulting reduction in strength and degradation in stiffness of the damaged rock and structures leads to further deformation and release of stored elastic strain energy.

One portion of this released energy is consumed by the damage process - frictional sliding and the creation of new surfaces. This energy cannot be retrieved, so is counted as 'dissipated'. If the value of the released elastic energy is higher than the energy dissipated by the irreversible damage, the surplus is emitted into the surrounding rock. These release events are seismic events.

The magnitude (and/or the rate) of the released energy during these events can be measured in a mine using a seismic monitoring system or calculated using a model. The instantaneous, peak (i.e. maximum) rate of energy release from a volume of rock (i.e. the energy that is not dissipated) is the Rate of Energy Release (RER).

The calculated rate of energy release (RER) is used to represent seismic potential in the model. Levkovitch et al. (2013) describe RER in some detail. RER is calculated as follows:

Each model frame comprises many numerical time steps as part of the explicit FE solution procedure. For each time step, the instantaneous rate of energy release is calculated for each finite element. This is the change in elastic strain energy less the dissipated plastic energy, and represents the energy radiated from the element out into the surrounding environment. The dissipated plastic energy represents irreversible work done on the rockmass through processes such as friction on joint surfaces and creation of new fractures and is calculated from the plastic strain condition of the element.

The RER is the maximum value of the instantaneous rate of energy release calculated all the time steps during a model frame.

RER is recorded for every tetrahedral element and every cohesive element in the FE simulation at every frame. This allows RER to be calculated for the homogenised rockmass (represented with tetrahedral elements), and for the explicit structures (represented with cohesive elements). Both are important: The largest events are expected on structures, but many lower magnitude events are expected in the homogenised rockmass.

6.9 Mechanical response in the presence of pore-water pressure

In the LR2 framework the governing rock or soil is regarded as a deformable porous medium, consisting of a solid skeleton and a pore space. A fluid (e.g., water) may partially or fully saturate this pore space and is allowed to flow through connected pores, i.e., to permeate through the rockmass. Within the conceptual modelling approach both the skeleton and the voids are considered to be homogeneously smeared within the Representative Volume Element (RVE), where the proportion of pore volume space to the bulk volume is denoted as porosity.

At any material point in the model, the fluid is subjected to a fluid pressure. The spatial distribution of the fluid pressure does vary and results from the respective hydro-geological setting. This pressure is obtained as a result of a separate hydrological analysis.

The fluid interacts with the solid rock skeleton. In case of a single-phase water flow the respective fluid pressure acting on the solid skeleton is referred to as pore-water-pressure p_w , or, in case of a multi-phase flow, as wetting phase pressure.

The stresses of the entire RVE, denoted as total stresses, can be decomposed in two parts. One part is represented by the effective stresses of the solid skeleton, and the other part by the fluid pressure acting onto the solid skeleton. This is referred to as effective stress concept of Terzaghi (1936):

$$\sigma_{tot} = \sigma_{eff} + \alpha_B p_w \mathbf{1} \quad (A.1 \ 18)$$

The sign convention is such that p_w being positive in compression, and of σ negative in compression, i.e., $p = -1/3 \text{tr}(\sigma)$. Further, α_B denotes the Biot coefficient which is a material parameter depending on the rock type that is generally bound between $0 < \alpha_B \leq 1$. Typical values for the Biot coefficient are summarized in the literature for a range of materials. Total stresses are always used to fulfil the linear momentum (equilibrium). The constitutive response of the porous material, however, is always updated using the effective stresses. Hence, the presence of pore-water pressure reduces the skeleton stresses such that the effective confinement pressure is reduced and the material may be subject to earlier yielding. As a special case, a pore-water pressure exceeding the total confining pressure, i.e., $p_w > -1/3 \text{tr}(\sigma_{tot})$, results in a plastic apex-mode deformation, also referred to as tensile cracking. This situation may arise in cases where a large p_w is present in a de-stressed material region, such as near a free surface.

6.10 References

- (1) Terzaghi, K. (1936) "The shear resistance of saturated soils." Proceedings for the 1st. Intl. Conf. on Soil Mechanics and Foundation Engineering (Cambridge, MA), 1, 54-56.
- (2) Menetrey P. & Willam K.: "Triaxial failure criterion for concrete and its generalization", ACI Structural Journal. 92(3): 311-317, 1995.
- (3) Hoek, E. & Brown E.T.: "Empirical strength criterion for rockmasses", Journal of the Geotechnical Engineering Division. 106(9): 1013-1035, 1980.
- (4) Hoek, E., Wood, D. and Shah, S.: "A modified Hoek-Brown criterion for jointed rockmasses", Proc. rock characterization, symp. Int. Soc. Rock Mech.: Eurock '92, (J.Hudson ed.). 209-213, 1992
- (5) M. Cai et al. / International Journal of Rock Mechanics & Mining Sciences 44 (2007) 247–265
- (6) Reusch, F., Levkovitch, V. & Beck, D. : "Multi-scale, non-linear numerical analysis of mining induced deformation in complex environments" in "Rock Mechanics in Civil and Environmental Engineering" , Jian Zhao (Editor), Vincent Labiouse (Editor), Jean-Paul Dudt (Editor), Jean-Francois Mathier (Editor), CRC Press, 2010, 697-700.
- (7) Levkovitch, V., Reusch, F. & Beck, D. : "Application of a non-linear confinement sensitive constitutive model to mine scale simulations subject to varying levels of confining stress" in "Rock Mechanics in Civil and Environmental Engineering" , Jian Zhao (Editor), Vincent Labiouse (Editor), Jean-Paul Dudt (Editor), Jean-Francois Mathier (Editor), CRC Press, 161-164, 2010.

7 APPENDIX B – MATERIAL STRENGTH ENVELOPE PLOTS

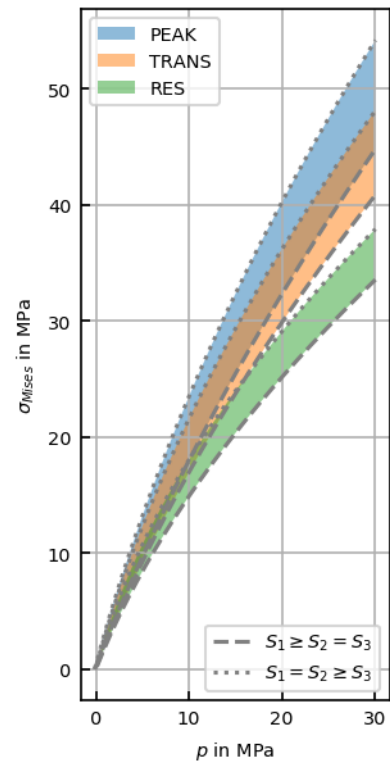
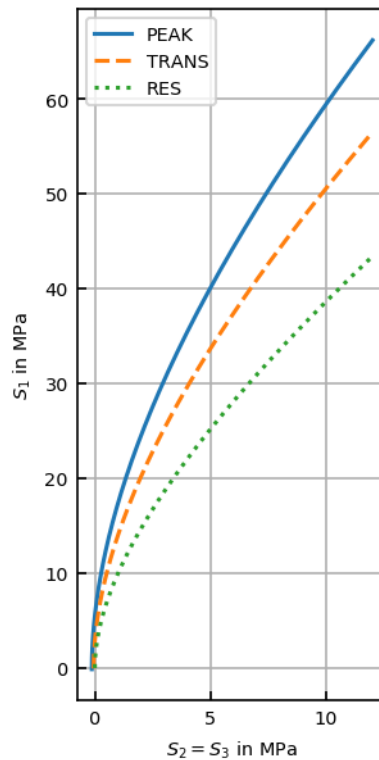
AN

General Properties

Type	Computator V14.3 PLR
ρ [kg/m ³]	2770.00
UCS_i [MPa]	125.00
GSI	65.00
n_{aniso}	1.00
s_{aniso}	1.00

LR2 Parameters

	PEAK	TRANS	RES
ϵ_{plast} [%]	0.00	0.96	7.32
E [GPa]	26.27	22.53	19.38
ν	0.25	0.25	0.25
s	2.10e-03	5.82e-04	1.00e-05
m_b	1.97	1.34	0.67
a	0.50	0.50	0.50
e	0.60	0.60	0.60
d	0.33	0.22	0.00



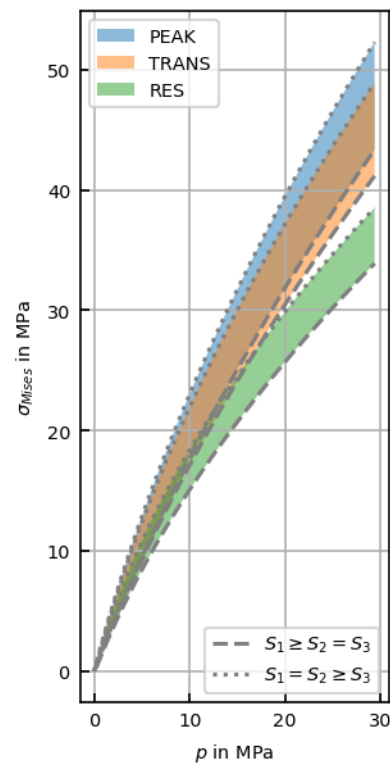
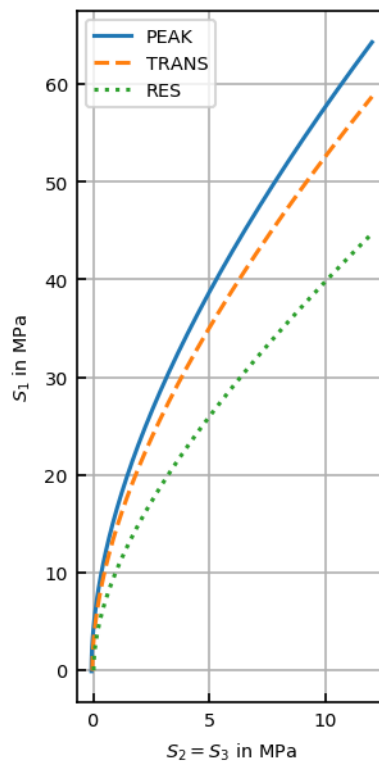
DIO

General Properties

Type	Computator V14.3 PLR
ρ [kg/m ³]	2800.00
UCS_i [MPa]	132.00
GSI	60.00
n_{aniso}	1.00
s_{aniso}	1.00

LR2 Parameters

	PEAK	TRANS	RES
ϵ_{plast} [%]	0.00	0.52	6.56
E [GPa]	25.17	23.14	19.80
ν	0.25	0.25	0.25
s	1.27e-03	6.12e-04	1.00e-05
m_b	1.75	1.40	0.70
a	0.51	0.51	0.51
e	0.60	0.60	0.60
d	0.29	0.23	0.00



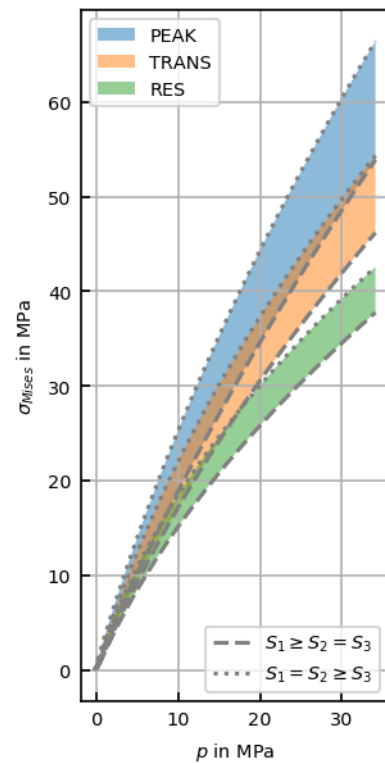
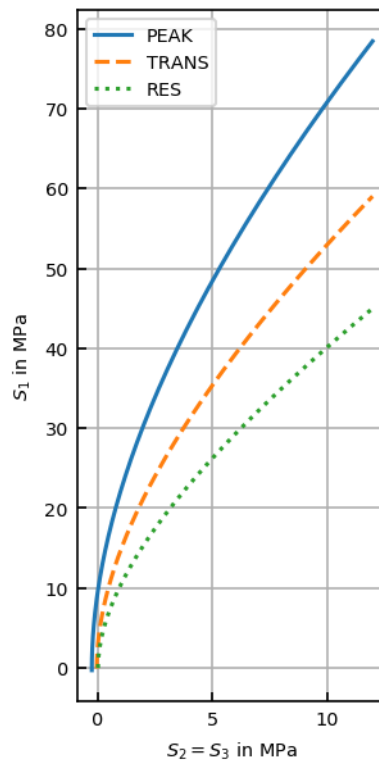
MODI

General Properties

Type	Computator V14.3 PLR
ρ [kg/m ³]	2800.00
UCS_i [MPa]	132.00
GSI	75.00
n_{aniso}	1.00
s_{aniso}	1.00

LR2 Parameters

	PEAK	TRANS	RES
ϵ_{plast} [%]	0.00	1.59	7.63
E [GPa]	30.58	23.14	19.80
ν	0.25	0.25	0.25
s	5.70e-03	6.12e-04	1.00e-05
m_b	2.74	1.40	0.70
a	0.50	0.50	0.50
e	0.60	0.60	0.60
d	0.46	0.23	0.00



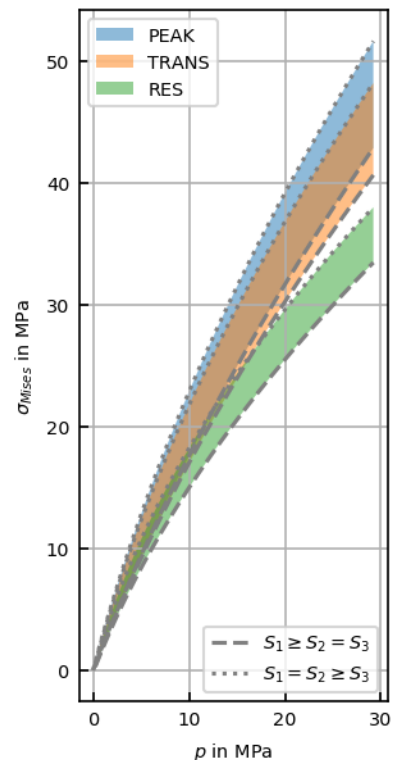
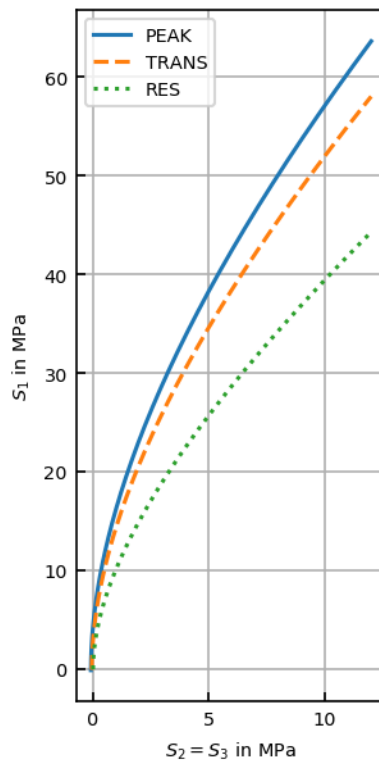
MOQ

General Properties

Type	Computator V14.3 PLR
ρ [kg/m ³]	2710.00
UCS_i [MPa]	130.00
GSI	60.00
n_{aniso}	1.00
s_{aniso}	1.00

LR2 Parameters

	PEAK	TRANS	RES
ϵ_{plast} [%]	0.00	0.54	6.66
E [GPa]	25.02	22.97	19.68
ν	0.25	0.25	0.25
s	1.27e-03	6.04e-04	1.00e-05
m_b	1.73	1.39	0.69
a	0.51	0.51	0.51
e	0.60	0.60	0.60
d	0.29	0.23	0.00



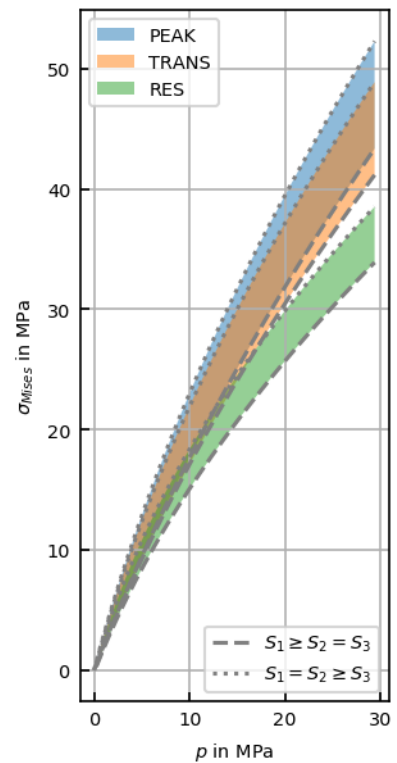
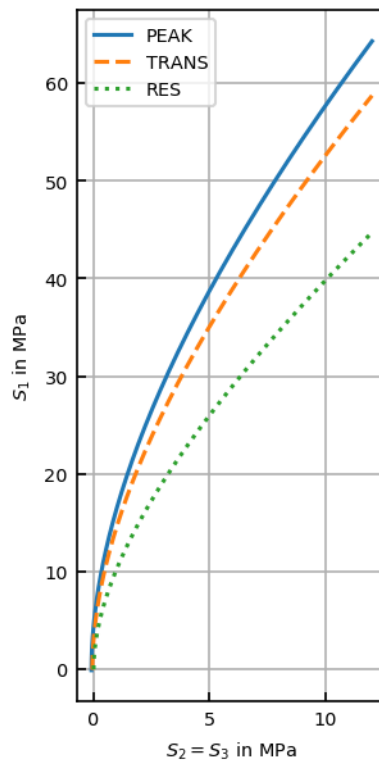
DIPP

General Properties

Type	Computator V14.3 PLR
ρ [kg/m ³]	2770.00
UCS_i [MPa]	132.00
GSI	60.00
n_{aniso}	1.00
s_{aniso}	1.00

LR2 Parameters

	PEAK	TRANS	RES
ϵ_{plast} [%]	0.00	0.52	6.56
E [GPa]	25.17	23.14	19.80
ν	0.25	0.25	0.25
s	1.27e-03	6.12e-04	1.00e-05
m_b	1.75	1.40	0.70
a	0.51	0.51	0.51
e	0.60	0.60	0.60
d	0.29	0.23	0.00



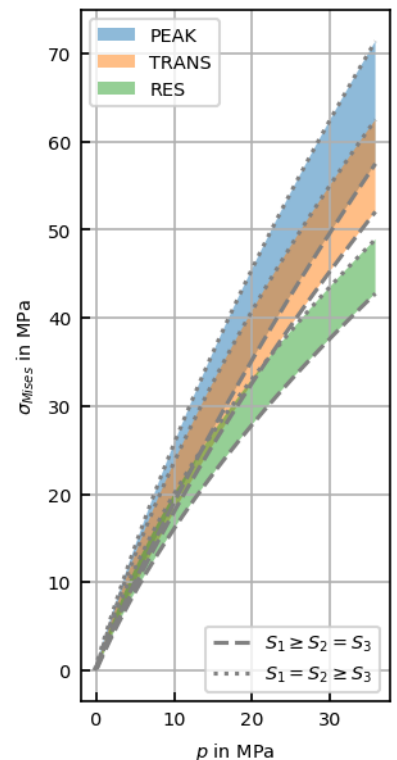
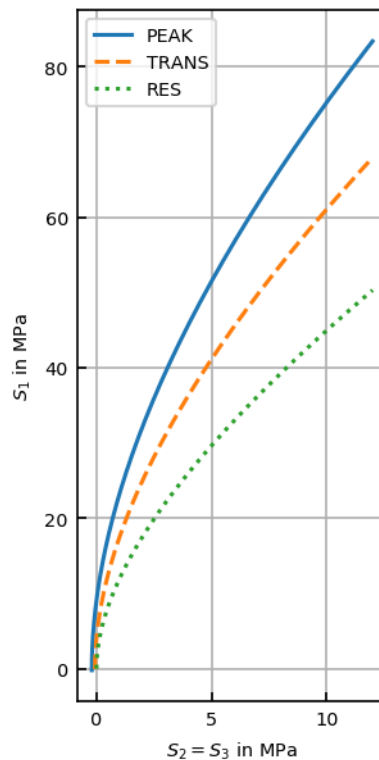
LAVA

General Properties

Type	Computator V14.3 PLR
ρ [kg/m ³]	2760.00
UCS_i [MPa]	159.00
GSI	70.00
n_{aniso}	1.00
s_{aniso}	1.00

LR2 Parameters

	PEAK	TRANS	RES
ϵ_{plast} [%]	0.00	0.96	5.99
E [GPa]	30.57	25.08	21.11
ν	0.25	0.25	0.25
s	3.46e-03	7.13e-04	1.00e-05
m_b	2.66	1.65	0.78
a	0.50	0.50	0.50
e	0.60	0.60	0.60
d	0.44	0.28	0.00



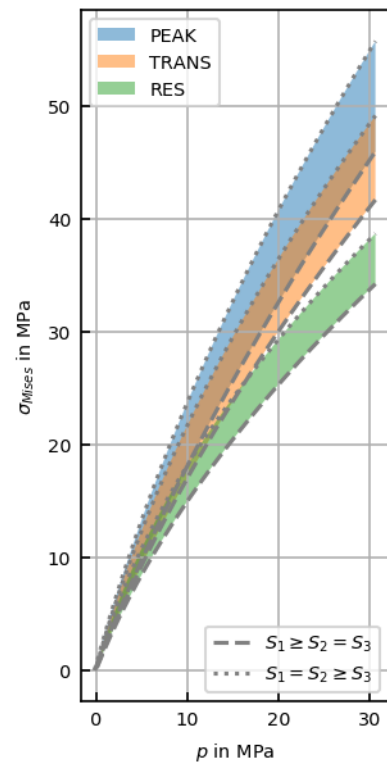
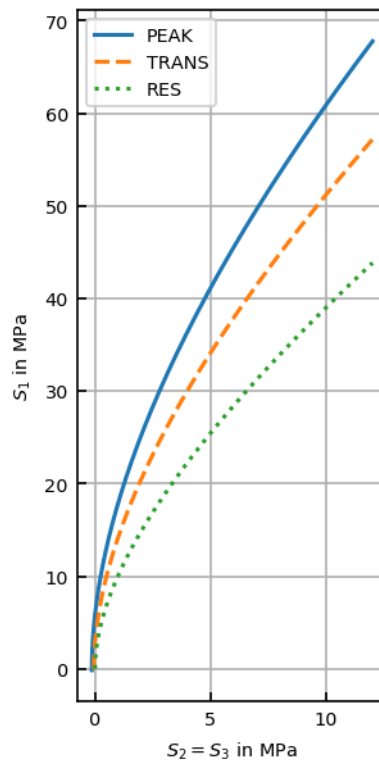
EVC

General Properties

Type	Computator V14.3 PLR
ρ [kg/m ³]	2770.00
UCS_i [MPa]	127.00
GSI	66.00
n_{aniso}	1.00
s_{aniso}	1.00

LR2 Parameters

	PEAK	TRANS	RES
ϵ_{plast} [%]	0.00	1.01	7.27
E [GPa]	26.79	22.71	19.50
ν	0.25	0.25	0.25
s	2.32e-03	5.91e-04	1.00e-05
m_b	2.04	1.36	0.68
a	0.50	0.50	0.50
e	0.60	0.60	0.60
d	0.34	0.23	0.00



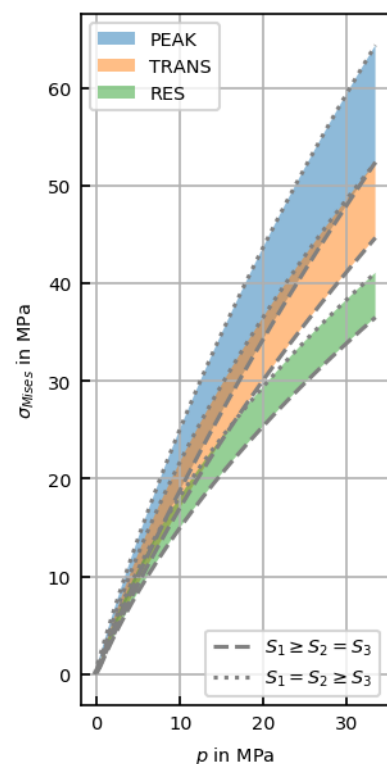
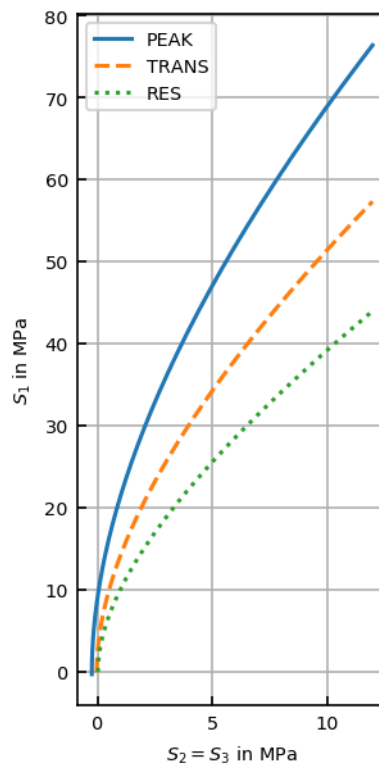
LVC

General Properties

Type	Computator V14.3 PLR
ρ [kg/m ³]	2770.00
UCS_i [MPa]	127.00
GSI	75.00
n_{aniso}	1.00
s_{aniso}	1.00

LR2 Parameters

	PEAK	TRANS	RES
ϵ_{plast} [%]	0.00	1.67	7.94
E [GPa]	30.12	22.71	19.50
ν	0.25	0.25	0.25
s	5.70e-03	5.91e-04	1.00e-05
m_b	2.68	1.36	0.68
a	0.50	0.50	0.50
e	0.60	0.60	0.60
d	0.45	0.23	0.00



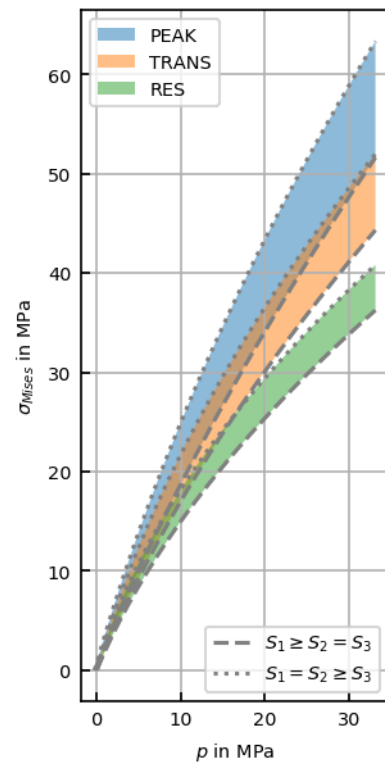
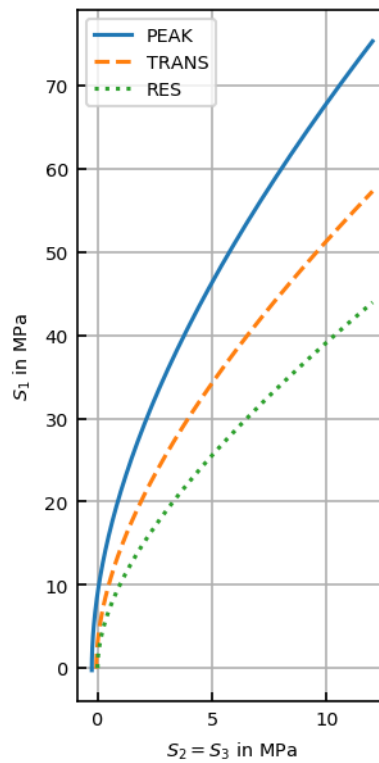
UVC

General Properties

Type	Computator V14.3 PLR
ρ [kg/m ³]	2700.00
UCS_i [MPa]	127.00
GSI	74.00
n_{aniso}	1.00
s_{aniso}	1.00

LR2 Parameters

	PEAK	TRANS	RES
ϵ_{plast} [%]	0.00	1.60	7.86
E [GPa]	29.74	22.71	19.50
ν	0.25	0.25	0.25
s	5.16e-03	5.91e-04	1.00e-05
m_b	2.60	1.36	0.68
a	0.50	0.50	0.50
e	0.60	0.60	0.60
d	0.43	0.23	0.00



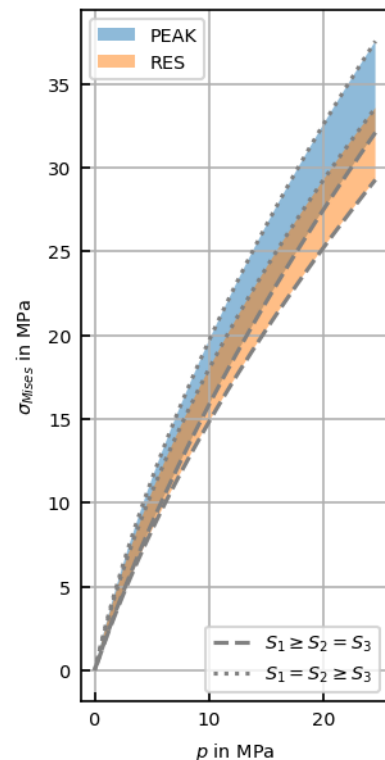
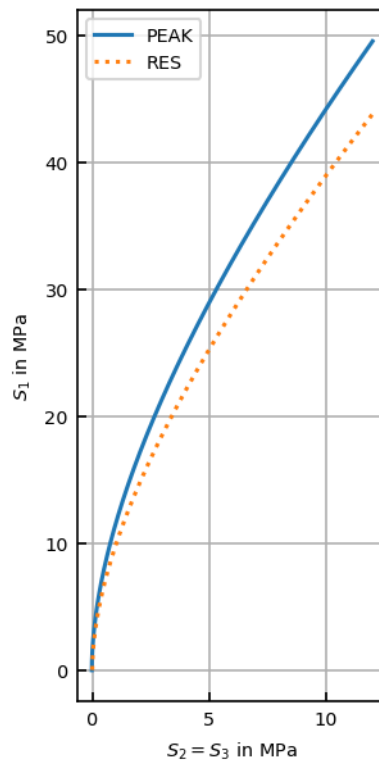
ZXP

General Properties

Type	Computator V14.3 PLR
ρ [kg/m ³]	2800.00
UCS_i [MPa]	132.00
GSI	40.00
n_{aniso}	1.00
s_{aniso}	1.00

LR2 Parameters

	PEAK	RES
ϵ_{plast} [%]	0.00	2.77
E [GPa]	20.83	19.80
ν	0.25	0.25
s	1.72e-04	1.00e-05
m_b	0.96	0.70
a	0.52	0.52
e	0.60	0.60
d	0.16	0.00



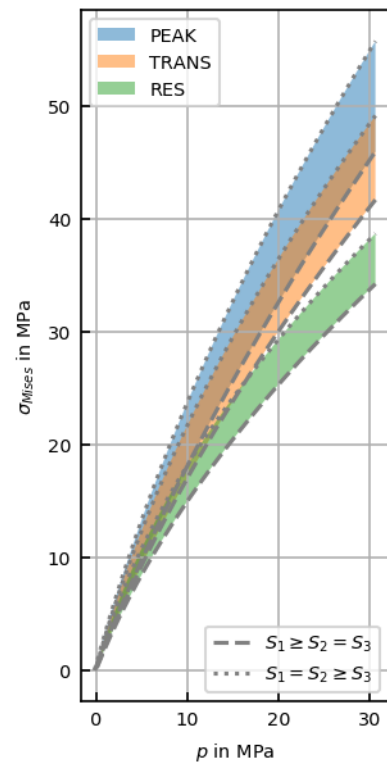
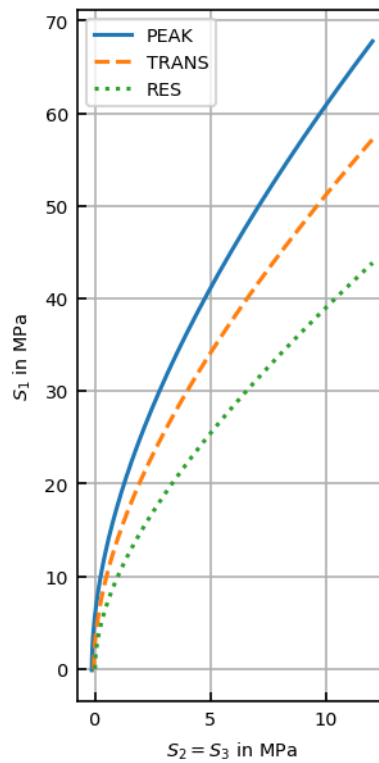
EAN

General Properties

Type	Computator V14.3 PLR
ρ [kg/m ³]	2800.00
UCS_i [MPa]	127.00
GSI	66.00
n_{aniso}	1.00
s_{aniso}	1.00

LR2 Parameters

	PEAK	TRANS	RES
ϵ_{plast} [%]	0.00	1.01	7.27
E [GPa]	26.79	22.71	19.50
ν	0.25	0.25	0.25
s	2.32e-03	5.91e-04	1.00e-05
m_b	2.04	1.36	0.68
a	0.50	0.50	0.50
e	0.60	0.60	0.60
d	0.34	0.23	0.00



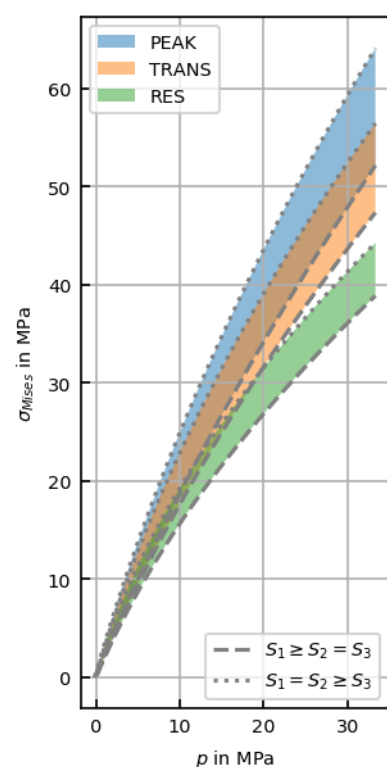
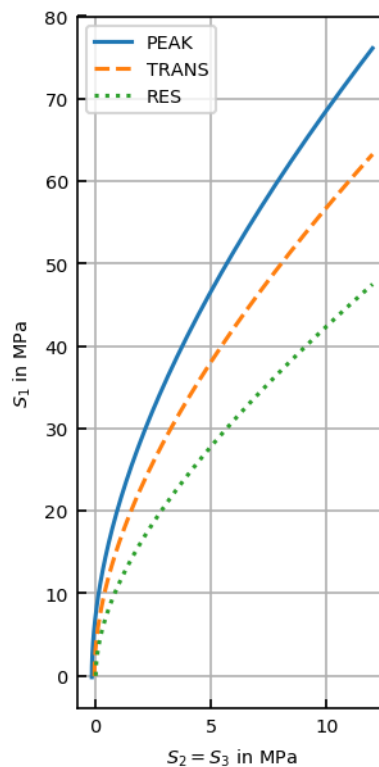
CSED

General Properties

Type	Computator V14.3 PLR
ρ [kg/m ³]	2700.00
UCS_i [MPa]	145.00
GSI	68.00
n_{aniso}	1.00
s_{aniso}	1.00

LR2 Parameters

	PEAK	TRANS	RES
ϵ_{plast} [%]	0.00	0.96	6.46
E [GPa]	28.90	24.15	20.49
ν	0.25	0.25	0.25
s	2.83e-03	6.64e-04	1.00e-05
m_b	2.36	1.53	0.74
a	0.50	0.50	0.50
e	0.60	0.60	0.60
d	0.39	0.25	0.00



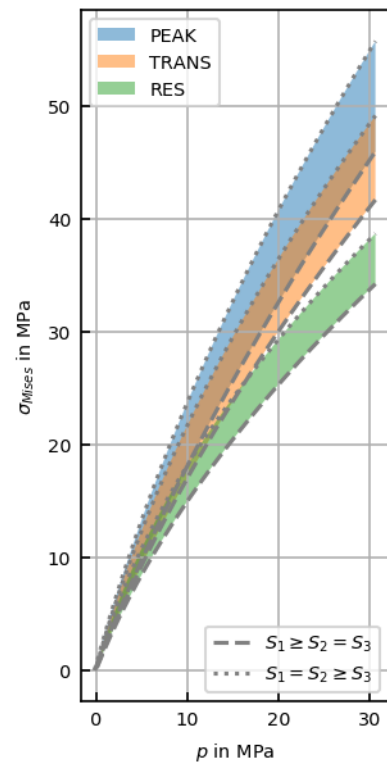
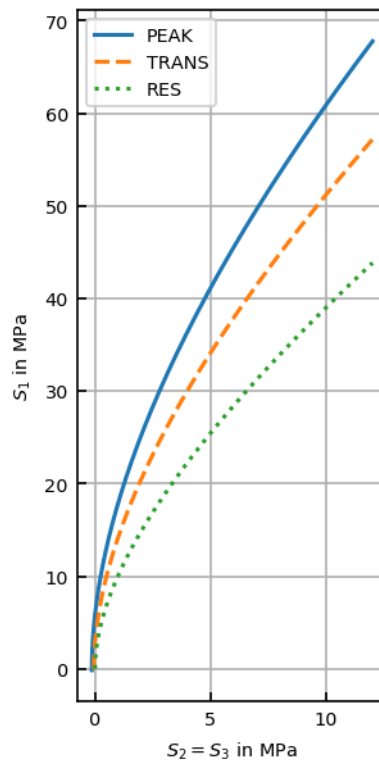
FSED

General Properties

Type	Computator V14.3 PLR
ρ [kg/m ³]	2800.00
UCS_i [MPa]	127.00
GSI	66.00
n_{aniso}	1.00
s_{aniso}	1.00

LR2 Parameters

	PEAK	TRANS	RES
ϵ_{plast} [%]	0.00	1.01	7.27
E [GPa]	26.79	22.71	19.50
ν	0.25	0.25	0.25
s	2.32e-03	5.91e-04	1.00e-05
m_b	2.04	1.36	0.68
a	0.50	0.50	0.50
e	0.60	0.60	0.60
d	0.34	0.23	0.00



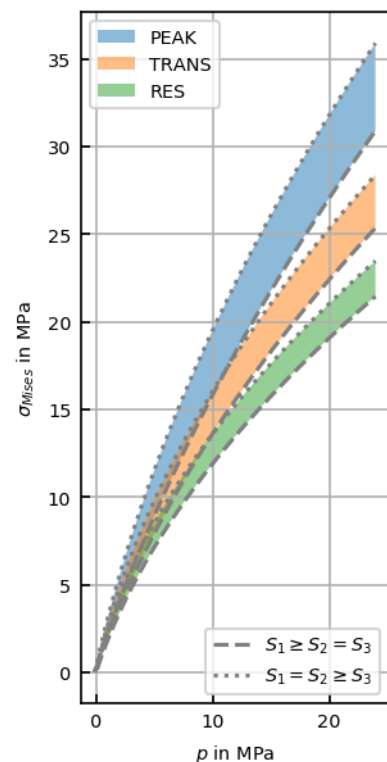
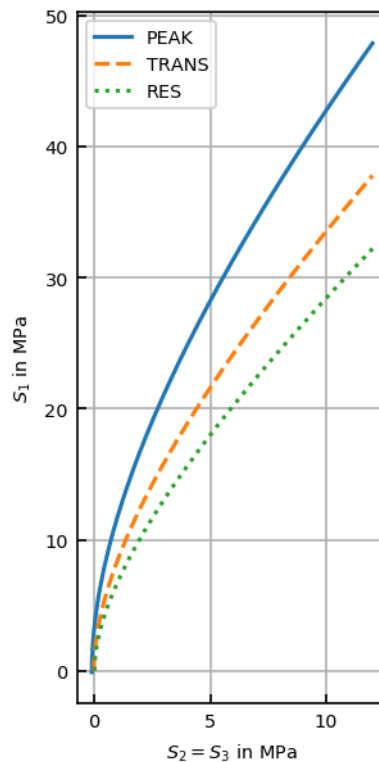
MUDS

General Properties

Type	Computator V14.3 PLR
ρ [kg/m ³]	2700.00
UCS_i [MPa]	70.00
GSI	67.00
n_{aniso}	1.00
s_{aniso}	1.00

LR2 Parameters

	PEAK	TRANS	RES
ϵ_{plast} [%]	0.00	2.34	12.41
E [GPa]	19.99	15.70	14.36
ν	0.25	0.25	0.25
s	2.56e-03	2.96e-04	1.00e-05
m_b	1.54	0.80	0.50
a	0.50	0.50	0.50
e	0.60	0.60	0.60
d	0.26	0.13	0.00



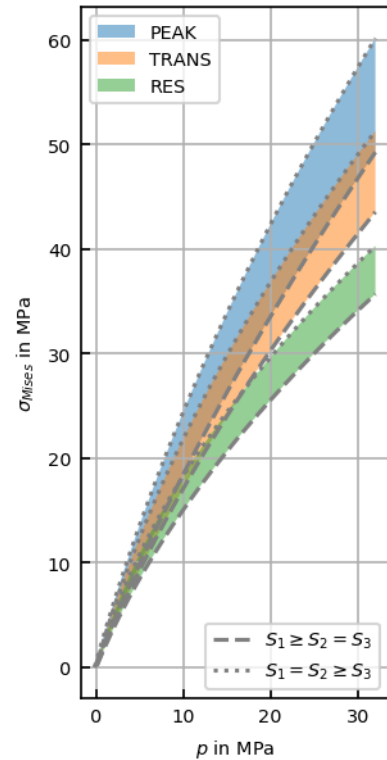
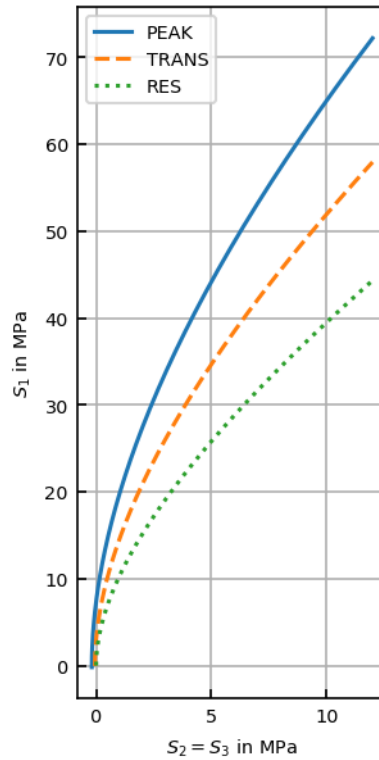
DYDA

General Properties

Type	Computator V14.3 PLR
ρ [kg/m ³]	2756.00
UCS_i [MPa]	129.00
GSI	70.00
n_{aniso}	1.00
s_{aniso}	1.00

LR2 Parameters

	PEAK	TRANS	RES
ϵ_{plast} [%]	0.00	1.28	7.45
E [GPa]	28.42	22.89	19.62
ν	0.25	0.25	0.25
s	3.46e-03	6.00e-04	1.00e-05
m_b	2.33	1.38	0.69
a	0.50	0.50	0.50
e	0.60	0.60	0.60
d	0.39	0.23	0.00



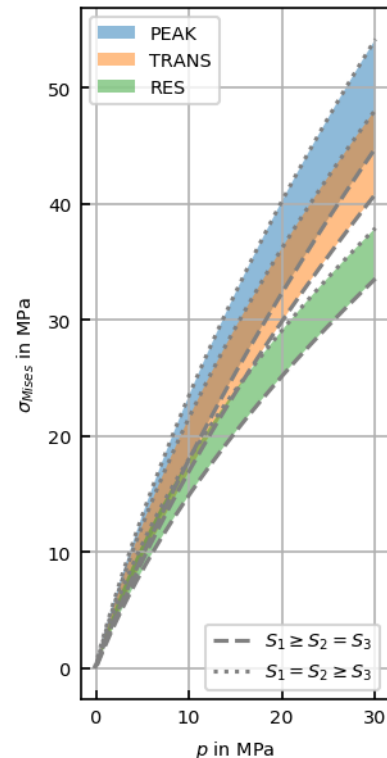
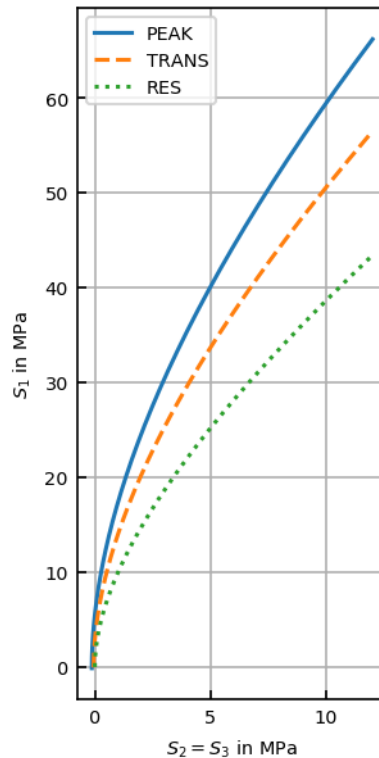
DYAN

General Properties

Type	Computator V14.3 PLR
ρ [kg/m ³]	2770.00
UCS_i [MPa]	125.00
GSI	65.00
n_{aniso}	1.00
s_{aniso}	1.00

LR2 Parameters

	PEAK	TRANS	RES
ϵ_{plast} [%]	0.00	0.96	7.32
E [GPa]	26.27	22.53	19.38
ν	0.25	0.25	0.25
s	2.10e-03	5.82e-04	1.00e-05
m_b	1.97	1.34	0.67
a	0.50	0.50	0.50
e	0.60	0.60	0.60
d	0.33	0.22	0.00



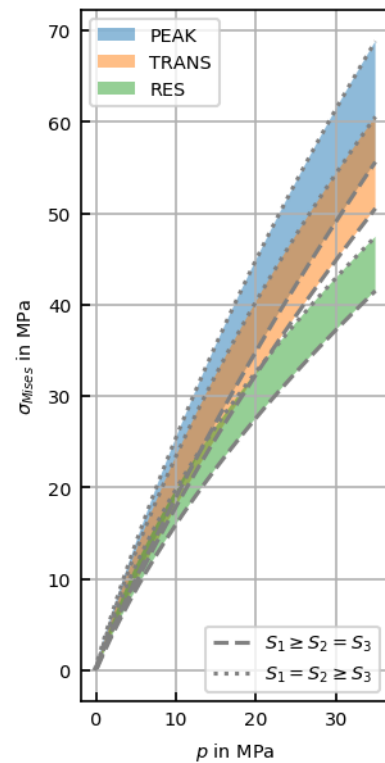
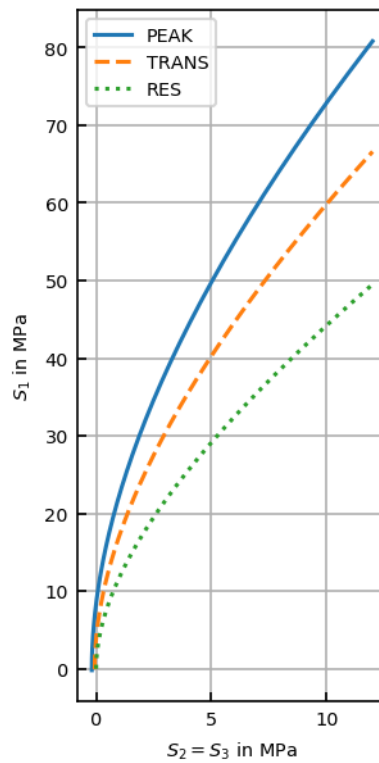
DYDI

General Properties

Type	Computator V14.3 PLR
ρ [kg/m ³]	2900.00
UCS_i [MPa]	155.00
GSI	69.00
n_{aniso}	1.00
s_{aniso}	1.00

LR2 Parameters

	PEAK	TRANS	RES
ϵ_{plast} [%]	0.00	0.93	6.09
E [GPa]	29.94	24.83	20.95
ν	0.25	0.25	0.25
s	3.13e-03	7.00e-04	1.00e-05
m_b	2.54	1.62	0.77
a	0.50	0.50	0.50
e	0.60	0.60	0.60
d	0.42	0.27	0.00



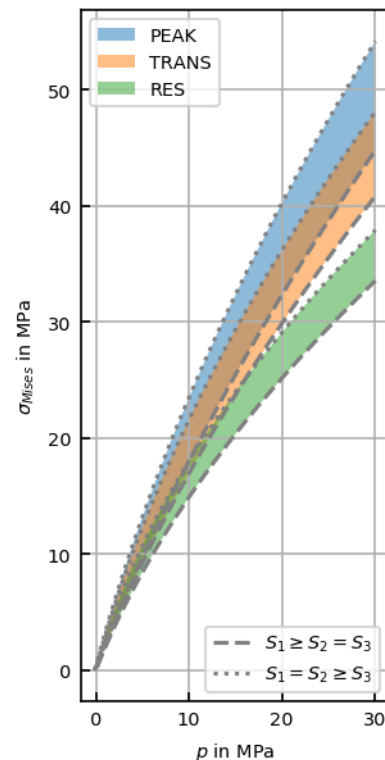
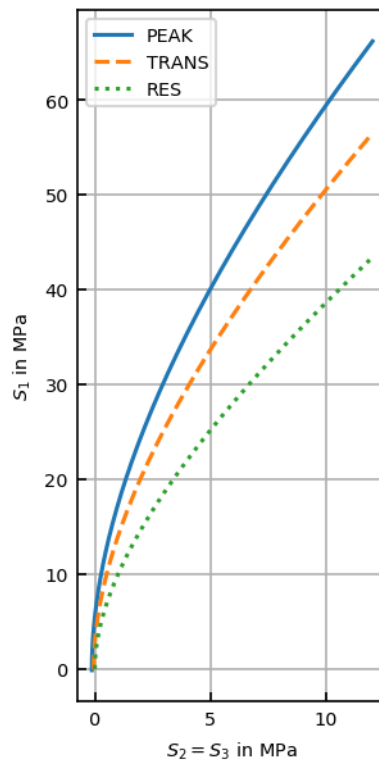
DYDM

General Properties

Type	Computator V14.3 PLR
ρ [kg/m ³]	2770.00
UCS_i [MPa]	125.00
GSI	65.00
n_{aniso}	1.00
s_{aniso}	1.00

LR2 Parameters

	PEAK	TRANS	RES
ϵ_{plast} [%]	0.00	0.96	7.32
E [GPa]	26.27	22.53	19.38
ν	0.25	0.25	0.25
s	2.10e-03	5.82e-04	1.00e-05
m_b	1.97	1.34	0.67
a	0.50	0.50	0.50
e	0.60	0.60	0.60
d	0.33	0.22	0.00



DYDO

General Properties

Type	Computator V14.3 PLR
ρ [kg/m³]	2800.00
UCS_j [MPa]	132.00
GSI	75.00
n_{aniso}	1.00
S_{aniso}	1.00

LR2 Parameters

	PEAK	TRANS	RES
ϵ_{plast} [%]	0.00	1.59	7.63
E [GPa]	30.58	23.14	19.80
ν	0.25	0.25	0.25
s	5.70e-03	6.12e-04	1.00e-05
m_b	2.74	1.40	0.70
a	0.50	0.50	0.50
e	0.60	0.60	0.60
d	0.46	0.23	0.00

